universität wien

DISSERTATION / DOCTORAL THESIS

Titel der Dissertation / Title of the Doctoral Thesis

„The role of asymmetric motion responses

in *Drosophila* object tracking“

verfasst von / submitted by

Dipl.-Phys. Univ. Andreas Pöhlmann

angestrebter akademischer Grad / in partial fulfilment of the requirements for the degree of

Doctor of Philosophy (PhD)

Wien, 2017 / Vienna 2017

Studienkennzahl lt. Studienblatt / degree programme code as it appears on the student record sheet:	A 794 685 490
Dissertationsgebiet lt. Studienblatt / field of study as it appears on the student record sheet:	Molekulare Biologie
Betreut von / Supervisor:	Andrew Straw, PhD

This thesis is dedicated to all the flies
which decided to fly towards the vertical black bar;
knowing they would never reach it.

Acknowledgements

This thesis wouldn't have been possible without the support of many people. First, I want to thank my supervisor Andrew for giving me an opportunity to join the field of neuroscience without prior field specific training, and having trust in my ability to acquire the required knowledge. I want to thank him for his guidance through the field of insect vision and his constant support and enthusiasm. Given my previous training as a physicist, he helped to improve my neuroscience skills significantly. I'd like to thank my committee members Wulf Haubensack, Alipasha Vaziri, and Ivan Yudushkin who helped me make the right choices at the right time.

I'd also like to thank all friends, collaborators and colleagues that made my time in Vienna a wonderful experience. In random order: John Stowers, Lisa Fenk, Sayan Soselisa, Santi Villalba, Etienne Campione, Max Hofbauer, Dan Bath, Dorothea Hörmann, Karin Panser, Katja Hellekes, Andi Hansen, everyone in the DnD group, everyone in the Dragonboat Team, and many more. (If I accidentally forgot you, I owe you a drink.) And a special thank you goes to Nina, my family and my friends for their support and everything else.

The role of asymmetric motion responses in *Drosophila* object tracking

Contents

1 Abstract

Understanding how behavior is generated on a neuronal level is a main goal of neuroscience. The complexity of the internal mechanisms governing neuronal computation lead the field to investigate complex behaviors of very simple model organisms with the goal of discovering common concepts. Indeed many biological commonalties are shared across species, with the work presented here having a focus on visual computation. This thesis, consisting of three manuscripts, aims to contribute to the advancement of the field.

In the first publication we present a novel method for thermogenetically modulating neuronal activity in freely walking *Drosophila* on sub-second timescales, called FlyMAD (the Fly Mind Altering Device). FlyMAD enhances current state-of-the-art thermogenetic methods, which lack temporal resolution, by using computer-vision based real-time systems to aim an infrared laser on a moving and behaving fly. Targeted heating enables us to increase the flies' internal temperature in fractions of the time current convection heating setups take. We test this capability by rapidly silencing and activating locomotion neurons. The fact that the visual system of *Drosophila* cannot detect infrared wavelengths, allows FlyMAD to be used orthogonally to visual stimulation, which we demonstrate by modulating neuronal activity in visual system neurons. The high spatial resolution even allows us to heat specific body parts of the fly preferentially, which we use to reveal timing relations of two well known neuron types involved in the generation of the courtship song.

The second publication investigates how motion-computation based visual system models with asymmetric motion responses can mediate object fixation in tethered flight. We demonstrate that flies with synaptically silenced motion-sensitive T4/T5 cells are unable to fixate small field objects under specific experimental conditions including figure-ground discrimination tasks. Additionally we show, that asymmetric motion visual system models based on properties of motion-sensitive neurons downstream of T4/T5 are sufficient to explain object tracking behavior under these conditions. We provide an analytical and numerical model that both use the asymmetry in the motion response towards progressive and regressive motion to derive small field object tracking behavior. The theoretical predictions together with the synaptic silencing experimental results suggest that object responses in *Drosophila* tethered flight can be mediated by a T4/T5 independent object system, as well as a T4/T5 dependent asymmetric motion system.

In the follow-up manuscript (unpublished) we continue to investigate T4/T5 mediated object tracking responses. We measure the dynamics of T4/T5-independent object tracking behavior in tethered flight, which allows us to estimate the transfer function of T4/T5 mediated object tracking. The estimated transfer function is in good agreement with that of an asymmetric motion based visual system model, indicating that indeed short timescale object tracking during flight is mediated by T4/T5 neurons. Additionally we show that many existing object tracking experiments under open and closed loop experimental conditions can be explained by the object responses calculated from our visual system model. These simulation results are in remarkable agreement with previously published experimental data, even for some experiments that have been argued to require motion-computation independent object tracking circuitry.

2 Zusammenfassung

Zu verstehen, wie Verhalten auf neuronaler Ebene generiert wird, ist ein Hauptziel der Neurowissenschaften. Die hohe Komplexität der internen Mechanismen, die neuronale Berechnungen steuern, bewegt Forscher dazu, komplexe Verhaltensweisen von sehr einfachen Modellorganismen zu untersuchen, mit dem Ziel gemeinsame Konzepte aufzudecken. In der Tat teilen verschiedene Spezies, viele biologische Gemeinsamkeiten, wobei die hier vorgestellte Doktorarbeit ihren Fokus auf die Untersuchung des visuellen Systems legt. Diese Doktorarbeit, setzt sich aus drei Manuskripten zusammen, und versucht einen kleinen Beitrag zur Weiterentwicklung des Forschungsfeldes zu leisten.

In der ersten Publikation wird ein neuartiges Verfahren, genannt FlyMAD (Fly Mind Altering Device), zur thermogenetischen Modulation neuronaler Aktivität präsentiert, welches in frei bewegenden *Drosophila* auf subsekunden Zeitskalen angewendet werden kann. FlyMAD verbessert derzeitige thermogenetische Methoden, die relativ niedrige zeitliche Auflösung aufweisen, indem computergesteuerte Echtzeit-Systeme dazu verwendet werden, um einen Infrarot-Laser auf sich bewegende und uneingeschränkt verhaltende Fliegen zu zielen. Diese gezielte Bestrahlung ermöglicht es, die interne Temperatur der Fliege in Bruchteilen der Zeit zu erhöhen, die derzeitige Konvektionsaufbauten benötigen. Demonstriert wird dies, durch schnelles Inhibieren und Aktivieren von Neuronen die in der Fortbewegung involviert sind. Da das visuelle System von *Drosophila* infrarot Wellenlängen nicht detektieren kann, ermöglicht es FlyMAD neuronale Modulation orthogonal zu visueller Stimulation zu verwenden, was experimentell nachgewiesen wird. Die hohe räumliche Auflösung erlaubt es, bestimmte Körperteile der Fliege bevorzugt aufzuwärmen. Dies wird genutzt, um die genaue Zeitabhängigkeit zweier bekannter Neuronentypen bei der Erzeugung des Balz Liedes zu untersuchen.

Die zweite Publikation untersucht, wie rein bewegungsbasierte Modelle des visuellen Systems, die eine Asymmetrie in ihren Übertragungseigenschaften aufweisen, Objekt-Fixation erklären können. Wir zeigen, dass Fliegen, deren bewegungsempfindliche T4/T5-Zellen synaptisch stummgeschalten wurden, nicht in der Lage sind, Objekte unter spezifischen experimentellen Bedingungen zu fixieren. Dies schliesst auch Objekt-Fixations-Verhalten ein, welches Figur-Grund-Wahrnehmung erfordert. Darüber hinaus zeigen wir, dass Modelle des visuellen Systems mit asymmetrischen Bewegungs-Übertragungseigenschaften, die auf wenigen Parametern von bewegungsempfindlichen Neuronen postsynaptisch von T4/T5 basieren, Objekt-Fixation unter diesen Bedingungen vorhersagen. Wir stellen ein analytisches und ein numerisches Modell vor, welche beide die Herleitung von Objekt-Fixations-Verhalten aus der Asymmetrie in der Bewegungsantwort auf progressive und regressive Bewegung erlauben. Die theoretischen Vorhersagen zusammen mit den experimentellen Ergebnissen deuten darauf hin, dass *Drosophila* Objekt-Fixation unter eindimensional restriktierten Bedingungen durch ein T4/T5-unabhängiges Objekt-Detektions-System sowie ein T4/T5-abhängiges asymmetrisches Bewegungs-Detektions-System vermittelt werden können.

Im Nachfolge-Manuskript (unveröffentlicht) setzen wir die Untersuchung T4/T5-vermittelten Objekt-Fixations-Verhaltens fort. Um dies zu erreichen, messen wir die Übertragungseigenschaften des T4/T5-unabhängigen Objekt-Fixations-Verhaltens unter restrikierten Flug Bedingungen. Dies ermöglicht es, die Übertragungsfunktion T4/T5-basierter Objekt-Fixation zu approximieren. Wir zeigen, dass diese Approximation gut mit der berechneten Übertragungsfunktion eines asymmetrischen bewegungsbasierten visuellen Systemmodells übereinstimmt. Dies deutet darauf hin, dass Objekt-Fixation auf kurzen Zeitskalen während des Fluges durch T4/T5-Neuronen vermittelt wird. Darüber hinaus zeigen wir, dass viele bestehende Objekt-Fixations-Experimente mit und ohne Verhaltensrückkopplung, durch die vorgestellten Modelle vorhergesagt werden können. Die Simulationsergebnisse weisen eine bemerkenswerte Übereinstimmung mit veröffentlichten experimentellen Daten auf. Dies trifft sogar für einige Experimente zu, deren Ergebnisse verwendet wurden, um zu argumentieren, dass das beobachtete Verhalten Bewegungsberechnungs-unabhängige Objekt-Detektions-Systeme erfordert.

3 Synopsis

This thesis investigates how specific types of behavior in *Drosophila melanogaster* can emerge from neuronal circuit states under different experimental paradigms. It consists of three studies, which conceptually are split into two parts. The first part establishes a novel thermogenetic method for influencing neuronal signalling in freely-walking *Drosophila*, that circumvents many previous drawbacks of the use of thermogenetics in the fly (Bath *et al.*, 2014). The second and main part shows how visual object tracking responses can be derived from neuronal system models based on a single type of visual neurons in the *Drosophila* visual system, which show asymmetric neuronal circuit responses towards progressive and regressive motion (Fenk, Poehlmann, and Straw, 2014; Poehlmann *et al.*, unpublished). This synopsis will give a brief introduction into both parts, define the specific aims of the thesis and summarize its findings.

3.1 Introduction

A major goal of neuroscience is to understand how the nervous system translates sensory inputs into behavioral output. The field of neuroscience has branched off into several different subfields approaching the question on different levels. These range across molecular interactions, neuronal signaling, and extend up to the level of cognition. As an example of the investigative process that neuroscientific studies have to go through, we can do a thought experiment with synthetic agents — so called Braitenberg vehicles (Braitenberg, 1986). These vehicles of arbitrary complexity are constructed from very simple construction blocks: Sensors collect sensory information at a single point. Motors turn wheels to move the vehicle, and connections translate sensor values into motor speeds.

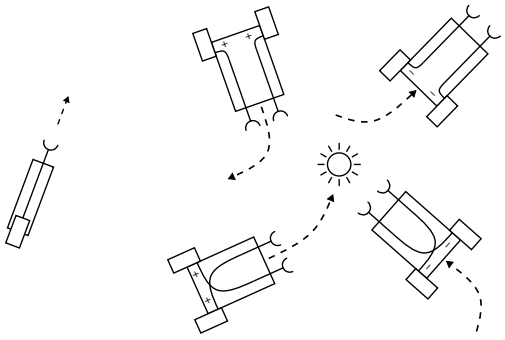

Figure 1: Braitenberg vehicles of low complexity. *(left)* Type 1 vehicle consisting of only one sensor connected to one motor. With increasing sensor value, the vehicle moves faster forward. *(right)* Type 2 and 3 vehicles. All have two sensors and two motors. Connections can cross and can be excitatory (+) and inhibitory (−). Simple behaviors can already be associated to these vehicles. Clockwise starting top-left interpreted as: *Fear*, *Exploration*, *Love*, *Aggression*.

Figure 1 (left) shows the least complex (type 1) versions of Braitenberg vehicles. They are constructed from one sensor connected to one motor. In this example the sensor measures light intensity, but this could be easily exchanged for other sensory modalities like temperature, or CO_2-sensing. With a normal connection from sensor to motor, the higher the intensity at the sensor, the faster the corresponding motor turns. If one imagines this vehicle to move around in a complex world, it can be easily seen, that dependent on slopes of the landscape, or asymmetries in the friction determined by the ground surface, it would move erratically. Given complex patterns of shade and illumination, one would observe, that this vehicle seems to rest in dark areas and will show increased movements when traversing brightly lit environments (photokinesis). More likely than not one would compare this vehicle to a living organism, rather than to an inanimate object. Increasing the complexity of these vehicles by doubling the number of sensors and motors, and allowing excitatory and inhibitory connections, one obtains type 2 and type 3 Braitenberg vehicles. Dependent on their wiring and mode of action, these vehicles show distinctly different behaviors, even in very simple environments that contain only one light source (see Fig. **??**, right). Given ipsi-lateral wiring and excitatory connections, the vehicle will display a behavior, which can be interpreted as *Fear* behavior. The closer the light source gets to the vehicle, the faster it tries to

get away from it. If the connections are kept excitatory but connect contra-laterally to the motors, the vehicle suddenly shows *Aggression* behavior towards the light source. It turns towards the light source and speeds up when it gets closer, ultimately ramming into it. Introducing inhibitory connections will transform the ipsi-laterally connected vehicle's *Fear* behavior into an *Exploration* behavior. It tries to move away from the light source, and the further it gets away the faster it goes. At last connecting contra-laterally with inhibitory connections will make the vehicle turn towards the light source and slow down to a halt. Staying in place and admiring the light source. Braitenberg calls this attraction behavior *Love*.

It is readily observed that the behavioral repertoire dramatically increases in complexity when the number of construction blocks used in the vehicles and the complexity of the surrounding world increase. It is remarkable how rich this behavioral output can be even for these simple agents. Considering that neuroscience is trying to solve the more complicated inverse problem by determining the internal workings of an organism from behavior, it becomes clear why care has to be taken in choosing the best suited model organism, and the best suited reproducible and robust behavior for the specific experimental studies.

In this thesis we focus on answering neuroscientific questions using the fruit fly *Drosophila melanogaster* (Fig. 2, left). The fruit fly is well a established model organism with an abundance of biological research available, genetic tractability, and state-of-the-art genetic access to the internal neuronal structure. *Drosophila* neuroscience benefits greatly from binary expression systems like the UAS-GAL4 system (Brand and Perrimon, 1993). Binary expression systems allow to cross two distinct genetically modified flies to produce offspring which expresses a predefined gene in a selected group of neurons. This is achieved by generating one fly stock (the driver line), which expresses the yeast transcription factor GAL4 in a specified subset of neurons, and a second fly stock (the effector line), which carries the UAS (Upstream Activation Sequence) enhancer sequence together with the coding DNA for the protein of choice in its genome. Large libraries of GAL4 driver lines offer a vast range of expression patterns, containing different neurons in different combinations (Jenett *et al.*, 2012). These can then be used in conjunction with an ever increasing number of genetic tools released as effector lines by the research community. *Drosophila's* short reproduction cycle allows for fast turnover times which enables the researcher to make full use of the versatility of this system.

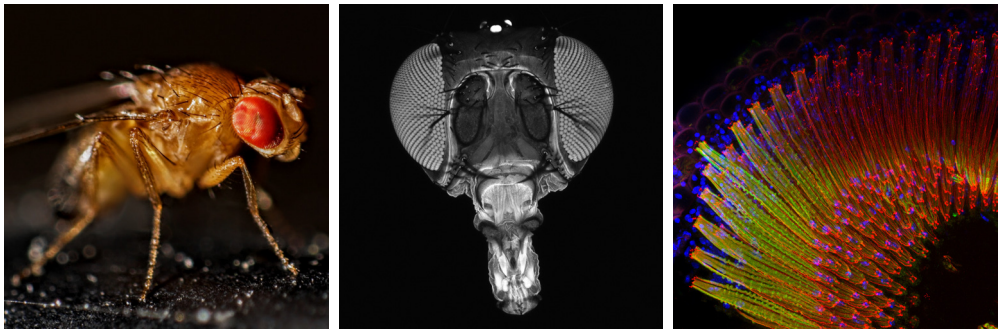

Figure 2: *(left)* The fruit fly, *Drosophila melanogaster (Image by Thomas Wydra, CC-BY-SA-3.0) (center)* Close up image of a fly head (autofluorescence, confocal imaging). The large facet eyes cover a wide field of view at low angular resolution. *(right)* Confocal image of the compound eye with photoreceptor cells marked in green (anti-chaoptin), cell nuclei in blue and cadherins in red, showing the columnar organization and neuro-crystalline structure. *(Images by Karin Panser)*

The fruit fly shows many reproducible, complex, and robust behavioral patterns (Sokolowski, 2001), that are produced by a relatively simple nervous system consisting of only about 100.000 neurons, orders of magnitude smaller than the human brain, or even that of the rat. When it comes to investigating vision, the large compound eyes of roughly 800 individual ommatidia (see Fig. 2, center) reduce the visual input dimensionality dramatically. Moreover, the *Drosophila* visual

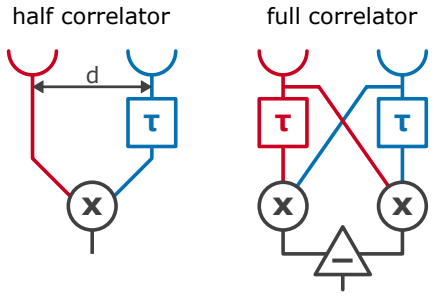

Figure 3: *(Adapted from Borst and Helmstaedter, 2015)* Hassenstein-Reichardt type elementary motion detectors. Simplest two photoreceptor correlator based motion computation. *(left)* Half correlator arm detecting motion in one direction. The signal of one photoreceptor is temporally delayed and multiplied with the signal from the adjacent photoreceptor. The output signal reaches its maximum when retinal pattern movement speed and direction corresponds to the speed defined by the photoreceptor distance and the temporal delay time. *(right)* Full correlator consisting of two opposing half correlators. Their outputs are subtracted to produce a signal which is sign correct for motion in both directions.

system is highly structured (neuro-crystalline, see Fig. 2, right) and precise maneuvering during free flight indicates that the fruit fly is a remarkably optimized organism. This makes *Drosophila melanogaster* not only an ideal candidate for neuroscience research in general, but visual processing specifically (Borst and Helmstaedter, 2015; Paulk, Millard, and Swinderen, 2013).

While the fruit fly is very well suited for neuroscientific research, there are also challenges, especially when studying the visual system. Optogenetic techniques, in which light is used to modulate the activity of neuronal populations, have contributed much to our understanding of neuronal processing in vertebrates, but have until recently not been used as extensively in *Drosophila*. The high intensity light that is required for most effectors to activate or inhibit neurons through the cuticle of the adult fly, also activates the photoreceptors in the eye. These are insufficiently spaced apart from the brain of the animal for the brain to be targeted separately, and are very sensitive to the wavelengths of blue and green light required for many activators. This makes well-controlled behavioral experiments virtually impossible. Even modern optogenetic activators, such as Chrimson, have to be operated at trade-off wavelengths where responses to photoreceptor activation in absence of other visual stimuli are still measurable (Klapoetke *et al.*, 2014), and is therefore not suited for all types of visual experiments.

Here, thermogenetics offer a potential alternative to optogenetics with virtually no interference with vision. Activation or inhibition of neurons can be achieved by expressing temperature sensitive ion channels in specific neurons and directly controlling the temperature of the fruit fly. Thermogenetics has been used effectively to find neurons that underlie a variety of behaviors (i.e. backwards locomotion — moonwalking, Bidaye *et al.*, 2014), by comparing fly behavior on large scales in temperature controlled setups, between sub- and super-threshold temperatures. However, these convection heating experiments also suffer from drawbacks, such as very poor spatial resolution, which prevents testing flies of the same genotype within the same setup independently of each other. Furthermore, the low temporal resolution complicates the fact that the activating temperature of the commonly used activator TrpA1 (Viswanath *et al.*, 2003; Hamada *et al.*, 2008) is in an aversive range for the fly, adding a confounding factor that makes thermogenetics less than optimal for many types of behavioral experiments, especially those requiring very short duration stimulation.

Many visual behaviors operate on short timescales. For example, during flight flies display very precise orientation behavior at remarkable speeds. When considering the relatively small brain size of the fly, this flight behavior is astounding. Computing optic flow (the apparant movement of objects in the visual field due to self motion) for flight stabilization and orientation, puts very high demands on the neuronal motion processing systems in the fly optic lobes. Understanding the fruit fly's solution to visual orientation and flight stabilization has been the focus of studies for decades. Roughly fifty years ago Hassenstein and Reichardt developed a mathematical description of motion-vision by observing turning behavior of a beetle on a spherical Y-maze (Hassenstein and Reichardt, 1956). Their model is a correlator based implementation of a moving edge detector,

which is able to reproduce the observed beetle behavior. To understand its operation we can look at the smallest constructional block required to create these elementary motion detectors. Figure 3 shows one half-correlator arm of a Hassenstein-Reichardt correlator. The visual input based on local intensity is fed downstream from two adjacent photoreceptors (ommatidia) which are spaced apart at distance d. In one of the signaling paths, the intensity signal is temporally delayed by a time τ. Following the delay, the two signals are multiplied with each other. The resulting signal reaches maximum value if a visual edge, that moves perpendicular to the visual axis, moves at a velocity corresponding to $v = d/\tau$ from the delayed to the undelayed arm. The half correlator is therefore sensitive to moving edges of certain velocity in its corresponding preferred direction. Two mirrored half correlators make up an elementary motion detector. The Hassenstein-Reichardt model is in remarkable agreement with many motion responses observed in *Drosophila melanogaster* and other species. Other correlator-type models have been postulated that work in similar ways, but use an inhibitory non-linearity (division) instead of an excitatory non-linearity (multiplication) to generate output. Recently, Haag *et al.*, 2016 have shown that the fly uses a combination of both correlators to determine motion.

Parts of the specific neuronal circuit representation of the correlator are already known, and major building blocks of the correlator have been found in the *Drosophila* optic lobes (Takemura *et al.*, 2013). Chief among these are Lobula Plate Tangential Cells that respond proportionally to large field motion in either the vertical or horizontal direction, the Vertical System (VS) and Horizontal System (HS) cells. Due to their anatomical structure and very large size, these have been prominent targets in electrophysiological studies in *Drosophila*, and have therefore been well-studied. More recent are the discoveries of various cells upstream in the optic lobes that provide input to the VS and HS cells (see Fig. 4) (Borst and Helmstaedter, 2015). T4 and T5 neurons are direction-sensitive neurons that respond to ON (T4) and OFF (T5) edges and are very important structural components of the correlators neuronal circuitry. These in turn receive input from medulla neurons that are thought to represent the arms of the correlator. Mi1 and Tm3 provide input to T4 neurons and Tm1, Tm2, Tm4 and Tm9 provide input to T5 neurons. It is then lamina cells L1 (ON) and L2-L4 (OFF) that bring information to these medulla neurons from the photoreceptors.

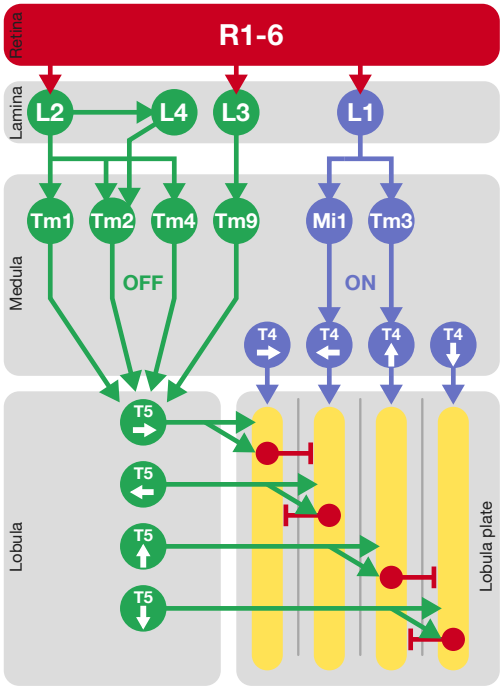

Figure 4: *(Adapted from Borst and Helmstaedter, 2015)* Schematic of the ON and OFF edge motion vision system in *Drosophila*. Initial forking of visual information delivered by R1-6 photoreceptors happens in the lamina. ON edge responses are dependent on L1 signaling, OFF edge responses are dependent on L2, L3, and L4 signaling. In the medulla Mi1 and Tm3 get input from L1 and further connect to directional selective T4 cells. Tm1, Tm2, and Tm4 get input from L2 and L4. Tm9 gets input from L3. All of these connect further to T5 cells in the lobula. Sorted by direction selectivity T4 and T5 cells transmit visual information to the lobula plate, which is layered according to the 4 major retinal directions. Here tangential cells pick up the visual information for further processing. Related lobula plate layers are predicted to connect via inhibitory local interneurons.

While optomotor responses in *Drosophila* are very well described by the correlator models, small field object tracking behavior is mediated by currently unknown circuitry in the fly visual system.

Reichardt and Poggio developed a theory of object tracking responses, which was acquired by simply linearizing the dynamic equation underlying tracking in a tethered flight paradigm (Poggio and Reichardt, 1973). The mathematical description of tracking behavior can be split into two terms, one of which is solely dependent on the position of a small field object, and another which is dependent on the velocity of the object. Since measurements of the motion response in tethered flight correspond well with the correlator model, position dependent object responses are often ascribed to other currently unknown neuronal circuits mediating small field object responses. The neuronal substrate responsible for object tracking behavior is yet to be discovered.

3.2 Goals of the Thesis

Understanding how behavior emerges from neuronal circuit activity requires methods that allow modulation of neuronal activity in the living organism. Precise activation and inhibition of neurons in behaving animals has been a challenge in *Drosophila* neuroscience, due to the difficulty of using optogenetics in the adult fly, and the temporal imprecision of thermogenetic setups. Part of this thesis aims to address this gap, by developing a method of targeted heating that brings thermogenetics the spatial and temporal specificity previously only seen in optogenetics, without any of the drawbacks associated with optogenetics, such as visual interference.

The main goal of this thesis is to determine if small field object responses are mediated by motion-vision based visual systems or not. Previous analytical descriptions of tracking behavior in insects suggested that tracking behavior can arise from dedicated non-motion-computation based object tracking circuitry as well as from motion-vision circuitry with asymmetric motion responses (Poggio and Reichardt, 1981). It has been shown that behavioral motion responses and neuronal responses of specific visual system neurons in *Drosophila* are in agreement with symmetric motion-computation systems (Bahl *et al.*, 2013). Motion computation in the fly relies largely on so called T4 and T5 neurons, which respond to moving ON and OFF edges. Object responses are often thought to be mediated by separate neuronal circuits and i.e. Fox *et al.*, 2014 argues that "[...] a [motion]-only system is ill-suited to [object] tracking, because it is susceptible to low-frequency drift away from the target being tracked". This argumentation, that object responses and motion responses operate through distinct neural processes is then supported by the fact that wide-field optomotor responses depend on intact T4/T5 neurons and that object responses in walking flies are mostly unaffected by blocking T4/T5 cells (Bahl *et al.*, 2013). Taken together these findings are used to hypothesize that an independent non-motion-computation based system is exclusively responsible for tracking behavior in flies. But this assumption is based on necessity of intact T4/T5 cells for motion responses and sufficiency of T4/T5-independent circuits for object tracking. It still requires proof of the necessity of T4/T5-independent circuits for all object tracking, which is currently complicated since the neural substrate for object tracking is still unknown. Here, we want to ascertain if object responses can also be mediated by a T4/T5 based motion system. If this is the case, we want to investigate if dynamics of object tracking differ between non-motion-vision and motion-vision based circuitry and determine the necessity and sufficiency of having intact T4/T5 cells for object tracking. This would allow us to potentially give guidelines for future experiments to separate different types of tracking behavior via specific optical stimulation and improve the investigative process towards a better understanding of tracking behavior in *Drosophila*.

3.3 Results and Discussion

In the first part of this thesis, we focus on enhancing thermogenetic experimental tools in freely walking fruit flies. The study establishes a novel method for targeted rapid thermogenetic activation and inhibition of neuronal signalling in *Drosophila*. By using real time tracking of freely-walking *Drosophila* and control of a focused infrared laser we can apply targeted heating on specific body parts of a walking fruit fly. The fact that the visual system of the fly is insensitive to infrared wavelength photons makes it possible to use this neuronal stimulation orthogonally to visual stim-

uli. Strong heating by the laser renders this thermogenetic method competitive with optogenetic methods and superior in comparison to conventional convection heating. Additionally FlyMAD can be used for optogenetic activation by switching to a laser with the corresponding wavelengths for the optogenetic activator or inhibitor of choice. Given an experimental paradigm, where visual and thermal stimulation can be applied independently, FlyMAD can be used to modulate two different types of neurons even in different flies if necessary. To demonstrate its applicability we chose to investigate the role of two previously identified neuron types (P1 and pIP10) in generating the courtship song. Convection heating experiments could, so far, only loosely determine the causal dependence of courtship song generation on activity in P1 and pIP10. The subsecond temporal resolution of FlyMAD activation was used to gather timing information of courtship song generation. Given the collected data, we propose, that pIP10 activity correlates more closely with the actual activity of singing, because after stopping pIP10 stimulation, singing stopped immediately. Whereas P1 activity correlates more with the persistent state of courtship activity, because song generation continued on for several minutes after stimulation had been stopped.

The second and main part of the thesis, consisting of two studies, focuses on object tracking behavior in tethered flight. In the first study we show that object tracking behavior of a black vertical bar in tethered flight does not require intact T4/T5 neurons. We also show, that given a figure-ground discrimination task, intact T4/T5 neurons seem to be required for reliable object fixation. Moreover we present one analytical and one numerical visual system model with asymmetric motion responses, which both are able to mediate object fixation behavior, and are based on properties of known downstream neurons like the Horizontal System cells. Our model implementations allow for analytical and numerical prediction of tethered flight responses to arbitrarily complex visual stimuli. Differences in the response towards artificially weak coupled closed-loop object tracking stimuli, led us to hypothesize, that T4/T5 independent object tracking systems are likely to have slower response times compared to T4/T5 dependent object tracking circuitry.

In a follow-up study we continue to investigate T4/T5 dependent and independent object tracking behavior. We show that while object tracking behavior under perturbed conditions can be explained by non T4/T5 dependent object tracking systems, higher frequency tracking compensations require intact T4/T5 neurons. This suggests that under slowly varying conditions motion-vision independent systems are sufficient to mediate tracking behavior, but under fast varying conditions, i.e. during flight, where operating timescales are way below the order of 1 s, object tracking has to be mediated by motion-vision dependent T4/T5 neuron based systems. Moreover we recreate a variety of different object tracking experiments with our asymmetric motion vision based numerical model. We show that multiple different object responses are reproduced by these models, even some which have been argued to require motion-vision independent neuronal circuitry.

To conclude, in the first part of this thesis we improve the current state-of-the-art in thermogenetic activation and inhibition experiments for freely moving *Drosophila* with FlyMAD. Its applicability is demonstrated under a variety of different experimental paradigms. Additionally, we use our novel methodology to investigate causal dependencies in the neuronal circuitry underlying courtship behavior. In the main body of the work, focused on visual processing, we show that short timescale object tracking behavior, as well as figure-ground discrimination based object tracking, requires motion-vision processing mediated by T4 and T5 neurons. Furthermore, we implemented analytical and numerical visual system models based on asymmetric motion processing, that can predict a large variety of *Drosophila* object tracking behavior. Using the models and carefully designed experiments, we gain a better understanding of the range of behaviors which can be mediated by motion-sensitive circuitry. All studies have worked to match neuronal substrates to specific fly behaviors, and provide methods and tools to help other researchers continue to unravel how behavior is generated on a neuronal level.

3.4 References

Bahl, A *et al.* (2013). "Object tracking in motion-blind flies". In: *Nature Neuroscience* 16.6, pp. 730–738. DOI: 10.1038/nn.3386.

Bath, DE *et al.* (2014). "FlyMAD: rapid thermogenetic control of neuronal activity in freely walking Drosophila". In: *Nature Methods* 11.7, pp. 756–762. DOI: 10.1038/nmeth.2973.

Bidaye, SS *et al.* (2014). "Neuronal Control of Drosophila Walking Direction". In: *Science* 344.6179, pp. 97–101. DOI: 10.1126/science.1249964.

Borst, A and Helmstaedter, M (2015). "Common circuit design in fly and mammalian motion vision". In: *Nature Neuroscience* 18.8, pp. 1067–1076. DOI: 10.1038/nn.4050.

Braitenberg, V (1986). *Vehicles: Experiments in Synthetic Psychology.* MIT press. ISBN: 0262521121.

Brand, AH and Perrimon, N (1993). "Targeted gene expression as a means of altering cell fates and generating dominant phenotypes." In: *Development (Cambridge, England)* 118.2, pp. 401–15. DOI: 10.1101/lm.1331809.

Fenk, LM, Poehlmann, A, and Straw, AD (2014). "Asymmetric processing of visual motion for simultaneous object and background responses". In: *Current Biology* 24.24, pp. 2913–2919. DOI: 10.1016/j.cub.2014.10.042.

Fox, JL *et al.* (2014). "Figure-ground discrimination behavior in Drosophila. I. Spatial organization of wing-steering responses". In: *Journal of Experimental Biology* 217.4, pp. 558–569. DOI: 10.1242/jeb.097220.

Haag, J *et al.* (2016). "Complementary mechanisms create direction selectivity in the fly". In: *eLife* 5. DOI: 10.7554/eLife.17421.001.

Hamada, FN *et al.* (2008). "An internal thermal sensor controlling temperature preference in Drosophila". In: *Nature* 454.7201, pp. 217–220. DOI: 10.1038/nature07001.

Hassenstein, B and Reichardt, W (1956). "Systemtheoretische Analyse der Zeit, Reihenfolgen, und Vorzeichenauswertung bei der Bewegungsperzepion des Rüsselkäfers Chlorophanus." In: *Naturforsch* 11b.9-10, pp. 513–524.

Heisenberg, M and Buchner, E (1977). "The role of retinula cell types in visual behavior of Drosophila melanogaster". In: *Journal of Comparative Physiology A* 117.2, pp. 127–162. DOI: 10.1007/BF00612784.

Jenett, A *et al.* (2012). "A GAL4-Driver Line Resource for Drosophila Neurobiology". In: *Cell reports* 2.4, pp. 991–1001.

Klapoetke, NC *et al.* (2014). "Independent optical excitation of distinct neural populations". In: *Nature Methods* 11.3, pp. 338–346. DOI: 10.1038/nmeth.2836.

Paulk, A, Millard, SS, and Swinderen, B van (2013). "Vision in Drosophila: Seeing the World Through a Model's Eyes". In: *Annual Review of Entomology* 58.1, pp. 313–332. DOI: 10.1146/annurev-ento-120811-153715.

Poehlmann, A *et al.* (unpublished). "Quantifying T4/T5 motion-vision dependent object tracking in Drosophila tethered flight". In: *This Thesis, Chapter* 6, pp. 64–87.

Poggio, T and Reichardt, W (1973). "A theory of the pattern induced flight orientation of the fly Musca domestica". In: *Kybernetik* 12.4, pp. 185–203. DOI: 10.1007/BF00270572.

— (1981). "Visual fixation and tracking by flies: Mathematical properties of simple control systems". In: *Biological Cybernetics* 40.2, pp. 101–112. DOI: 10.1007/BF00344289.

Sokolowski, MB (2001). "Drosophila: genetics meets behaviour." In: *Nature reviews. Genetics* 2.11, pp. 879–90. DOI: 10.1038/35098592.

Takemura, S *et al.* (2013). "A visual motion detection circuit suggested by Drosophila connectomics". In: *Nature* 500.7461, pp. 175–181. DOI: 10.1038/nature12450.

Viswanath, V *et al.* (2003). "Ion channels: Opposite thermosensor in fruitfly and mouse". In: *Nature* 423.6942, pp. 822–823. DOI: 10.1038/423822a.

4 FlyMAD: rapid thermogenetic control of neuronal activity in freely walking *Drosophila*

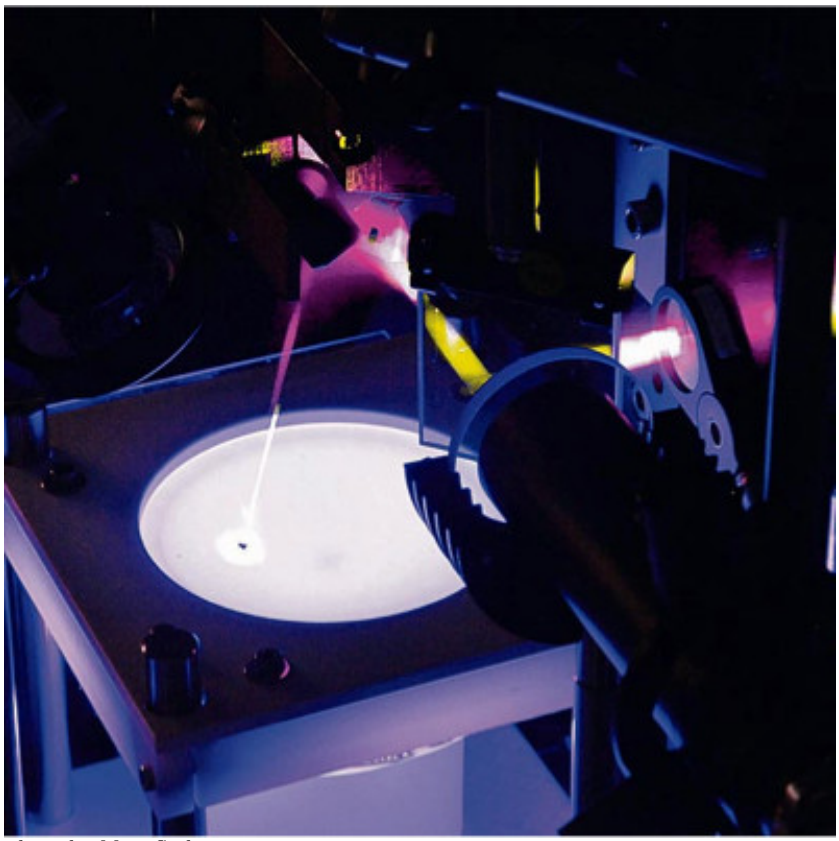

photo by Matt Staley

type	*published* Nature Methods 11, 756 - 762 (2014) **doi:10.1038/nmeth.2973**
authors	Daniel E. Bath[1] (DEB), John R. Stowers[1] (JRS), Dorothea Hörmann (DH), Andreas Poehlmann (AP), Barry J. Dickson (BJD) & Andrew D. Straw (ADS) [1] *equal contribution*
contributions	DEB, BJD, and ADS conceived of the project. DEB, JRS, DH, AP, and ADS developed the hardware and software. DEB and DH performed experiments. All authors contributed to data analysis, interpretation and writing the manuscript.

FlyMAD: rapid thermogenetic control of neuronal activity in freely walking *Drosophila*

Daniel E Bath[1,2,4], John R Stowers[1,3,4], Dorothea Hörmann[1], Andreas Poehlmann[1], Barry J Dickson[1,2] & Andrew D Straw[1]

Rapidly and selectively modulating the activity of defined neurons in unrestrained animals is a powerful approach in investigating the circuit mechanisms that shape behavior. In *Drosophila melanogaster*, temperature-sensitive silencers and activators are widely used to control the activities of genetically defined neuronal cell types. A limitation of these thermogenetic approaches, however, has been their poor temporal resolution. Here we introduce FlyMAD (the fly mind-altering device), which allows thermogenetic silencing or activation within seconds or even fractions of a second. Using computer vision, FlyMAD targets an infrared laser to freely walking flies. As a proof of principle, we demonstrated the rapid silencing and activation of neurons involved in locomotion, vision and courtship. The spatial resolution of the focused beam enabled preferential targeting of neurons in the brain or ventral nerve cord. Moreover, the high temporal resolution of FlyMAD allowed us to discover distinct timing relationships for two neuronal cell types previously linked to courtship song.

Methods to modulate activity in genetically defined cell types are essential for establishing relationships between neuronal activity and behavior. Such methods are most informative when applied with high spatial and temporal resolution to behaving animals. Spatial resolution can generally be provided by genetic methods[1,2], though with considerable limitations. Temporal resolution, however, is constrained by the properties of the genetically encoded effectors and the external stimuli used to control them. Furthermore, to characterize distinct neuronal types in a behavior, it is desirable to have two or more orthogonal systems to independently and acutely modulate activity of multiple cell types in the same animal.

Light-gated optogenetic tools are commonly used to acutely modulate neuronal activity[3,4]. They offer high temporal precision, revolutionizing the functional analysis of neural circuits and behavior. Nonetheless, using light as an external trigger poses several challenges. Spectral overlap with photoreceptors of the eye[5] can cause flash blindness or trigger artifactual visual responses, and surrounding tissue can limit light penetration to the target region. For larger animals, such as rodents, optic fibers can be used to deliver light to deeper tissue without constraining movement[6]. However, these fiber optic systems would disrupt the movement of smaller animals such as adult *Drosophila*. This problem may be alleviated by the use of higher light intensities. Red-shifted optogenetic tools provide another solution, with the deeper penetration of longer-wavelength light and greater spectral separation from fly visual sensitivity. Although progress in the development of red-shifted channelrhodopsins has been reported[7–9], independent and bidirectional optogenetic control of multiple cell types in behaving flies is not yet possible.

Fortunately, ectotherms such as *Drosophila* are suitable for an alternative approach: thermogenetics, which exploits temperature-gated ion channels and other proteins to activate or silence neurons[10]. As a trigger, temperature is orthogonal to light, and for small animals, heat can be applied without physical manipulation of the animal. The challenge with thermogenetics has been poor temporal resolution. Typical protocols use convection heating of the environment. Radiant heating with infrared (IR) light can greatly improve the kinetics of thermogenetic modulation, but this requires precise targeting of a focused laser beam. Thus far, this method has only been applied to immobilized flies[11,12].

Here we present FlyMAD, a device that overcomes this problem by focusing a laser on a freely walking fly. FlyMAD uses real-time video tracking to determine animal position and target the laser. Using a dichroic mirror, a second camera provides high-resolution videos for behavioral analysis and allows through-the-mirror (TTM) tracking to target the laser to specific body parts. Used with an IR laser to apply heat, FlyMAD brings high temporal and spatial resolution to the thermogenetic investigation of neuronal activity and behavior in *Drosophila*. By incorporating an additional visible-light laser, the system is also suitable for optogenetic activation, enabling rapid and independent activity modulation of distinct cell types in the same animal.

RESULTS

Implementation of FlyMAD

In FlyMAD (**Fig. 1a**, **Supplementary Figs. 1** and **2** and **Supplementary Video 1**), flies walk freely in a 9-cm diameter circular chamber with a transparent cover. The chamber is concave[13] so

[1]Research Institute of Molecular Pathology, Vienna Biocenter, Vienna, Austria. [2]Janelia Farm Research Campus, Howard Hughes Medical Institute, Ashburn, Virginia, USA. [3]Automation and Control Institute, Vienna University of Technology, Vienna, Austria. [4]These authors contributed equally to this work. Correspondence should be addressed to B.J.D. (dicksonb@janelia.hhmi.org) or A.D.S. (andrew.straw@imp.ac.at).

RECEIVED 9 DECEMBER 2013; ACCEPTED 20 APRIL 2014; PUBLISHED ONLINE 25 MAY 2014; DOI:10.1038/NMETH.2973

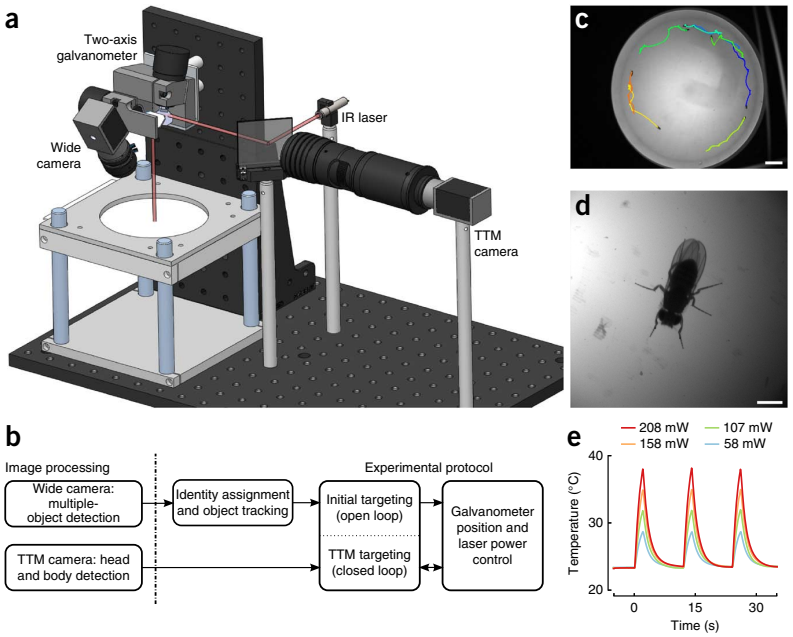

Figure 1 | FlyMAD system overview. (**a**) Drawing of selected components. The red line area denotes the optical beam path of the IR laser. (**b**) Schematic of the information flow within the tracking, galvanometer and laser-control systems. (**c**) Wide-field view of the arena through the tracking camera, and tracked trajectories of several flies. Scale bar, 1 cm. (**d**) Higher-magnification TTM view of the targeted fly. Scale bar, 1 mm. (**e**) Temperature changes inside the thorax of an immobilized fly upon IR stimulation over a range of laser powers (14-d-old male fly, unfocused 808-nm laser).

that the fly maintains a constant distance from a galvanometer mounted 10 cm above the chamber. The position of the fly is determined by real-time tracking through a camera with a view of the entire arena, mounted next to the galvanometer[14] (**Fig. 1b**,**c**), and these coordinates are used to control galvanometer mirrors that target the laser beam directly at the fly. To facilitate low-latency tracking, we simplify image processing by uniformly illuminating the background (**Supplementary Fig. 2**). The tracking algorithm (Online Methods) is capable of tracking multiple flies simultaneously (**Fig. 1c**); the laser is automatically targeted to the first fly detected by default (**Supplementary Fig. 3**). A second camera is aligned with the laser beam, imaging the fly TTM (**Fig. 1d**) to provide high-resolution videos for behavioral analysis. These high-resolution images can also be used to further refine the laser position (TTM tracking). The tracking software can be obtained from http://flymad.strawlab.org/ and is also available as **Supplementary Software**.

The reliability of the laser targeting depends on the speed and precision with which the tracking system can respond to changes in the fly's motion (**Supplementary Figs. 4** and **5**). Without TTM tracking, we estimated the average latency between the software command and the laser illumination to be ~32 ms and the spatial accuracy to be 0.8 mm (Online Methods). We measured the temperature inside the thorax of an immobilized fly over a range of laser conditions (**Fig. 1e** and **Supplementary Fig. 6**). With unfocused light, the temperatures reached were comparable to thresholds reported in conventional thermogenetic experiments[15]. With focused light, the laser powers used in our study could yield larger temperature changes than are typically used in thermogenetic studies. A moving fly may not be as efficiently heated owing to residual targeting error (**Supplementary Fig. 5**) and small beam diameter (**Supplementary Fig. 7**); measurements from a stationary fly represent an upper-bound for a mobile fly.

Rapid activation and silencing of neurons

To test the efficacy of FlyMAD for rapid thermogenetic modulation of neuronal activity and behavior, we first examined locomotor behavior with wide-field tracking. An 808-nm diode laser was slightly defocused to cover the whole body with an ~4.0 mm × 1.7 mm rectangular spot in our video image. We used the *GAL4*–upstream activating sequence (*GAL4*-UAS) system[16] to target specific neurons and either silence (using Shibire^{ts1}; refs. 17–19) or activate them (using TrpA1; refs. 20,21) at temperatures above 25 °C.

We predicted that silencing all motoneurons would disrupt locomotion. We silenced the motoneurons by expressing *UAS-shi^{ts1}* under the control of *VGlut-GAL4* (*OK371-GAL4*)[22]. For control flies, we observed an immediate and transient (<1 s) decrease in speed followed by a more sustained (>10 s) and pronounced increase in speed (**Fig. 2a**). We interpret these locomotion effects as aversive reactions to heat. In contrast, in experimental flies, speed decreased even further after the immediate aversive response, being significantly slower than that of control flies within just 2.5 s ($P < 0.01$; **Supplementary Fig. 8a** and **Supplementary Video 2**). The locomotion of experimental flies returned to baseline within 12.5 s after the laser was turned off.

Next we examined the optomotor response, an innate behavior in which a fly turns toward visual motion. This response is mediated by the R1–R6 photoreceptors[23], so silencing photoreceptors with Shi^{ts1} should eliminate the optomotor response. Using the *Rh1* (*ninaE*)*-GAL4* driver line[24], we expressed *UAS-shi^{ts1}* in R1–R6 and recorded the turning rate as we induced the optomotor response by presenting a high-contrast rotating grating around the edge of the arena (**Fig. 2b**). Prior to laser activation, the mean angular velocity of both control and experimental flies correlated with direction of the rotating visual stimulus. Upon stimulation, the mean angular velocity of experimental flies was significantly reduced ($P < 0.001$; **Supplementary Table 1** and **Supplementary Video 3**), although overall velocity remained unchanged.

For activation experiments, we targeted the 'moonwalker' neurons with *VT50660-GAL4* (ref. 25). The activity of these neurons is both necessary and sufficient to trigger backward walking. In control flies lacking the *UAS-TrpA1* effector or the *GAL4* driver, laser activation induced a rapid transient decrease followed by an increase in forward velocity, again reflecting the aversive heat response (**Fig. 2c**). By contrast, forward velocity of *VT50660-GAL4 UAS-TrpA1* flies continued to decrease and differed from

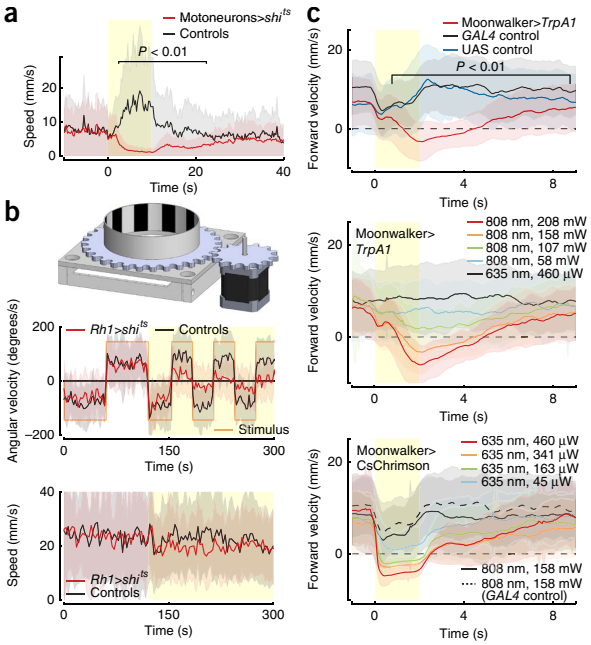

Figure 2 | Behavioral responses to acute neuronal silencing and activation. (**a**) Silencing motoneurons with Shi^{ts1}. Speeds of *OK371-GAL4/UAS-shi^{ts1}* (red) and *+/UAS-shi^{ts1}* (black) flies (n = 25 and 19 flies, respectively, one trial each). P values in **a** and **c** were computed using a two-tailed Kruskal-Wallis test. (**b**) Silencing photoreceptors. Top, rotating grating apparatus to induce optomotor response. Center, angular velocity of *Rh1-GAL4/UAS-shi^{ts1}* (red) and pooled *Rh1-GAL4/+* and *UAS-shi^{ts1}/+* (black) flies presented with a rotating grating (n = 18 and 9 + 12 flies, respectively). Angular velocity of the grating is indicated by the orange square wave. Bottom, translational speed before and during stimulus. (**c**) Activating moonwalker neurons. Top, forward velocity of *VT50660-GAL4/UAS-TrpA1* (red, n = 11 flies, 10 trials per fly), *+/UAS-trpA1* (blue, n = 10 flies, 10 trials each) and *VT50660-GAL4/+*; (black, n = 9 flies, 10 trials each). Forward velocity is the component of locomotion speed toward the fly's head. Center, dose-response activation of *VT50660-GAL4/UAS-TrpA1* using an 808-nm IR laser at varying power (n = 10 flies per condition) and a 635-nm red laser at high power (n = 10). Bottom, dose-response activation of *VT50660-GAL4/UAS-CsChrimson* using a 635-nm red laser at varying power (n = 10 flies per condition) and an 808-nm IR laser at 158 mW (n = 10). In all panels, the yellow shaded region indicates time of IR or red stimulation, solid lines indicate mean values, and corresponding color shadings represent s.d.

controls within 0.75 s of laser activation (P < 0.01; **Supplementary Fig. 8**), becoming negative within 1.0 s (**Supplementary Video 4**). Locomotion returned to control velocity within 6.8 s after the laser was turned off. Recently, acute activation of freely moving flies has also been demonstrated with optogenetic techniques using the red-shifted channelrhodopsins Chrimson[9] and ReaChR[8]. We tested the orthogonality of optogenetic and thermogenetic activation strategies in moonwalker neurons. *VT50660-GAL4 UAS-TrpA1* flies showed neither aversive slowing nor backward walking in response to stimulation with the 635-nm laser but walked backwards in response to the 808-nm laser (P < 0.001; **Fig. 2c** and **Supplementary Figs. 9–12**). *VT50660-GAL4 UAS-CsChrimson* flies walked backwards when exposed to 635-nm light (P < 0.001). The 808-nm IR laser did not induce backward walking in these flies, and the aversive response was not different from that of control flies (P > 0.05; **Fig. 2c** and **Supplementary Fig. 9e**). These data demonstrate the potential for FlyMAD to be used in experiments that combine thermogenetics and optogenetics to independently control the activity of two distinct sets of neurons.

Through-the-mirror targeting of specific body parts

IR heating can deliver body region–specific thermogenetic modulation when targeted with a focused beam[11]. For more precise targeting with FlyMAD, we implemented a TTM tracking system, which uses the high-resolution camera axially aligned with the laser beam. In this mode, the laser was focused to a 105-µm-diameter spot (**Fig. 3a–c** and **Supplementary Fig. 7**). Using template-matching image processing, we could target the laser beam directly at specific body parts such as the antennae, head or thorax (**Supplementary Video 5**). *Post hoc* analysis of saved TTM images during thorax targeting showed a mean initial tracking error of 300 µm at 50-ms latency. Upon continual TTM tracking, the mean tracking error improved to ~100 µm by 100 ms over a range of velocities (Online Methods and **Supplementary Fig. 5**). We compared thorax temperature in stationary head-targeted and thorax-targeted fly bodies (**Fig. 3b**). Owing to the size of the thermocouple, we were unable to measure temperature in the head.

We first tested whether TTM targeting could ameliorate the heat-aversion response by comparing the effect of TTM targeting a 2-s laser pulse to the antennae, head or thorax on the locomotion of wild-type flies. The transient slowing response was observed only upon antennal targeting (P < 0.05; **Fig. 3d** and **Supplementary Fig. 13**), consistent with reports that antennal heat receptors are involved in a rapid heat response[26,27]. The subsequent acceleration was observed in all three TTM conditions but was most pronounced for head targeting. This response might reflect activation of the anterior cell neurons within the head that express endogenous TrpA1 (refs. 21,28).

One potential application of TTM targeting is to preferentially activate neurons in the head or thorax. To explore this possibility, we examined the proboscis extension reflex (PER) and production of courtship song. PER can be elicited by activation of TH-VUM, a dopaminergic neuron in the brain[12]. Using *TH* (*ple*)*-GAL4*, which is expressed in dopaminergic neurons of both the brain and ventral nerve cord (VNC), we found that PER was induced more rapidly and robustly during head targeting than thorax targeting (P < 0.001; **Fig. 3e**, **Supplementary Table 2** and **Supplementary Video 6**). Courtship song can be elicited by optogenetic or thermogenetic activation of *fruitless*-expressing neurons[29] including the descending neuron pIP10 and the VNC neurons dPR1, vPR6 and vMS11 (ref. 30). For the thoracic song neurons, we tested using restricted *GAL4* drivers (Online Methods) and targeted the laser alternately to the head and thorax (**Fig. 3f–h**). Compared to head targeting, thorax targeting elicited wing extension with lower latency, higher frequency or both (P < 0.001; **Fig. 3f–h**, **Supplementary Table 2** and **Supplementary Video 7**). For the descending neuron pIP10, targeting the head induced a slightly more rapid response (P < 0.05; **Fig. 3i** and **Supplementary Table 2**), but overall levels of wing extension were similar in the head- and thorax-targeted trials (**Fig. 3i**). Although the resolution of this method is inevitably limited by targeting inaccuracies and gradual transfer of heat from one body part to

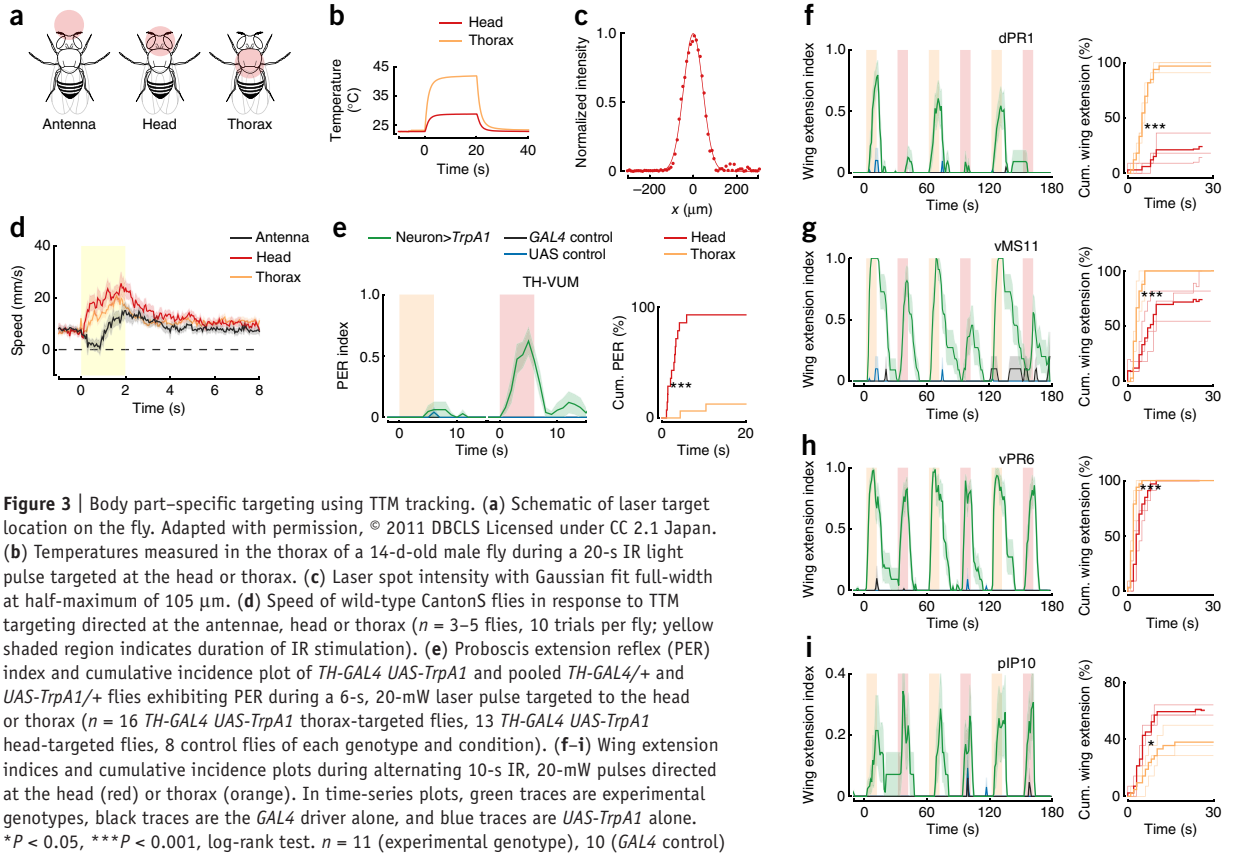

Figure 3 | Body part–specific targeting using TTM tracking. (**a**) Schematic of laser target location on the fly. Adapted with permission, © 2011 DBCLS Licensed under CC 2.1 Japan. (**b**) Temperatures measured in the thorax of a 14-d-old male fly during a 20-s IR light pulse targeted at the head or thorax. (**c**) Laser spot intensity with Gaussian fit full-width at half-maximum of 105 µm. (**d**) Speed of wild-type CantonS flies in response to TTM targeting directed at the antennae, head or thorax (n = 3–5 flies, 10 trials per fly; yellow shaded region indicates duration of IR stimulation). (**e**) Proboscis extension reflex (PER) index and cumulative incidence plot of *TH-GAL4 UAS-TrpA1* and pooled *TH-GAL4/+* and *UAS-TrpA1/+* flies exhibiting PER during a 6-s, 20-mW laser pulse targeted to the head or thorax (n = 16 *TH-GAL4 UAS-TrpA1* thorax-targeted flies, 13 *TH-GAL4 UAS-TrpA1* head-targeted flies, 8 control flies of each genotype and condition). (**f–i**) Wing extension indices and cumulative incidence plots during alternating 10-s IR, 20-mW pulses directed at the head (red) or thorax (orange). In time-series plots, green traces are experimental genotypes, black traces are the *GAL4* driver alone, and blue traces are *UAS-TrpA1* alone. $^*P < 0.05$, $^{***}P < 0.001$, log-rank test. n = 11 (experimental genotype), 10 (*GAL4* control) and 10 (UAS control) flies in **f**; 11, 10 and 10 flies in **g**; 11, 10 and 7 flies in **h**; and 14, 10 and 7 flies in **i**, with 3 head and 3 thorax trials each (pooled in thick lines in cumulative wing extension plots). In all cumulative incidence plots, red lines show head targeting and orange show thorax targeting. For all plots, solid lines represent mean values, and colored shaded regions represent s.e.m.

another, these experiments nonetheless demonstrated that TTM targeting can localize thermogenetic control to specific regions in a moving fly.

Temporal properties of courtship-song neurons

The improved kinetics of thermogenetics afforded by FlyMAD make it possible to distinguish between neuronal activities that relate to persistent behavioral states versus those associated with transient motor actions. We explored this issue in the context of courtship behavior. Conventional thermogenetic experiments have demonstrated that activating either P1 or pIP10 triggers courtship song[30,31] and that P1 induces other components of courtship behavior including following[31]. pIP10 neurons are potentially postsynaptic to P1 in the brain and innervate the wing neuropil of the VNC[32]. We used FlyMAD to examine whether activation of each cell type induces a courtship-like state, in which song would be triggered by (but temporally uncoupled from) the laser stimulus, or the specific action of singing, in which case song would be time locked to the laser stimulus.

In these experiments, we placed fly-size Plasticine targets in the chamber to serve as surrogate courtship targets (**Fig. 4**). P1 neurons were targeted using the genetic intersection of *NP2361-GAL4* and fru^{FLP} (ref. 32) and pIP10 as the intersection of *VT40347-GAL4* and fru^{FLP} (**Supplementary Fig. 14**), in both cases driving the combinatorial effector *UAS>stop>TrpA1*^{myc} (ref. 30; *>stop>* indicates a transcriptional stop cassette that can be excised by Flp recombinase).

As predicted[30,31], acute activation of either P1 or pIP10 in FlyMAD induced wing extension within 5 s ($P < 0.05$; **Fig. 4e**, **Supplementary Fig. 15** and **Supplementary Videos 8** and **9**). In the case of pIP10 activation, wing extension ceased within 10 s when the laser was turned off ($P > 0.05$; **Fig. 4e**). In contrast, wing extension triggered by P1 activation persisted intermittently for at least 5 min ($P < 0.05$). In both cases, most wing extensions elicited during laser stimulation were not directed toward the targets; the flies generally remained near the periphery of the arena. Indeed, for pIP10 activation, the average distance to the nearest target did not change during the course of the experiment (**Fig. 4c**). Following P1 activation, however, the fly increasingly spent more time near the target ($P < 0.01$; **Fig. 4c** and **Supplementary Fig. 15d**). We classified 'proximal' and 'distal' position using a threshold defined by the bimodal distribution of P1-activated flies relative to targets (**Fig. 4f**). Most wing extensions during the P1 stimulus period occurred when the fly was distant from a target (**Fig. 4c**,**e**). During the post-stimulus period, wing extensions increasingly occurred close to a target ($P < 0.0001$, χ^2 test; **Supplementary Table 3**) and often appeared to be directed specifically at the target (**Supplementary Video 8**). These data suggest that, just

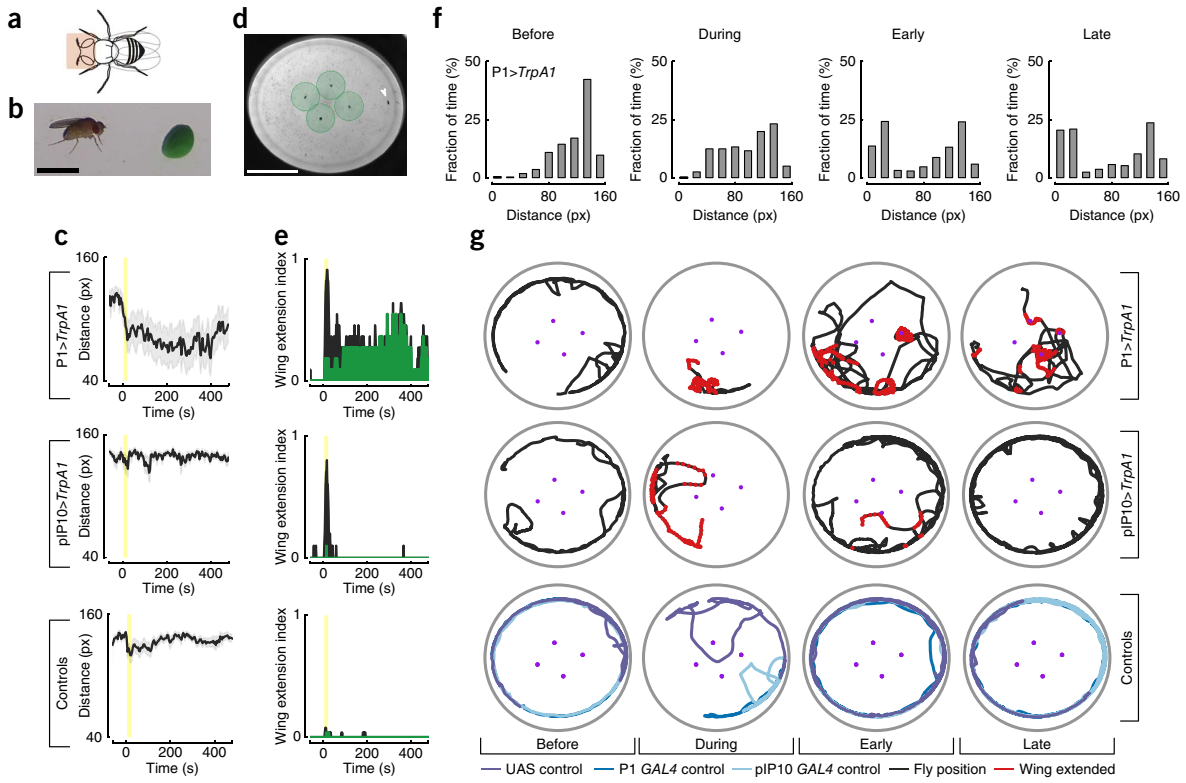

Figure 4 | Acute activation of courtship neurons. (**a**) Location of IR stimulation. Adapted with permission, © 2011 DBCLS Licensed under CC 2.1 Japan. (**b**) Fly approaching a Plasticine ball. Scale bar, 3 mm. (**c**) Mean (solid line) and s.e.m. (shading) of the distance to the nearest target for the indicated strains. Yellow shaded regions represent 20-s IR stimulation. (**d**) Image of a fly (white arrowhead) within the FlyMAD arena. The green shaded region indicates proximal zone, which encompasses a 50-pixel (px) radius from the Plasticine targets. Scale bar, 3 cm. (**e**) Total (black) and proximal (green) wing extension indices for the indicated strains. (**f**) Histograms of distance to nearest target for P1>*TrpA1* flies during the 60-s period before the stimulus ("Before"), during the 20-s laser pulse ("During"), during the first 220 s after the stimulus ("Early") and 220–440 s after the stimulus ("Late"). (**g**) Representative position traces of single flies. Black, purple or blue indicates fly trajectory; red indicates wing extension. Purple points show the location of Plasticine balls. Genotypes: P1>*TrpA1*: +;*UAS>stop>TrpA1*^{myc}*NP2361-GAL4;fru*^{FLP} (n = 11, black); pIP10>*TrpA1*: +;*UAS>stop>TrpA1*^{myc};*fru*^{FLP}*/VT40347-GAL4* (n = 10, black); controls have pooled data from +;*UAS>stop>TrpA1*^{myc};*fru*^{FLP} (n = 9, purple), +;*NP2361-GAL4/+* (n = 7, dark blue) and +;*VT40347-GAL4/+* (n = 10, light blue).

as normal courtship behavior unfolds as a gradual progression between distinct component actions, the persistent courtship induced by direct activation of P1 is also a dynamic state.

DISCUSSION

FlyMAD directs an IR laser beam onto freely walking flies using low-latency real-time computer vision, thereby dramatically improving the temporal resolution possible in thermogenetic experiments. Using convection heating, silencing with Shi^{ts1} has been shown to produce behavioral effects within 60 s (ref. 17), and TrpA1 kinetics are tightly correlated with crossing threshold temperatures[15]. With FlyMAD, we have drastically reduced these latencies, with behavioral changes occurring within just a few seconds or even fractions of a second. This time course compares favorably with that normally achieved using optogenetic approaches.

With FlyMAD, neuronal activity can be controlled by either heat or light. This versatility is important for several reasons. First, until long-wavelength optogenetic silencers are developed, FlyMAD and Shi^{ts1} is the only option for acute silencing in behaving flies. Second, IR light penetrates deeper, scatters less and interferes less with visual responses than red light, making fast thermogenetics with FlyMAD an attractive alternative to red-shifted optogenetic tools in experiments in which these factors might be critical. Third, and most notably, in cases where both optogenetics and thermogenetics can be applied, FlyMAD can combine both approaches to independently modulate the activity of distinct cell types in the same experiment. Such dual control will introduce many new possibilities. For example, one might modulate the activity of a given neuron type according to the behavior observed when modulating—in either the same fly or another fly in the same arena—a different class of neuron.

The importance of high temporal resolution in thermogenetic experiments is exemplified here by our analysis of courtship neuron activation. Most complex behaviors, such as courtship, involve the integration of multiple sensory cues and coordinated, timely execution of multiple actions. These actions might unfold over relatively long time scales, during which time the specific sensory cues might be only intermittently present. With no precise temporal coupling between specific sensory cues and motor patterns, it

thus becomes imperative to discern whether any neuronal activity is temporally coupled to the presence of specific sensory inputs or the execution of specific actions or whether it might instead represent a more persistent state that is independent of moment-to-moment sensation and action.

In the context of courtship song, thermogenetic experiments relying on convection heating previously identified two distinct neuron types, P1 and pIP10, whose activities were causally linked to singing. Causation was, however, only loosely defined, as these experiments lacked the temporal resolution to discriminate between a long-lasting courtship state and directly elicited wing extension and vibration. We propose, on the basis of the data we obtained here and recent findings using red-shifted optogenetic tools[8], that P1 activity more closely correlates with a persistent state of courtship, temporally uncoupled from instantaneous sensory input and motor output, whereas pIP10 activity more closely correlates with the specific action of singing. This model derives from the critical observation that with P1 activation, courtship persisted for several minutes after the laser was turned off, whereas with pIP10 activation, song ceased immediately. It will now be of considerable interest to assess how long P1 activity persists after stimuli are removed. Imaging data are not yet available for pIP10 neurons, but their anatomy suggests that they constitute a key descending pathway from P1 neurons to the wing motor centers in the VNC.

By enabling fast thermogenetic and optogenetic modulation of neuronal activity in freely walking flies, FlyMAD is a powerful tool for the functional investigation of neuronal circuits in *Drosophila*. We anticipate that FlyMAD will be useful in studies that address timing, an important and poorly understood aspect of courtship, learning and other complex behaviors. Future technical developments will further extend FlyMAD's capabilities. For example, the existing tracking software can target a single fly within a group, and the process of selecting a target or modulating laser power could be automated on the basis of spatial location, body posture, sex or any other detectable physical or behavioral contingency. Time-multiplexing the laser across many flies and integrating automated behavior recognition[33,34] should increase the throughput and experimental sophistication without sacrificing the precision of FlyMAD. Finally, with adjustable focus optics and improved tracking, FlyMAD could be used with larger and even three-dimensional arenas, bringing even more of the fly's rich behavioral repertoire into its target.

METHODS

Methods and any associated references are available in the online version of the paper.

Note: Any Supplementary Information and Source Data files are available in the online version of the paper.

ACKNOWLEDGMENTS

We thank S. Bidaye for data on the *VT50660-GAL4* genotype, the Institute of Molecular Pathology (IMP) workshop for help fabricating the hardware, M. Palfreyman and M. Dickinson for insightful discussion, L. Fenk for technological support and P. Masek for insight into IR activation of TrpA1. We thank J.H. Simpson (Howard Hughes Medical Institute, Janelia Farm Research Campus) for providing UAS-Shibire^{ts1} flies. The fruit fly drawings in **Figure 3** are modified from versions made available by Database Center for Life Science (DBCLS) under a CC 2.1 license. This work was supported by the Natural Sciences and Engineering Research Council of Canada by a postgraduate scholarship to D.E.B., European Research Council (ERC) Starting grant 281884 and Wiener Wissenschafts-, Forschungs- und Technologiefonds (WWTF) grant CS2011-029 to A.D.S., ERC Advanced grant 233306 to B.J.D. and IMP core funding.

AUTHOR CONTRIBUTIONS

D.E.B., B.J.D. and A.D.S. conceived of the project. D.E.B., J.R.S., D.H., A.P. and A.D.S. developed the hardware and software. D.E.B. and D.H. performed experiments. All authors contributed to data analysis, interpretation and writing the manuscript.

COMPETING FINANCIAL INTERESTS

The authors declare no competing financial interests.

1. Pfeiffer, B.D. *et al.* Tools for neuroanatomy and neurogenetics in *Drosophila*. *Proc. Natl. Acad. Sci. USA* **105**, 9715–9720 (2008).
2. Jenett, A. *et al.* A GAL4-driver line resource for *Drosophila* neurobiology. *Cell Rep.* **2**, 991–1001 (2012).
3. Lima, S.Q. & Miesenböck, G. Remote control of behavior through genetically targeted photostimulation of neurons. *Cell* **121**, 141–152 (2005).
4. Boyden, E.S., Zhang, F., Bamberg, E., Nagel, G. & Deisseroth, K. Millisecond-timescale, genetically targeted optical control of neural activity. *Nat. Neurosci.* **8**, 1263–1268 (2005).
5. Heisenberg, M. & Buchner, E. The role of retinula cell types in visual behavior of *Drosophila melanogaster*. *J. Comp. Physiol. A Neuroethol. Sens. Neural Behav. Physiol.* **117**, 127–162 (1977).
6. Aravanis, A.M. *et al.* An optical neural interface: *in vivo* control of rodent motor cortex with integrated fiberoptic and optogenetic technology. *J. Neural Eng.* **4**, S143–S156 (2007).
7. Lin, J.Y., Knutsen, P.M., Muller, A., Kleinfeld, D. & Tsien, R.Y. ReaChR: a red-shifted variant of channelrhodopsin enables deep transcranial optogenetic excitation. *Nat. Neurosci.* **16**, 1499–1508 (2013).
8. Inagaki, H.K. *et al.* Optogenetic control of *Drosophila* using a red-shifted channelrhodopsin reveals experience-dependent influences on courtship. *Nat. Methods* **11**, 325–332 (2014).
9. Klapoetke, N.C. *et al.* Independent optical excitation of distinct neural populations. *Nat. Methods* **11**, 338–346 (2014).
10. Bernstein, J.G., Garrity, P.A. & Boyden, E.S. Optogenetics and thermogenetics: technologies for controlling the activity of targeted cells within intact neural circuits. *Curr. Opin. Neurobiol.* **22**, 61–71 (2012).
11. Keene, A.C. & Masek, P. Optogenetic induction of aversive taste memory. *Neuroscience* **222**, 173–180 (2012).
12. Marella, S., Mann, K. & Scott, K. Dopaminergic modulation of sucrose acceptance behavior in *Drosophila*. *Neuron* **73**, 941–950 (2012).
13. Simon, J.C. & Dickinson, M.H. A new chamber for studying the behavior of *Drosophila*. *PLoS ONE* **5**, e8793 (2010).
14. Straw, A.D. & Dickinson, M.H. Motmot, an open-source toolkit for realtime video acquisition and analysis. *Source Code Biol. Med.* **4**, 5 (2009).
15. Pulver, S.R., Pashkovski, S.L., Hornstein, N.J., Garrity, P.A. & Griffith, L.C. Temporal dynamics of neuronal activation by Channelrhodopsin-2 and TRPA1 determine behavioral output in *Drosophila* larvae. *J. Neurophysiol.* **101**, 3075–3088 (2009).
16. Brand, A.H. & Perrimon, N. Targeted gene expression as a means of altering cell fates and generating dominant phenotypes. *Development* **118**, 401–415 (1993).
17. Kitamoto, T. Conditional modification of behavior in *Drosophila* by targeted expression of a temperature-sensitive shibire allele in defined neurons. *J. Neurobiol.* **47**, 81–92 (2001).
18. Grigliatti, T.A., Hall, L., Rosenbluth, R. & Suzuki, D.T. Temperature-sensitive mutations in *Drosophila melanogaster*. *Mol. Gen. Genet.* **120**, 107–114 (1973).
19. Poodry, C.A. & Edgar, L. Reversible alterations in the neuromuscular junctions of *Drosophila melanogaster* bearing a temperature-sensitive mutation, shibire. *J. Cell Biol.* **81**, 520–527 (1979).
20. Viswanath, V. *et al.* Opposite thermosensor in fruitfly and mouse. *Nature* **423**, 822–823 (2003).
21. Hamada, F.N. *et al.* An internal thermal sensor controlling temperature preference in *Drosophila*. *Nature* **454**, 217–220 (2008).
22. Mahr, A. & Aberle, H. The expression pattern of the *Drosophila* vesicular glutamate transporter: a marker protein for motoneurons and glutamatergic centers in the brain. *Gene Expr. Patterns* **6**, 299–309 (2006).

23. Yamaguchi, S., Wolf, R., Desplan, C. & Heisenberg, M. Motion vision is independent of color in *Drosophila*. *Proc. Natl. Acad. Sci. USA* **105**, 4910–4915 (2008).
24. Ellis, M.C., O'Neill, E.M. & Rubin, G.M. Expression of *Drosophila* glass protein and evidence for negative regulation of its activity in non-neuronal cells by another DNA-binding protein. *Development* **119**, 855–865 (1993).
25. Bidaye, S.S., Machacek, C., Wu, Y. & Dickson, B.J. Neuronal control of *Drosophila* walking direction. *Science* **344**, 97–101 (2014).
26. Ni, L. *et al.* A gustatory receptor paralogue controls rapid warmth avoidance in *Drosophila*. *Nature* **500**, 580–584 (2013).
27. Tang, X., Platt, M.D., Lagnese, C.M., Leslie, J.R. & Hamada, F.N. Temperature integration at the AC thermosensory neurons in *Drosophila*. *J. Neurosci.* **33**, 894–901 (2013).
28. Gallio, M., Ofstad, T.A., Macpherson, L.J., Wang, J.W. & Zuker, C.S. The coding of temperature in the *Drosophila* brain. *Cell* **144**, 614–624 (2011).
29. Clyne, J.D. & Miesenböck, G. Sex-specific control and tuning of the pattern generator for courtship song in *Drosophila*. *Cell* **133**, 354–363 (2008).
30. von Philipsborn, A.C. *et al.* Neuronal control of *Drosophila* courtship song. *Neuron* **69**, 509–522 (2011).
31. Kohatsu, S., Koganezawa, M. & Yamamoto, D. Female contact activates male-specific interneurons that trigger stereotypic courtship behavior in *Drosophila*. *Neuron* **69**, 498–508 (2011).
32. Yu, J.Y., Kanai, M.I., Demir, E., Jefferis, G.S.X.E. & Dickson, B.J. Cellular organization of the neural circuit that drives *Drosophila* courtship behavior. *Curr. Biol.* **20**, 1602–1614 (2010).
33. Dankert, H., Wang, L., Hoopfer, E.D., Anderson, D.J. & Perona, P. Automated monitoring and analysis of social behavior in *Drosophila*. *Nat. Methods* **6**, 297–303 (2009).
34. Branson, K., Robie, A., Bender, J., Perona, P. & Dickinson, M.H. High-throughput ethomics in large groups of *Drosophila*. *Nat. Methods* **6**, 451–457 (2009).

ONLINE METHODS

Fly stocks. *UAS-TrpA1*, *UAS>stop>TrpA1^{myc}*, *UAS-CsChrimson*, *UAS-shi^{ts1}NP2361-GAL4*, *VT41688-GAL4*, *VT43702-GAL4*, *VT5534-GAL4*, *VT50660-GAL4*, *TH-GAL4*, *Rh1-GAL4* (also called *ninaE-GAL4*) and *OK371-GAL4* lines were previously described[9,12,17,21,22,24,25,28,30]. *VT40347-GAL4* was generated as part of the VT library (B.J.D., unpublished data). *UAS-shi^{ts1}* flies were provided by J.H. Simpson. Flies were raised at 22 °C, and males were collected up to 24 h after eclosion and raised at 22 °C in groups of 15–20 for 7–9 d (locomotion experiments) or 15–17 d (courtship experiments). For PER and optomotor experiments, female flies were used, age 6–8 d and 4 d, respectively. For moonwalker experiments, flies were raised in 0.1 mM *trans*-retinal in darkness.

We activated the TH-VUM neurons using *TH-Gal4* (ref. 35) and vMS11 and dPR1 with *VT43702* and *VT41688*, respectively[30]. P1 neurons were targeted using the genetic intersection of *NP2361-GAL4* and *fru^{FLP}* (ref. 32), pIP10 as the intersection of *VT40347-GAL4* and *fru^{FLP}* (**Supplementary Fig. 14**) and vPR6 as the intersection of VT5534 (ref. 32) and *fru^{FLP}*, in all three cases driving the combinatorial effector *UAS>stop>TrpA1^{myc}* (ref. 32; *>stop>* indicates a transcriptional stop cassette that can be excised by Flp recombinase).

Behavior assays. The surface of the FlyMAD arena is white nylon (Delrin polyacetyl copolymer). The arena was coated with fly odors by housing 50–100 virgin females overnight. The arena was backlit with diffuse white or 440-nm LED light. To prevent flies from walking on the enclosure lid, we coated the glass with a silicon lubricant (SigmaCote). To provide targets for courtship behavior, we placed four small (approximately 2–3 mm) round pieces of Plasticine in the center of the arena. Flies were introduced to the FlyMAD arena by gentle aspiration and allowed to acclimatize for a minimum of 30 s before we began experiments. For head- and thorax-targeting experiments, acclimatization was increased to minimum 120 s.

For moonwalker experiments, each fly was given repeated stimuli (2-s stimuli at 7- or 12-s intervals; 10 trials), and locomotion data were pooled by trial. For PER and song-neuron activation in TTM experiments, the laser was focused to 105 µm, and in the song experiments, each fly was given six 10-s stimuli at 20 mW, alternating between thorax and head, with 20-s recoveries. For TTM targeting experiments on wild-type flies (**Fig. 3d**), each fly was given ten repeated stimuli with a 90-s rest period, and the laser was powered to 46.8 mW. For all other experiments each fly was given only a single stimulus. For experiments with an unfocused beam (**Fig. 2a**,**c**), the laser was powered as indicated and focused to 4 by 1.7-mm beam size as seen in the video camera. For optomotor experiments, flies were stimulated for 3 min with TTM thorax targeting focused to 105 µm and 19.3-mW laser power. The visual stimulus (a 42-mm-wavelength square-wave grating that was laser printed on white paper) changed direction every 30 s and rotated at 144° per second about the arena via gear coupling to a stepper motor (**Fig. 2b**).

Some components of fly behavior were manually scored. For moonwalker experiments, head direction was manually assigned a quadrant, which was applied to the tracked body axis to determine heading, which otherwise has a 180° uncertainty (either head or tail could potentially be identified as head). For PER, video frames in which the proboscis was visible in front of the head were scored as positive. Wing extension was defined as extension of one or both wings by more than 15° from their baseline posture, except during righting after a fall and grooming (when the hind legs are stroking the wings or abdomen). The PER index and wing extension index are the fraction of time spent in PER and wing extension, respectively, as defined using these criteria.

Temperature was measured with a Type T (Farnell 8598258) or Type K (Farnell 859-8240) thermocouple after obtaining reference measurements with PT100 temperature probe. Laser power was measured in the arena using an optical power meter (Thorlabs PM100A and Thorlabs S120C).

Statistics and general methods. All experiments were performed on *D. melanogaster*. Our stopping criterion was to end experiments after three working days spent across all genotypes and a particular experimental design. We did not specify an effect size before running the experiments. If flies were not moving before the experiment or underwent seizures during heating, they were excluded. Within a given experimental design, flies of different genotypes were raised side by side in different vials or bottles. Experiments on different genotypes were performed sequentially. For dose-response curves on the same genotype, conditions were tested in sets of one or two and repeated several times until the final sample size was reached for all conditions. The experiments were done with prior knowledge of the genotype. Analysis that required manual scoring was done blindly (no knowledge of the genotype) in random order.

As described in the relevant figure captions and supplementary figures and tables, we used the Kruskal-Wallis, Mann-Whitney *U*, χ^2 and log-rank tests, which are not sensitive to the variance of the distributions.

Cameras and optical equipment. Wide-field tracking cameras were acA640-120gm (Basler); monochrome 659 pixels × 494 pixels operating at 100 frames/s. Through-the-mirrors cameras were as follows: piA1000-60gm (Basler) at 60 frames/s in courtship experiments and acA640-120gm at 100 frames/s in TTM experiments. Wide-field lenses were 2.9–8.2 mm 1:1.0⅓" CS (Computar). Through-the-mirrors lenses were VS-TC1-220CO (VS Technologies) or 200-mm ED AF Nikkor (Nikon). Cameras were connected via gigabit Ethernet. Galvanometers were GVS012/M (Thorlabs). Infrared lasers were DB808-350-3(22x65) (Picotronic) and RLTMDL-808-1W-5 (Roithner), and red lasers were DA635-1-3(16x58) (Picotronic). For a full parts list, see **Supplementary Table 4**.

Real-time tracking and targeting architecture. Images were acquired using libcamiface (https://github.com/motmot/libcamiface). Detection of fly positions in the wide-field camera, and detection of fly head and body centers in the TTM camera were both implemented as FView (https://github.com/motmot/fview) plug-ins. Both image streams were analyzed in real time at 100 frames/s. All image processing was implemented using OpenCV (http://www.opencv.org/) compiled with SSE optimizations.

Processes responsible for the subsequent tracking, targeting, and experimental tasks were implemented as ROS (http://www.ros.org/) processes and communicated using the ROS interprocess communication protocol. The tracking and data-association method was a simplified version of one described previously[36].

Briefly, putative 2D pixel locations of flies were sent from the real-time tracking FView plug-in to a tracker node that assigned these observations to existing models for each fly. If new observations arrived with no corresponding model, a new model was created. Likewise, if a model existed for some time with no observational support, it was destroyed. The model was implemented as a linear Kalman filter with a 4D state space (x, y, x velocity, y velocity) in pixels. The motion model was a constant velocity model, and the observation model was a 2×4 portion of the identity matrix. Important software packages and respective versions used are shown in **Supplementary Table 5**.

Galvanometer positions were set using an analog reference input between −10 V and +10 V. Each axis was put into 0.5 V/° mode and the reference input generated using a custom printed circuit board (PCB). The PCB contained an ATmega328-based Arduino microprocessor board, and analog reference voltages were generated using DAC714 16-bit digital-to-analog converters (Texas Instruments) referenced to ±12 V taken from the galvanometer power supply (**Supplementary Fig. 16**). Communication between the ROS targeting process on the host computer and the ATmega328 occurs over USB. Latencies were quantified and are shown in **Supplementary Figure 5**.

TTM head and body detection. After acquisition, images are downsampled by 4 (**Supplementary Fig. 2**). An adaptive threshold is applied, followed by a morphological open filter to remove noise, resulting in a binary image. A contour detection step is performed on the binary image to find closed contours. The largest contour is taken to outline the entire fly and fitted with an ellipse. Using the major axis of the ellipse, an affine transform is applied in order to rotate the contour points so the fly is orientated vertically. Because of the direction ambiguity of the major axis, the fly head may now be above or below the horizontal after the affine transform. A temporary binary image is created, and points contained in the contour in the temporary image are filled with white. The filled and upright fly silhouette is compared with the previously collected template of the fly head in both orientations using a cross-correlation template-matching strategy to compute a 'difference image'. By the normalized squared difference metric, the best matching template (absolute minimum cross-correlation) indicates whether the fly head is above or below the horizontal. The index of the pixel with the minimum value in the difference image is declared the coordinates of the center of the template. An offset ('template fraction' in the GUI shown in **Supplementary Fig. 3**) relative to the center of the template is added here to target regions along the fly's long axis, before the previous transformation and downsampling is reversed, giving the location of the template target in the original image.

The computationally expensive template operation may also be performed on the GPU if a large template is required, such as if one wishes to define the whole fly body to allow directed targeting within the thorax, for example.

The algorithm was implemented with a focus on graceful degradation and efficiency. The relatively expensive affine transform operation was performed on only the contour points (and not on the image pixels). Furthermore, by performing an ellipse fit early in the algorithm, the center of the fly body is returned in addition to the location of the template target; allowing graceful degradation of the control system (by pointing the laser at the body momentarily) for the small number of instances where the template is not matched correctly.

Latency and accuracy estimation. In wide-field mode (without TTM), the camera configuration is similar to that previously described[13]. As the camera shutter integration time was set to 8 ms, and assuming a gigabit Ethernet delay of 5 ms, the predicted latency of images available for processing is a distribu tion between 5 and 13 ms, depending on whether a given photon arrived at the beginning or end of the integration period. With image processing times of ~8 ms, USB transmission delay of ~4 ms and galvanometer response time of ~7 ms, the predicted latency in wide-field mode is 24–32 ms. Indeed, when we measured total latency of the time from the initial target command to the switch to TTM mode, the mode of this distribution was at 32 ms.

Closed-loop performance of TTM control is influenced by accuracy of the template-matching operation and system latency. Both important image processing operations, ellipse fitting to contour points and template matching via cross-correlation, return estimates without returning quality or confidence. Thus, direct quantification of their accuracy is challenging. Instead, we estimated them in two ways. The first was by performing measurements a single fly whose size we presumed to be constant over the trial (**Supplementary Fig. 4**). TTM head detection measured contour area between 1,400 and 1,800 pixels, compared with the true value measured offline of 1,544 pixels. Furthermore, TTM measured distances from head to contour center ranging from 70 to 85 pixels, with the mode at 77 pixels, for a true head-contour distance of 74.2 pixels.

The second way we estimated TTM accuracy was by analyzing the signal sent to control the galvanometers (**Supplementary Fig. 5**). By definition, this corrective action represents the system's best estimate of spatial error. By aiming the laser in another quadrant of the arena from a fly and then enabling TTM mode, FlyMAD asymptotically approaches the maximal performance of ~100-µm error (thorax targeting mode) or ~200-µm error (head targeting mode) with this value being reached within 200 ms. At 50 ms, mean error ± s.d. was 400 ± 200 µm for head targeting and 300 ± 100 µm for thorax targeting error. Together, these two estimates of TTM accuracy suggest pixel errors were <7 and around 200 µm.

Alignment and calibration. The floor of the arena forms a spherical bowl that was aligned with the galvanometer such that the center of the sphere was coincident with the center of the galvanometer's secondary axis mirror. The TTM camera and laser beams were aligned with a dichroic mirror such that the transmitted and reflected light paths (respectively) were coaxial before reaching the galvanometer.

The wide-angle targeting system was calibrated by delivering a range of known voltages to the galvanometer while wide-field tracking with the tracking camera's IR blocking filter was removed. Targeting the entire arena was accomplished by interpolating the resultant lookup table of corresponding voltages and tracked positions.

35. Friggi-Grelin, F. *et al.* Targeted gene expression in *Drosophila* dopaminergic cells using regulatory sequences from tyrosine hydroxylase. *J. Neurobiol.* **54**, 618–627 (2003).
36. Straw, A.D., Branson, K., Neumann, T.R. & Dickinson, M.H. Multi-camera real-time three-dimensional tracking of multiple flying animals. *J. R. Soc. Interface* **8**, 395–409 (2011).

Supplementary Text and Figures

FlyMAD: Rapid thermogenetic control of neuronal activity in freely-walking *Drosophila*

Daniel E. Bath[1,2,4], John R. Stowers[1,3,4], Dorothea Hörmann[1], Andreas Poehlmann[1], Barry J. Dickson[1,2] and Andrew D. Straw[1]

[1] Research Institute of Molecular Pathology, Vienna, Austria

[2] Janelia Farm Research Campus, Howard Hughes Medical Institute, Ashburn, U.S.A.

[3] Automation and Control Institute, Vienna University of Technology, Vienna, Austria.

[4] These authors contributed equally to this work.

Correspondence should be addressed to B.J.D (dicksonb@janelia.hhmi.org) or A.D.S. (andrew.straw@imp.ac.at).

Supplementary Figure 1. Photograph of FlyMAD apparatus.

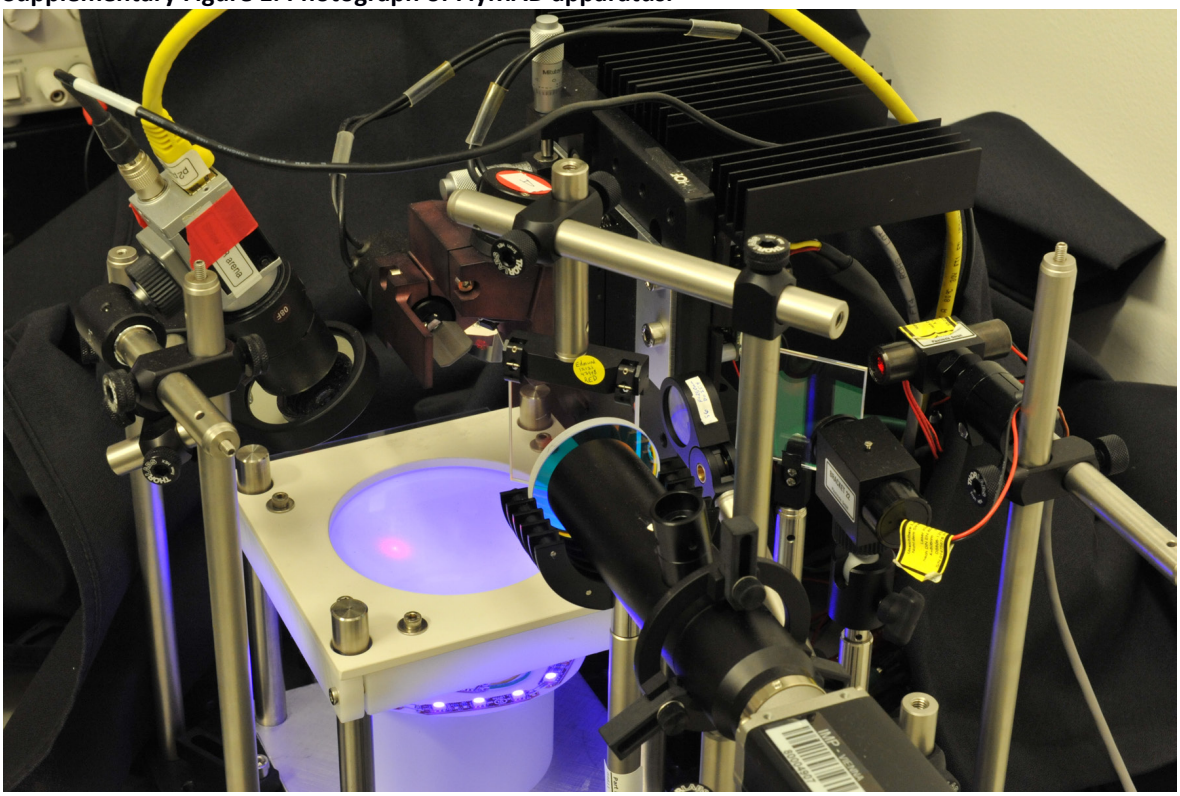

(Photo by Matt Staley.)

Supplementary Figure 2. Realtime image processing.

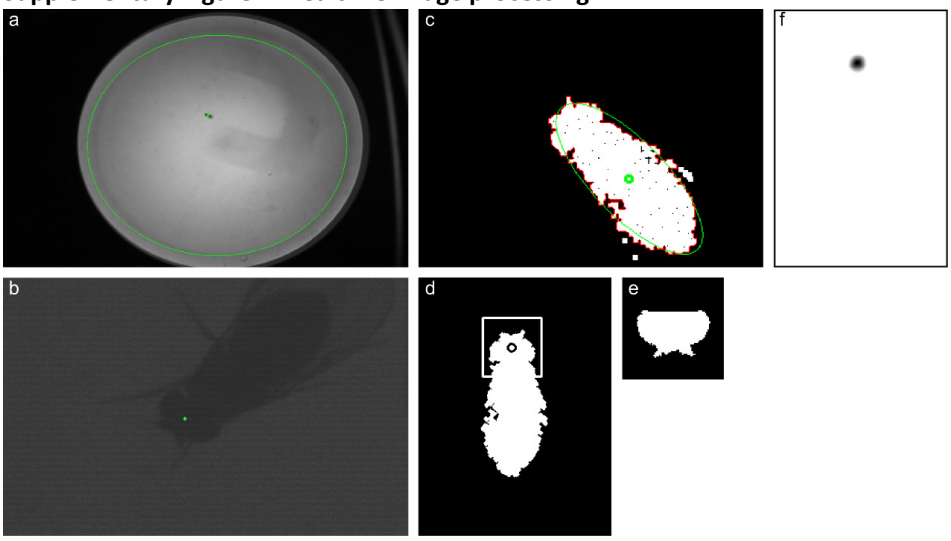

(**a**) View of arena from wide-field tracking camera showing tracking region (green circle) and tracked fly (green point). (**b**) View of fly from TTM camera and identified head projected onto raw image. (**c**) Downsampled, thresholded and filtered TTM image showing the fly contour (red line outlining white thresholded pixels) and best fit ellipse (green line, and center green circle). (**d**) Affine transformed upright fly image and location identified as head (circle). (**e**) Template used for detecting the fly head. (**f**) Normalized cross correlation result image between upright fly image and fly head template.

Supplementary Figure 3. Graphical user interfaces for controlling FlyMAD.

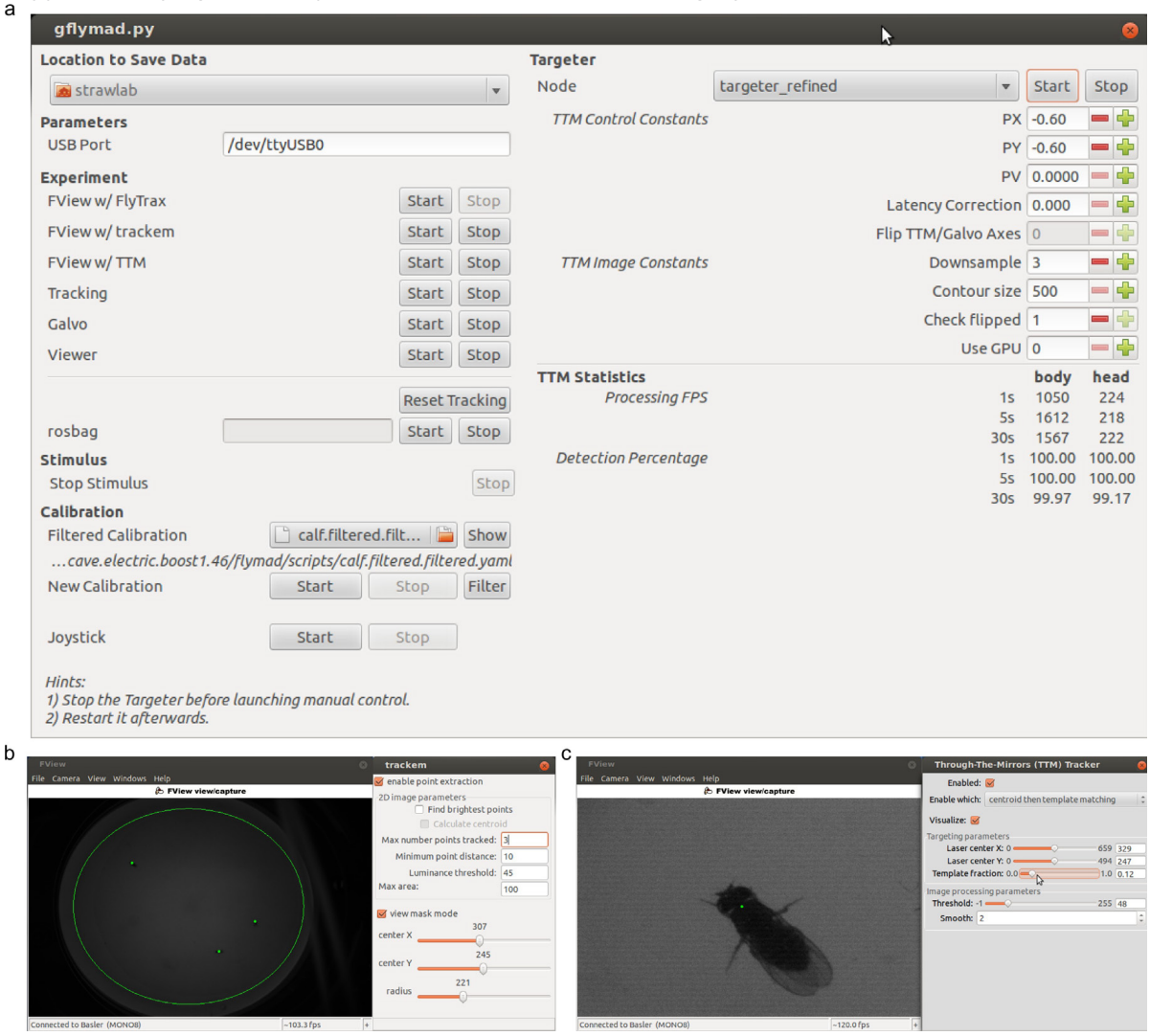

(**a**) gFlyMAD GUI for launching the major components of the system (targeter, tracker, etc), visualization, recording data, and adjusting control gains. (**b**) Wide-field tracking software (FView with Trackem plugin) and associated configuration interface for adjusting the number of flies tracked. (**c**) TTM tracking software (FView with TTM head detection plugin) and associated GUI for adjusting targeting and image processing parameters. gFlyMAD displays realtime statistics showing the effect of any change on tracking accuracy.

Supplementary Figure 4. Measurements of spatial accuracy of head and body detection.

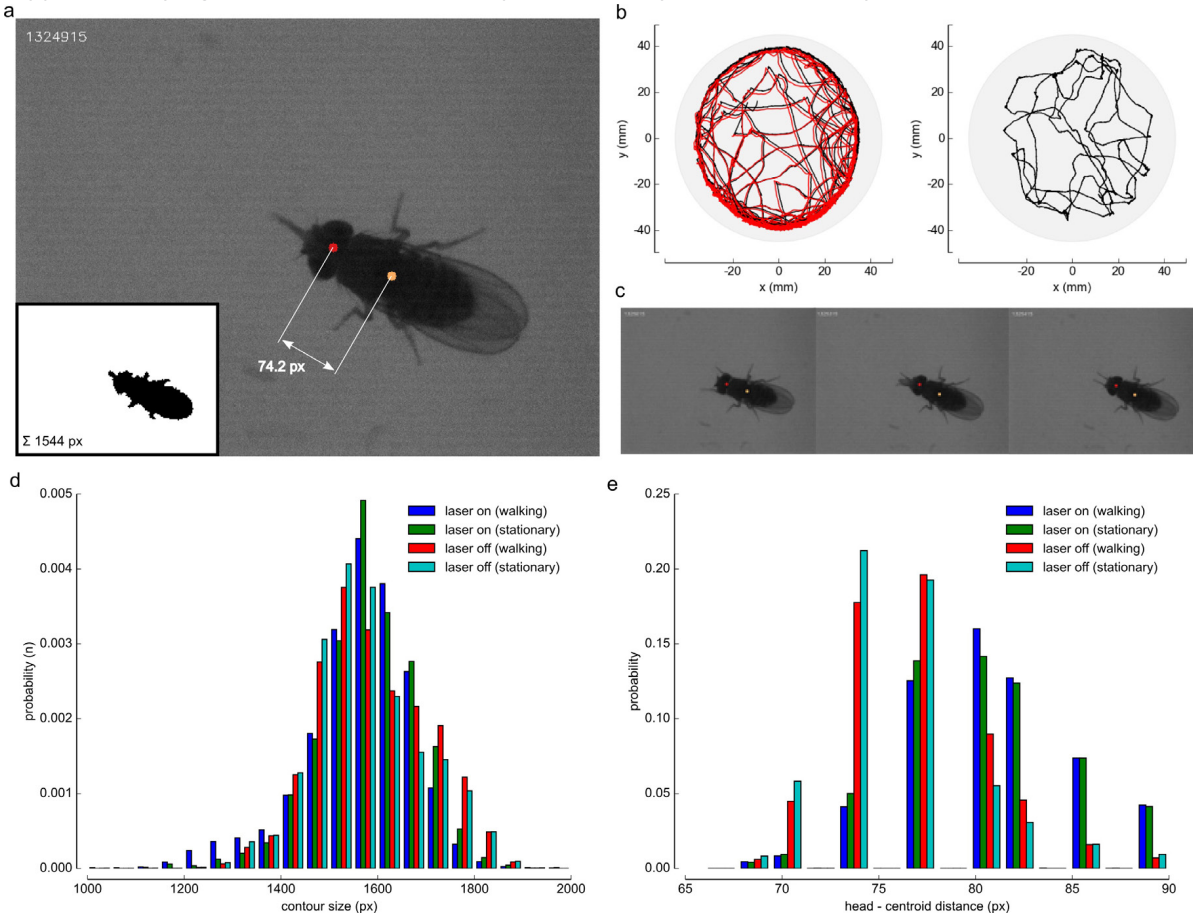

(**a**) Image of the fly from the TTM camera with the true distance from head to centroid (white dimensions) and fly body contour length (inset, black). (**b**) Trajectories (black) and associated periods of laser stimulation (red) for two 5 minute trials of the same fly. The fly was head targeted for the duration of the experiment with the laser powered ('laser on') or not ('laser off') respectively. (**c**) Representative images from both trials showing head detection. (**d**) Distribution of estimated centroid area for the two trials, split into stationary and walking (< 5mm/s) groups. (**e**) Estimated distance between fly body centroid and head for the same experiments.

Supplementary Figure 5. Measurements of spatial and temporal performance.

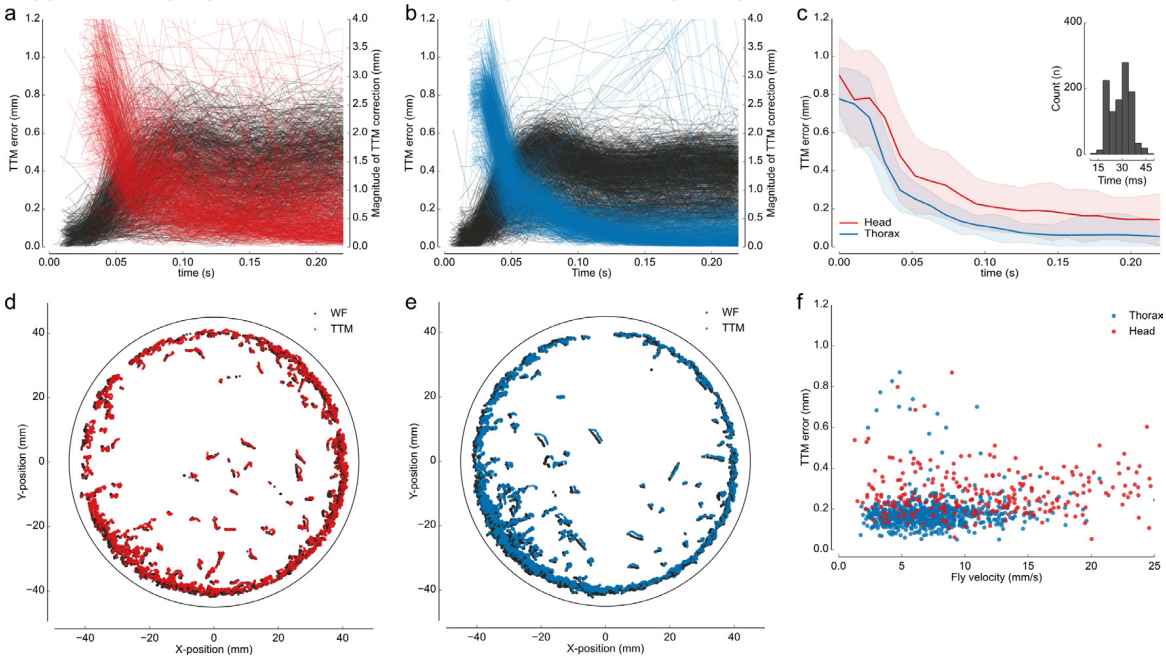

(**a-c**) Measurement of error (distance between optical path center and targeted location) as a function of time since commanding a switch to the targeted fly. Individual trials in head targeting mode (**a**) and thorax targeting mode (**b**) showing distance between optical path center and targeted location (red, blue) and magnitude of TTM-correction command (black). Average error (**c**) (mean ± standard deviation). Inset shows histogram of latency of time to switch to TTM targeting. (**d-e**) Top view of fly position estimate from wide-field (WF) camera compared with actual position required to hit the target using TTM refinement for head (**d**, red) and thorax (**e**, blue). In both panels, only periods where the laser was on are plotted. (**f**) TTM error as a function of fly velocity for head (red) and thorax (blue) targeting.

Supplementary Figure 6. Temperature measurements.

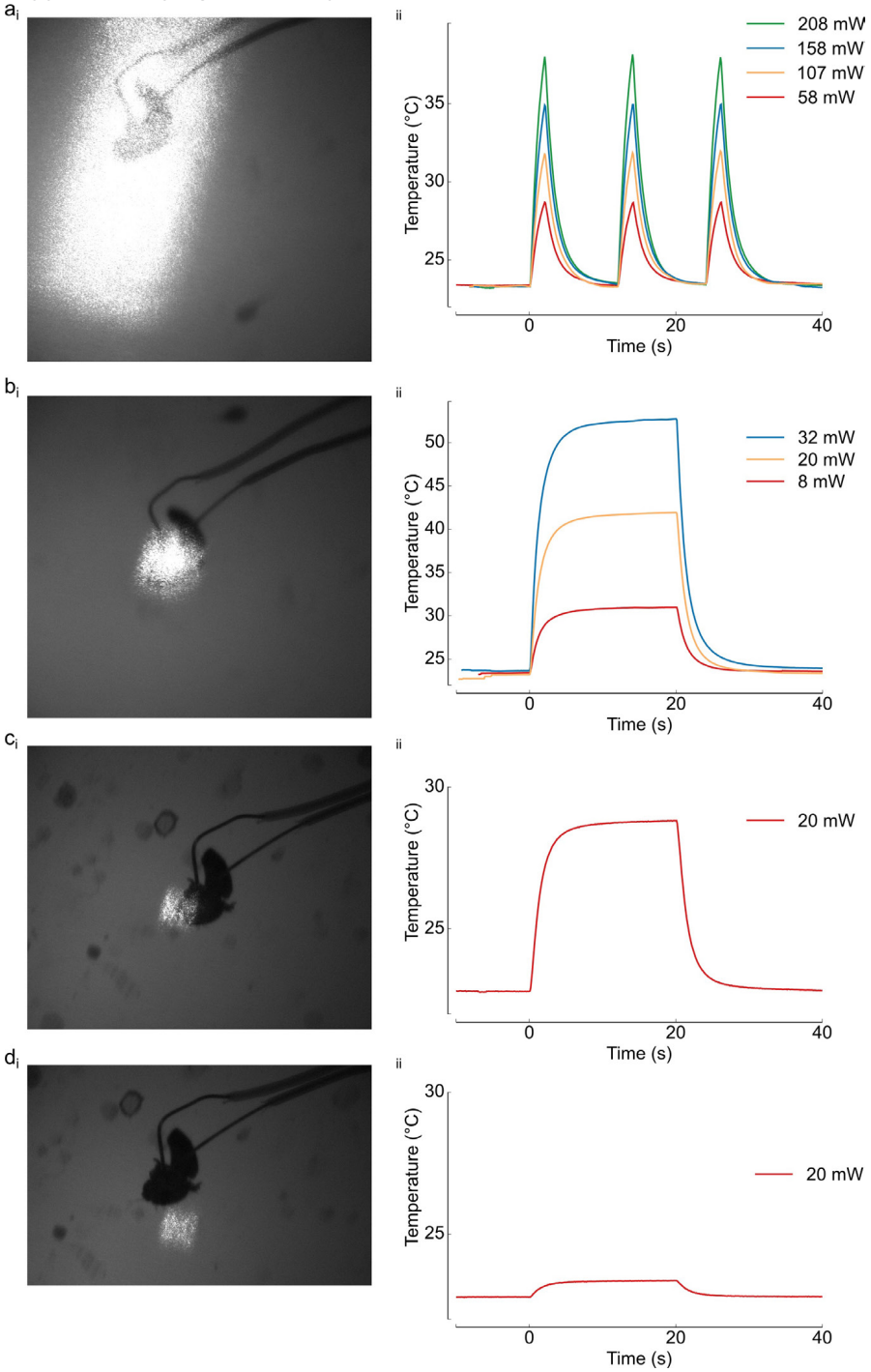

Temperatures measured by a thermocouple in 14-day old male fly with thermocouple inserted in thorax. (**a**) Unfocused laser. (**b**) Focused laser aimed at thorax. (**c**) Focused laser aimed at head. (**d**) Laser focused off-target. Laser powers and wavelengths as specified. All traces from 808nm IR laser.

Supplementary Figure 7. Measurement of laser spot size and optical power.

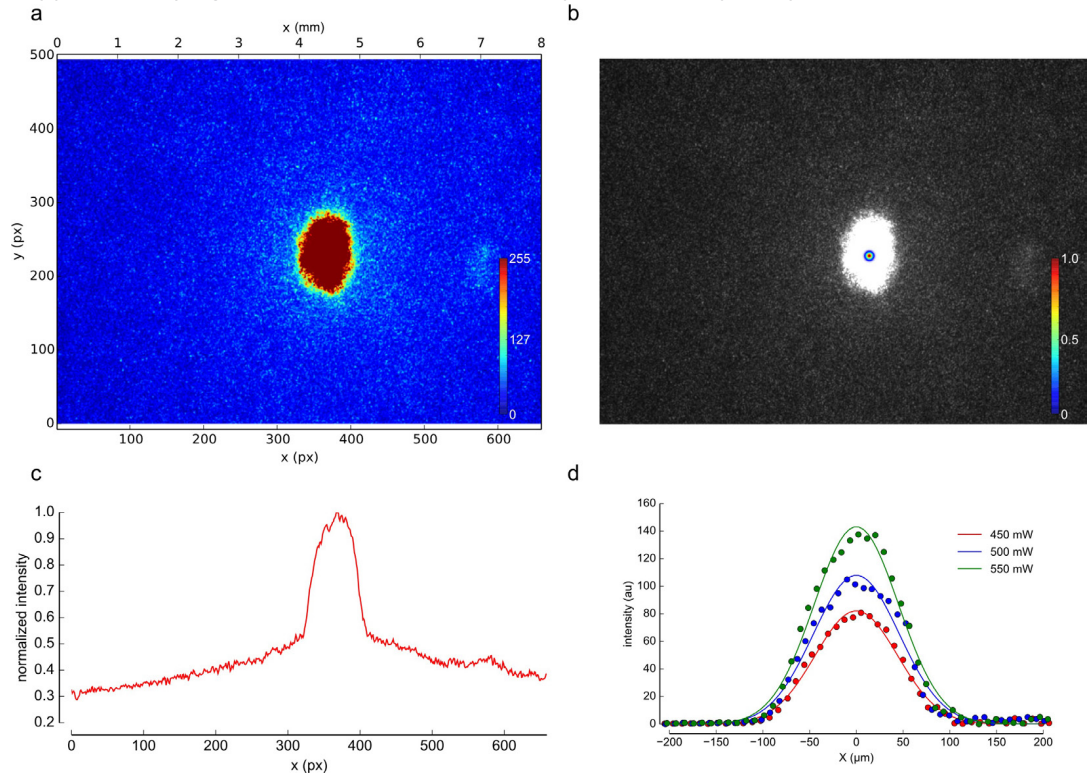

(**a**) Laser spot viewed from the TTM camera displayed in false color. (**b**) Comparison of the laser spot size as seen in the TTM camera (grayscale image) and the real spot size (false color point). (**c-d**) Laser spot intensity profile from the TTM camera view (**c**) and the real profile (**d**) with Gaussian fit FWHM of 105 µm. The laser intensity was measured using a power meter by partially blocking the beam with a razorblade mounted on a motorized stage moving in the focal plane. Blade position was changed incrementally from non-blocking to fully-blocking, to allow measurement of the spatial integral of the beam. The derivative of this measurement is plotted as the spot profile and fit with a Gaussian.

Supplementary Figure 8. Statistical analysis for Figure 2a and upper panel of Figure 2c.

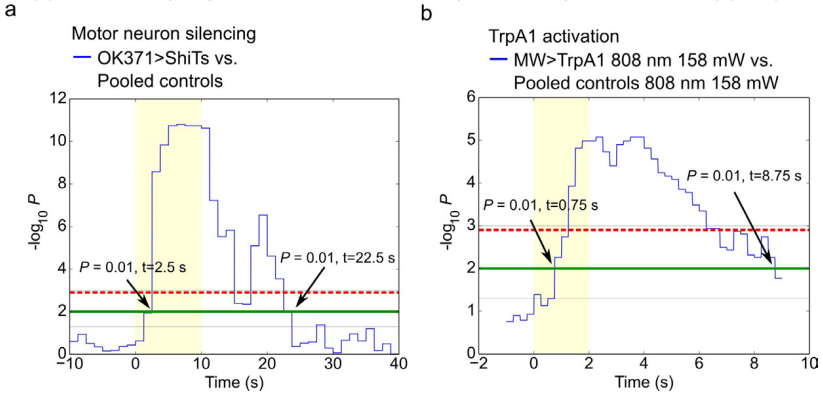

P values are shown on a negative $\log_{10}$ scale. Bonferroni-corrected significance level was computed by dividing significance level (0.05) by number of bins and is indicated by red a dashed line. To measure on- and off- time of the thermogenetic tools, we used a threshold of *P*=0.01 rather than using a more conservative Bonferroni corrected value. For both panels (**a**) Kruskal-Wallis tests applied to data of Fig. 2a. *P* values cross *P*=0.01 threshold (green line) at 2.5s after the onset of laser stimulation, returning at 22.5s (12.5s after laser off). (**b**) Kruskal-Wallis tests applied to data of Fig. 2ci. **b** shows data from repeated trials where controls were pooled into a single analysis. *P* values cross *P*=0.01 threshold (green line) at 0.75s after the onset of laser stimulation, returning above this threshold at 8.8s (6.8s after laser off). For both panels, thin horizontal lines correspond to *P* values of 0.05, 0.001.

Supplementary Figure 9. Statistical analysis for middle and lower panels of Figure 2c.

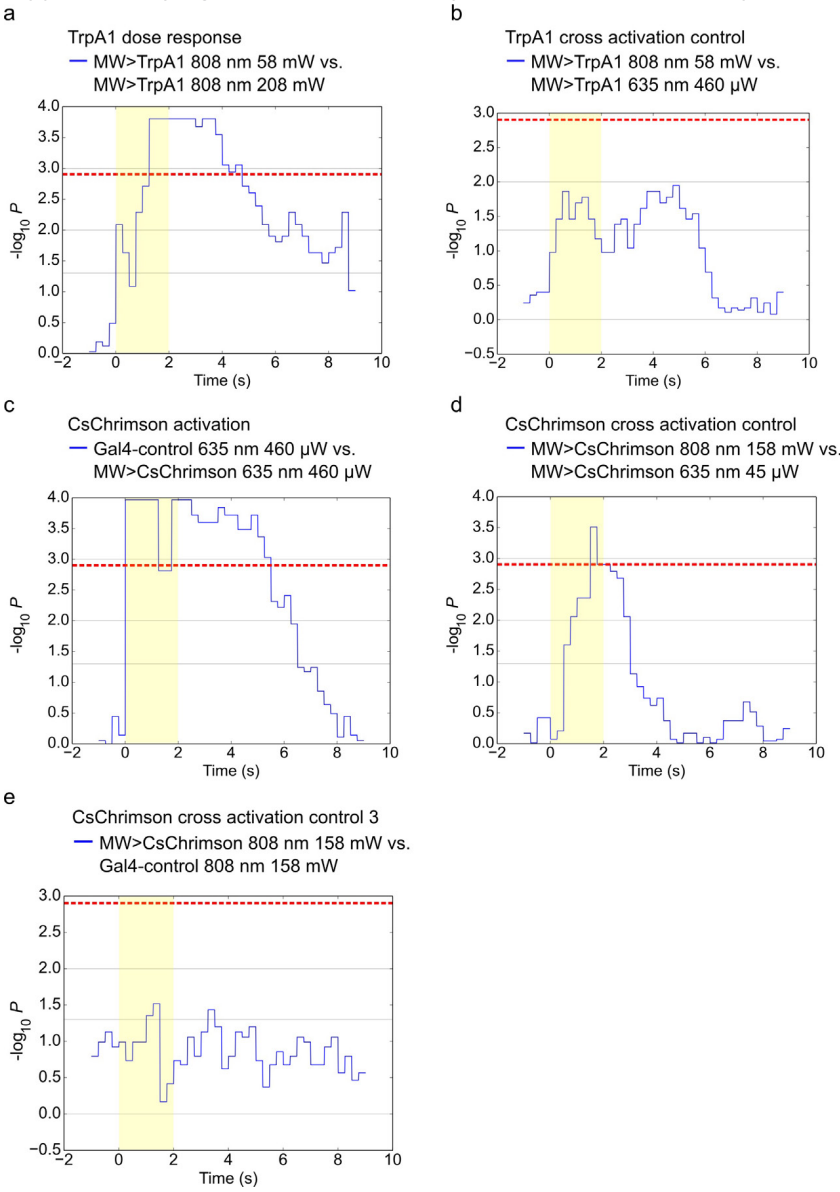

P values are shown on a negative $\log_{10}$ scale. Kruskal-Wallis test was used for all tests. Bonferroni-corrected significance level was computed by dividing significance level (0.05) by number of bins and is indicated by a red dashed line. In all panels, data from repeated trials were pooled into a single analysis. (**a-b**) Kruskal-Wallis tests applied to the data of Fig. 2c (middle panel). **a** compares responses of Moonwalker>*trpA1* flies to low (58mW) and high (208mW) IR laser. **b** compares responses of Moonwalker>*trpA1* to 58 mW IR light and 460 µW red light. (**c-f**) Kruskal-Wallis tests applied to the data of Fig. 2c (lower panel). **c** compares responses of MW>*CsChrimson* flies with MW-Gal4 controls, both to 460 µW red light. **d** compares responses of MW>*CsChrimson* flies to 158 mW IR light and 45 µW red light. **e** compares responses of MW>*CsChrimson* flies and MW-Gal4 control flies exposed to 158 mW IR light. For all panels, thin horizontal lines correspond to *P* values of 1.0, 0.05, 0.01, 0.001.

Supplementary Figure 10. Replotted data of middle and lower panels of Figure 2c.

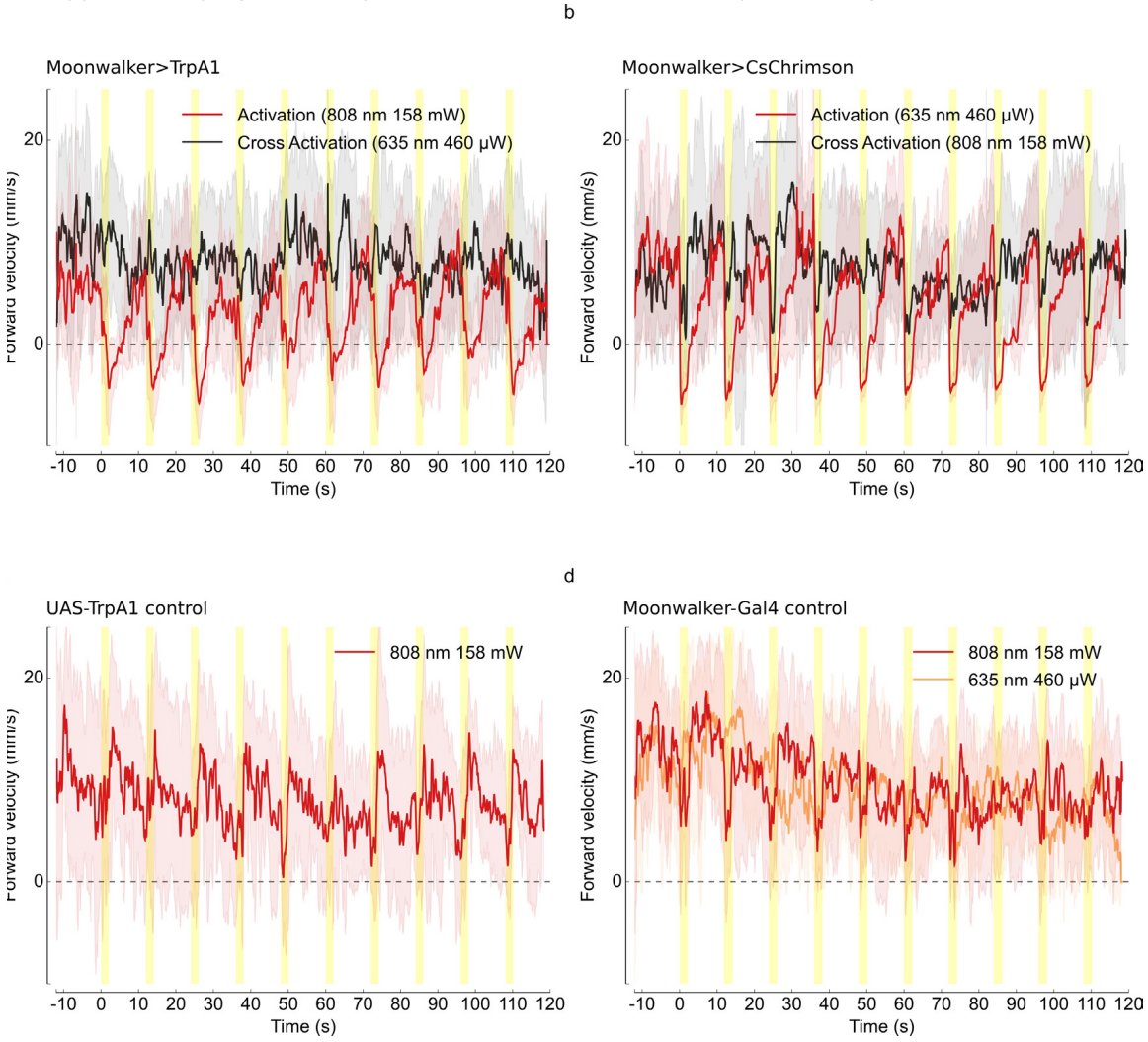

(**a**) Moonwalker>*trpA1* traces shown without pooling across repeated trials. (**b**) Moonwalker>*CsChrimson* traces shown without pooling across repeated trials. (**c**) *UAS*>*trpA1* trace shown without pooling across repeated trials. (**d**) Moonwalker-Gal4 trace shown without pooling across repeated trials.

Supplementary Figure 11. Statistical analysis of lower panel of Figure 2c.

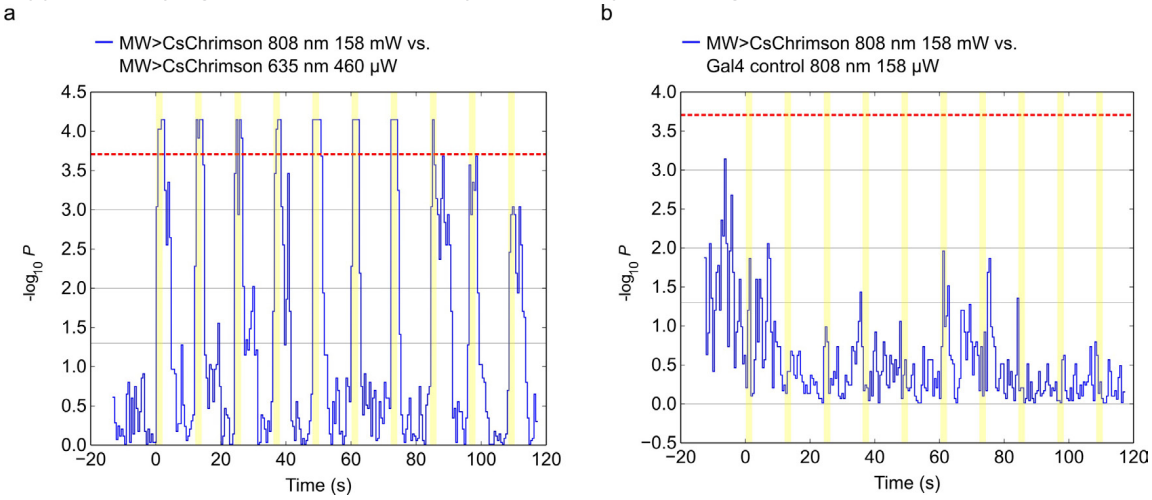

Kruskal-Wallis test was used for all tests. Bonferroni-corrected significance level was computed by dividing significance level (0.05) by number of bins and is indicated by a red dashed line. In both panels, traces are shown without pooling across repeated trials (original data shown in Supplemental Figure 10). (**a**) Comparison between data in Supplementary Figure 10b, Moonwalker>*CsChrimson* flies in response to IR and red light. (**b**) Comparison between Moonwalker>*CsChrimson* and Moonwalker-GAL4 flies in response to IR light. For all panels, thin horizontal lines correspond to *P* values of 1.0, 0.05, 0.01, 0.001.

Supplementary Figure 12. Replotted data and statistical analysis for upper panel of Figure 2c.

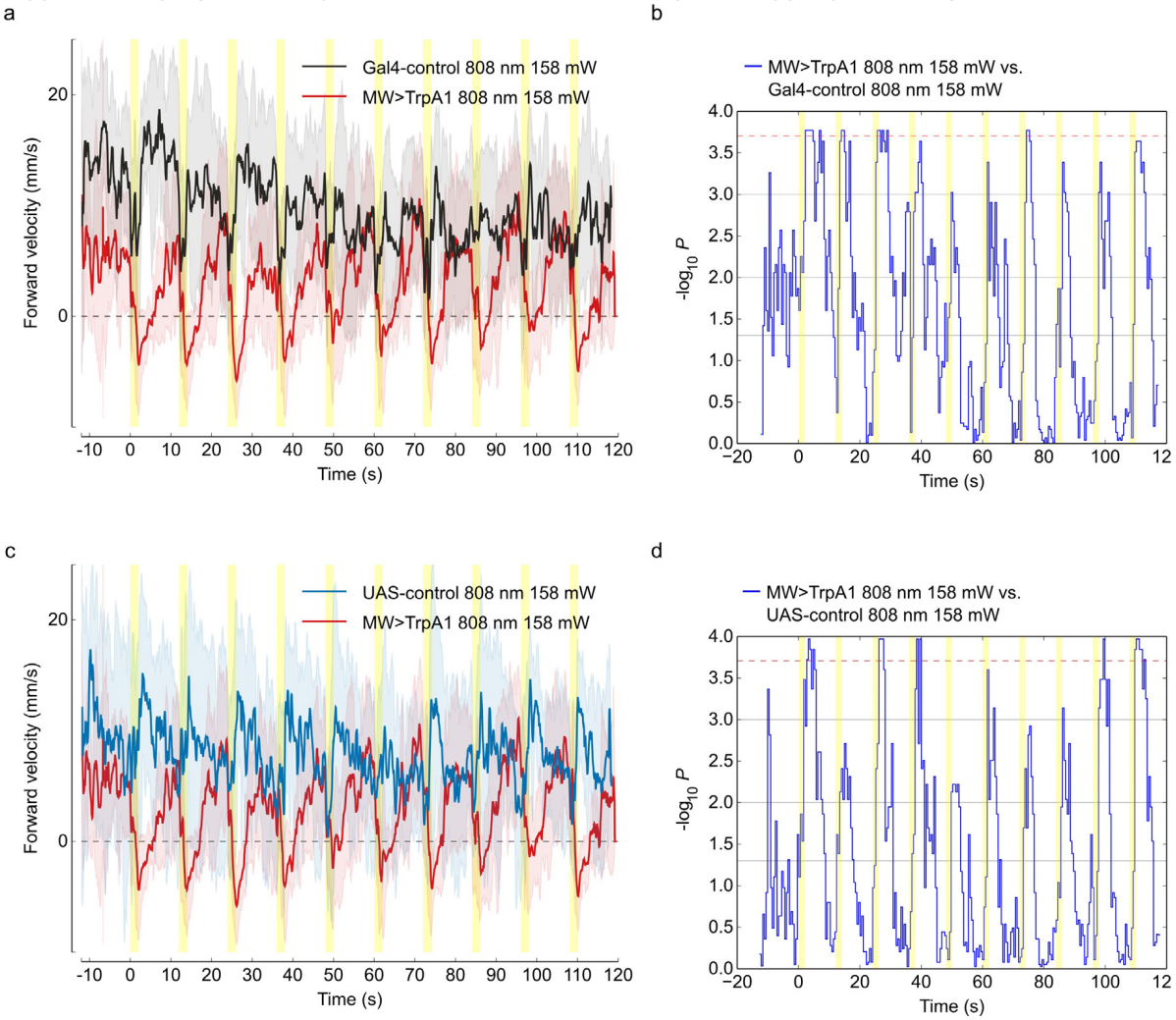

(**a**) Experimental and Gal4 control traces shown without pooling across repeated trials. (**b**) Kruskal-Wallis test for comparison shown in **a**. (**c**) Experimental and UAS control traces shown without pooling across repeated trials. (**d**) Kruskal-Wallis test for comparison shown in **c**. For panels **b** and **d**, *P* values are shown on a negative $\log_{10}$ scale, Bonferroni-corrected significance level was computed by dividing significance level (0.05) by number of bins and is indicated by a red dashed line, and thin horizontal lines correspond to *P* values of 0.05, 0.01, 0.001.

Supplementary Figure 13. Statistical analysis for Figure 3c.

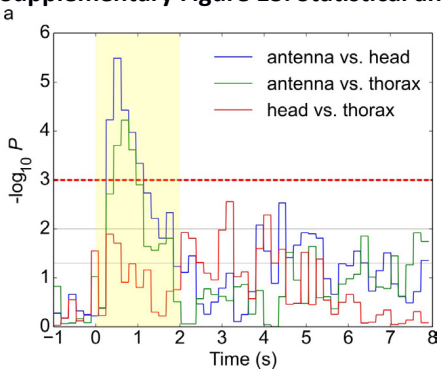

(**a**) *P* values are shown on a negative $\log_{10}$ scale. Kruskal-Wallis test was used. Bonferroni-corrected significance level was computed by dividing significance level (0.05) by number of bins and is indicated by a red dashed line. Thin horizontal lines correspond to *P* values of 0.05, 0.01, 0.001.

Supplementary Figure 14. *VT40347-GAL4* targets pIP10 neurons.

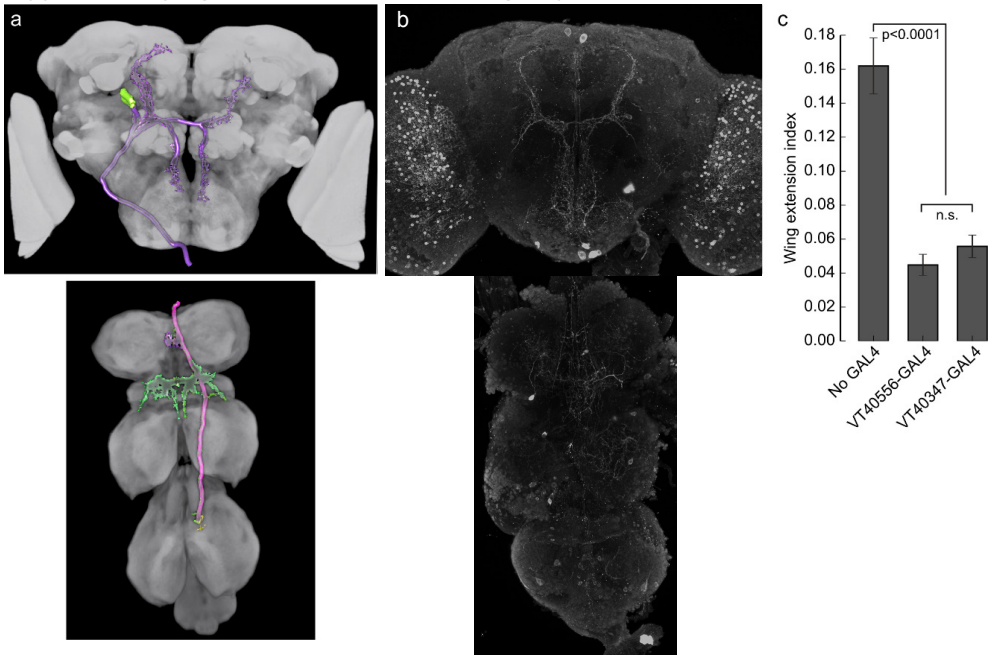

(**a**) 3D View of segmented representation of pIP10. (**b**) Maximum intensity Z-projection of brain (top) and ventral nerve cord (bottom) of a *VT40347-GAL4 UAS-mCD8GFP* male, stained with rabbit polyclonal anti-GFP (1:6,000; Torrey Pines, Fisher Catalog No.: NC9589665), and Alexa488-conjugated goat anti-rabbit IgG (1:1000; Life Technologies catalog no. A-11001). (**c**) Wing extension indices of males carrying the indicated *GAL4* driver and *fru*^{FLP} *UAS>stop>Kir2.1*, in single pair assays with wild-type virgin females. Comparable reductions in courtship song were observed upon silencing pIP10 with either *VT40556-GAL4* (ref. 30) or the more restricted *VT40347-GAL4*. n = 18 for no *GAL4* and *VT40556*; n = 36 for *VT40347*; *p<0.0001, Kruskal-Wallis test.

Supplementary Figure 15. Statistical analysis for Figure 4.

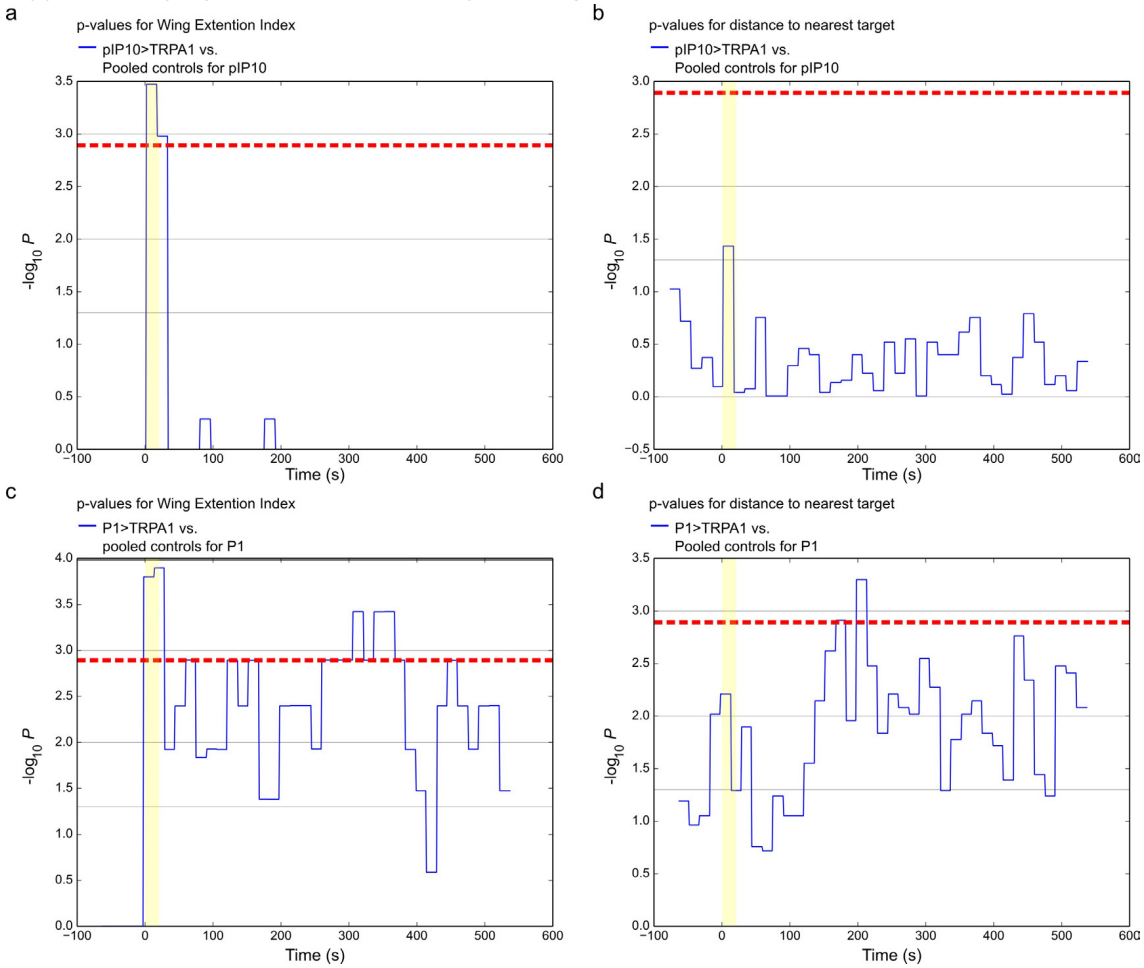

P values are shown on a negative log scale. Kruskal-Wallis test was used for all tests. Bonferroni-corrected significance level was computed by dividing significance level (0.05) by number of bins and is indicated by a red dashed line. For all panels, thin horizontal lines corresponding to *P* values of 1.0, 0.05, 0.01, 0.001.

Supplementary Figure 16. Mirror control electronics.

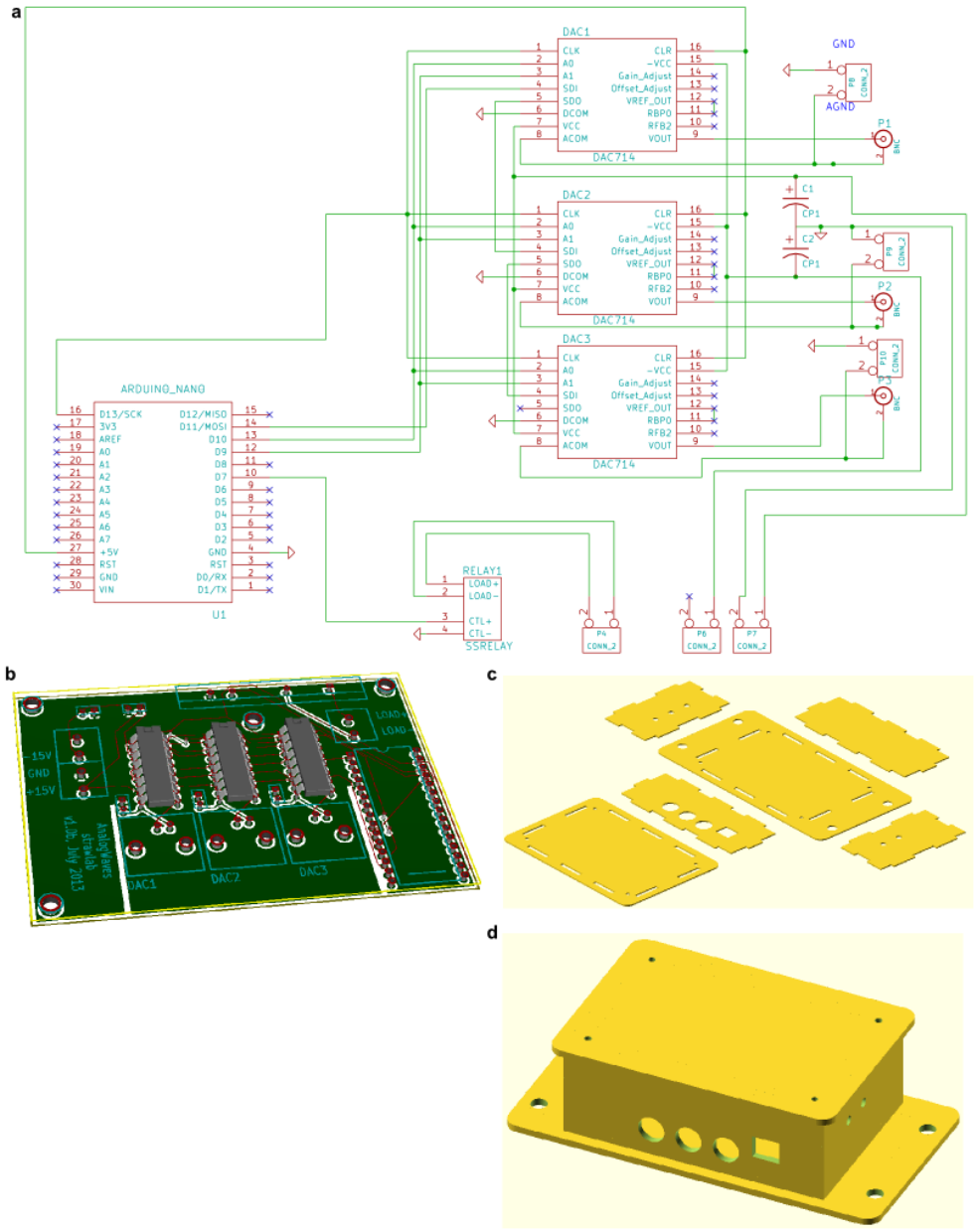

(**a-b**) Schematic (**a**) and rendering (**b**) of printed circuit board (PCB) used to generate analog voltages to control the galvanometer and a solid-state relay to control laser power. (**c-d**) Renderings of the enclosure to hold the PCB, including flat layout as used for laser cutting (**c**) and assembled (**d**).

Supplementary Table 1. Statistical analysis of data in Figure 2b.

start time (seconds)	stop time (seconds)	*P* (angular velocity *Rh1>shi*^{ts} vs. controls)	*P* (angular velocity *Rh1>shi*^{ts} vs. zero)	*P* (linear velocity *Rh1>shi*^{ts} vs. controls)	*P* (*Rh1>shi*^{ts} vs *Rh1>shi*^{ts} pre-stim)	*P* (controls vs controls pre-stim)	Laser on
0	60	0.050	*** 7.0e-08	0.81	-	-	no
60	120	0.21	*** 5.4e-10	0.83	-	-	no
120	154	* 0.041	*** 6.7e-09	0.92	0.62	0.28	yes
154	184	*** 9.1e-06	*** 0.00010	** 0.0036	*** 0.00014	0.11	yes
184	214	*** 3.6e-06	** 0.0076	** 0.0027	*** 0.00033	0.15	yes
214	244	*** 6.1e-06	0.13	* 0.016	*** 1.2e-05	0.21	yes
244	274	*** 0.00024	** 0.0068	0.24	*** 0.00067	0.82	yes
274	304	*** 0.00014	0.29	0.83	*** 7.6e-06	0.30	yes

A two-tailed Mann-Whitney U test was used to calculate "P (angular velocity *Rh1>shi*^{ts} vs. controls)" and "P (linear velocity *Rh1>shi*^{ts} vs. controls)". These tests were used to compare the effect of IR heating on the experimental and control genotypes. A t-test was used to compute "P (angular velocity *Rh1>shi*^{ts} vs. zero)", which tested whether mean angular velocity differed significantly from zero. "P (*Rh1>shi*^{ts} vs *Rh1>shi*^{ts} pre-stim)" was performed with a two-tailed Mann-Whitney U test to compare angular velocity between the pre-stimulus period and the stimulus period for *Rh1>shi*^{ts}flies. Likewise, "P (controls vs controls pre-stim)" is a similar test for control flies. All tests done with *Rh1-GAL4/UAS-shi*^{ts} and pooled *Rh1-GAL4/+* and *UAS-shi*^{ts}*/+* flies (n=18 and 9+12, respectively).

Supplementary Table 2. Statistical analysis of data in Figure 3d.

genotype	*P* (head vs. thorax)
TH>*trpA1*	*** 2.1e-07
dPR1>*trpA1*	*** 9.3e-12
vMS11>*trpA1*	*** 3.4e-07
vPR6>t*rpA1*	*** 9.4e-05
pIP10>*trpA1*	* 0.031

All analyses done using the log-rank test.

Supplementary Table 3. Statistical analysis of proximal and distal wing extension indices.

Test	***P*** (early vs. during)	***P*** (late vs. during)	***P*** (early vs. late)
Total W.E.I.	*** 1.9e-47	*** 2.9e-50	0.60
Proximal W.E.I.	*** 3.0e-41	*** 7.4e-59	*** 2.3e-04
Proximal visit frequency	*** 1.3e-102	*** 5.2e-110	0.29

Wing extension indices are abbreviated W.E.I. Pearson's Chi-squared test (1 degree of freedom) was used to test the null hypotheses that total and proximal W.E.I. and proximal visit frequency do not differ among different stages of the P1-activation experiment shown in figure 4. "During" refers to the time when the laser stimulus is on (t=0-20s), "early" refers to the first 220 seconds post-stimulus (t=20-240s), and "late" refers to the the 220 seconds immediately after "early" (t=240-460s). "Proximal" refers to a distance less than 50 pixels from a target. "Proximal visits" are defined as a 2 second period in which the fly entered a proximal area.

Supplementary Table 4. Parts list.

	Quantity	Part numbers	alternative
Arena			
Arena	1	custom, see accompanying specifications	
Arena mount	1	custom, see accompanying specifications	
Arena cover glass	1	custom, see accompanying specifications	
backlight LED	2	Superbright LEDS: NFLS-UV30x3-DI	or comparable
backlight LED, center	6	Mouser Electronics 604-WP710A10MBCK	or comparable
Wide field tracking system			
Wide field camera	1	Basler acA640-120gm	
Wide field camera lens	1	Computar 2.9-8.2mm 1:1.0 ⅓”	
camera post mount	1	Giottos MH1004	
Hot mirrors	2	Edmund Optics 43-955	
Galvanometer and TTM system			
Galvanometer	1	Thorlabs GVS012/M	
Galvanometer power supply	1	Thorlabs GPS011	
Galvanometer control circuit board	1	custom, see accompanying specifications	
TTM camera	1	Basler piA 1000-60gm	Basler acA640-120gm
TTM camera lens	1	VS Technologies VS-TC1-220CO	Nikon 200mm ED AF Nikkor
TTM lens mount	1	Thorlabs LH1/M	Thorlabs BA2T2/M
Bandpass filter, 435nm	1	Edmund Optics 86-360	
Mounting cell 50mm	1	Edmund Optics 55-007	
Short-pass filter 750nm	1	Thorlabs FES0750	
Galvanometer mounting common			
Breadboard – base	1	Thorlabs MB3045/M	or larger
Breadboard – right angle bracket	1	Thorlabs AP90RL/M	
Breadboard – Galvo base	1	Thorlabs MB1515/M	
Vibration isolators, set of 4	1	Thorlabs AV1/M	
Galvanometer mounting option A			
Pitch and Yaw mounting platform	1	Thorlabs PY003/M	
Galvanometer mounting option B			
Cage system cube	1	Thorlabs C6W	
Cage adapter for Galvanometer	1	Thorlabs GCM012/M	
Cage cube platform	1	Thorlabs B3C/M	
Cage assembly rod – ½"	4	Thorlabs ER05-P4	
Cage assembly rod – 2"	6	Thorlabs ER2-P4	
Cage assembly rod – 8"	8	Thorlabs ER8-P4	
Laser system			
Option A: two coaxial lasers			
Infrared (808nm) laser	1	Picotronic DB808-350-3(22x65)	
Infrared laser mount	1	Picotronic BALLHEAD-MOUNT-22(25x80)	
Red (635nm) laser	1	Picotronic DA635-1-3(16x58)	

Red laser mount	1	Picotronic BALLHEAD-MOUNT-16(25x75)
Short-pass 700nm dichroic mirror	1	Edmund Optics NT43-957
Short-pass 600nm dichroic mirror	1	Edmund Optics 69-216
IR filter	1	Thorlabs FGB37S
Filter mount	3	Thorlabs SFH2
Beam-focusing lens, f=250mm	1	Thorlabs LB1056
Beam-focusing lens mount	1	Thorlabs LMR1/M
Option B: small spotsize		
Infrared (808nm) laser	1	Roithner RLTMDL-808-1W-5
Short-pass filter mount	1	Thorlabs CP02T/M
Short-pass 700nm dichroic mirror	1	Edmund Optics 43955
Collimation Package	1	Thorlabs F810SMA-780
Dichroic mirror mount	1	Thorlabs B5C
Infrared laser mount	2	Thorlabs CP02/M, AD15F
IR filter	1	Thorlabs FGS900S
Filter mount	1	Thorlabs SFH2
Beam-focusing lens, f=100mm	1	Thorlabs LA1509
Beam-focusing lens, f=200mm	1	Thorlabs LA1708
Beam-focusing lens mount	3	Thorlabs CP08

MOUNTING & STRUCTURAL (for all options)

Optical posts – 30cm	3	Thorlabs TR300/M
Optical posts – 25cm	1	Thorlabs TR240/M
Optical posts – 15cm	8	Thorlabs TR150/M
Optical posts – 7.5cm	4	Thorlabs TR75/M
Optical posts – 5cm	2	Thorlabs TR50/M
Post holders – 2cm	7	Thorlabs PH20/M
Post holders – 7.5cm	3	Thorlabs PH75/M
Post holders – 15cm	1	Thorlabs PH150/M
Swivel base adapters	6	Thorlabs UPHA
M6 spring-loaded thumbscrews	5	Thorlabs TS6H/M
Swivel connectors	2	Thorlabs SWC/M
Right angle connectors	4	Thorlabs RA90/M
End connectors	3	Thorlabs RA180/M
Table clamps	2	Thorlabs CL3
Mounting base	14	Thorlabs BA1S(/M)

RECOMMENDED MINIMUM COMPUTER SPECIFICATIONS

Processor		Intel Core i7-2600 CPU @ 3.40GHz x 8
Memory		8GB
Solid-state hard drive		Intel SSD 320 series, 120GB
Video card		NVIDIA GeForce GTX 670/PCIe/SSE2
ethernet ports	2	GigE
operating system		Ubuntu 12.04 LTS, 64-bit

Supplementary Table 5. Software used.

Name	*Version*	*URL*	*Usage*
Robot Operating System (ROS)	Electric	http://ros.org	Inter-process communication
FView, FlyTrax, Trackem	2013-11-01 git master	http://code.astraw.com/projects/motmot/fview.html	Realtime image acquisition and analysis framework
OpenCV	2.4	http://opencv.org/	Realtime image analysis
Kicad	0.0.20110616-1	http://www.kicad-pcb.org/	Printed Circuit Board (PCB) design
py2scad	23:54eadbba357d	http://hg.iorodeo.com/py2scad	PCB enclosure
Aravis	0.1.13	https://wiki.gnome.org/Aravis	Camera drivers
libcamiface	0.8.4	http://code.astraw.com/projects/motmot/libcamiface.html	Camera interaction
Ubuntu GNU/Linux	12.04 LTS	http://ubuntu.com/	Operating system
Python	2.7.3	http://python.org/	Primary programming language
Scipy	0.9.0	http://scipy.org/	Kruskal-Wallis and Mann Whitney U statistics
Lifelines	0.2.3.0.3	http://lifelines.readthedocs.org/	Log-rank statistics
Numpy	1.6.1	http://numpy.org/	Numerical computation
Pandas	0.12.0	http://pandas.pydata.org/	Data analysis package
adskalman	0.3.3	http://github.com/astraw/adskalman	Kalman filtering
OpenSCAD	2011.09	http://openscad.org/	CAD modeller
SolidWorks	2010	http://www.solidworks.com/	CAD modeller

5 Asymmetric processing of visual motion for simultaneous object and background responses

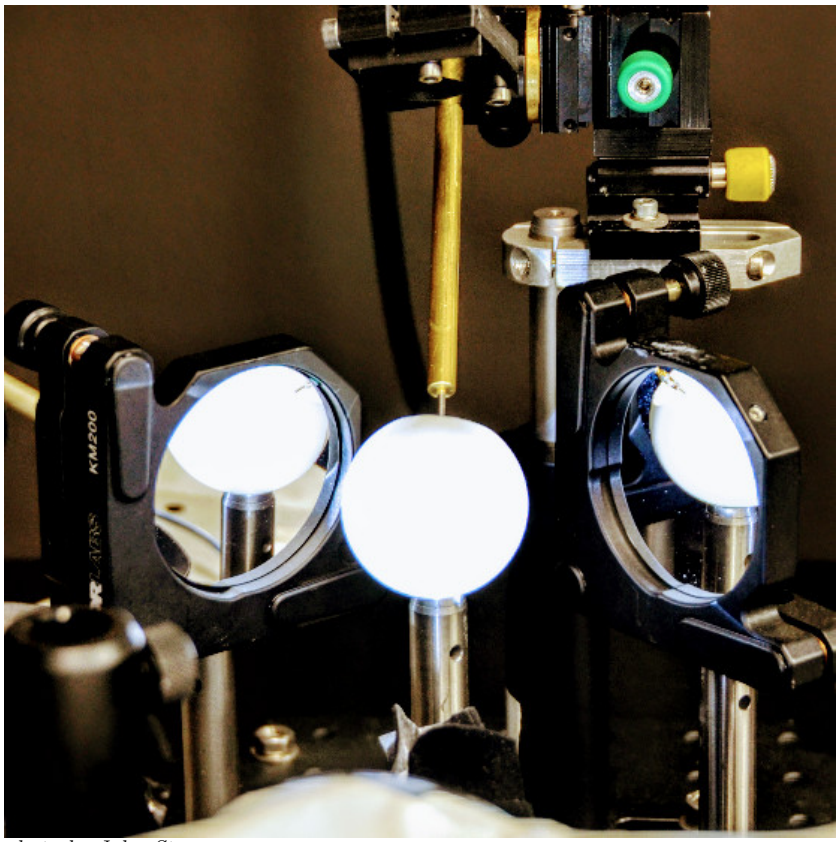

photo by John Stowers

type	*published* Current Biology, Volume 24, Issue 24, 2913 - 2919 **doi:10.1016/j.cub.2014.10.042**
authors	Lisa M. Fenk[1] (LMF), Andreas Poehlmann[1] (AP), Andrew D. Straw (ADS) [1] *Co-first author*
contributions	LMF, AP, and ADS conceived the experiments and performed the modeling. LMF performed the experiments. LMF, AP, and ADS analyzed the experimental data. LMF, AP, and ADS wrote the manuscript.

Report

Asymmetric Processing of Visual Motion for Simultaneous Object and Background Responses

Lisa M. Fenk,[1,2] Andreas Poehlmann,[1,2] and Andrew D. Straw[1,*]
[1]Research Institute of Molecular Pathology, Vienna Biocenter, Dr. Bohr-Gasse 7, 1030 Vienna, Austria

Summary

Visual object fixation and figure-ground discrimination in *Drosophila* are robust behaviors requiring sophisticated computation by the visual system, yet the neural substrates remain unknown. Recent experiments in walking flies revealed object fixation behavior mediated by circuitry independent from the motion-sensitive T4-T5 cells required for wide-field motion responses [1]. In tethered flight experiments under closed-loop conditions, we found similar results for one feedback gain, whereas intact T4-T5 cells were necessary for robust object fixation at a higher feedback gain and in figure-ground discrimination tasks. We implemented dynamical models (available at http://strawlab.org/asymmetric-motion/) based on neurons downstream of T4-T5 cells—one a simple phenomenological model and another, physiologically more realistic model—and found that both predict key features of stripe fixation and figure-ground discrimination and are consistent with a classical formulation [2]. Fundamental to both models is motion asymmetry in the responses of model neurons, whereby front-to-back motion elicits stronger responses than back-to-front motion. When a bilateral pair of such model neurons, based on well-understood horizontal system cells [3, 4], downstream of T4-T5 [5], is coupled to turning behavior, asymmetry leads to object fixation and figure-ground discrimination in the presence of noise. Furthermore, the models also predict fixation in front of a moving background, a behavior previously suggested to require an additional pathway [1]. Thus, the models predict several aspects of object responses on the basis of neurons that are also thought to serve a key role in background stabilization [6–12].

Results

Behavioral Experiments in Flies with Blocked T4-T5 Cells

To measure visuomotor responses of *Drosophila*, we used low-latency wing tracking [13] and display systems [14] to show visual stimuli to rigidly tethered flying flies (Figure S1A available online). One well-studied behavior elicited by rotating wide-field stimuli is the optomotor response (e.g., [15]). Flies steer in the direction of the stimulus, presumably to stabilize flight direction against external perturbations. Another prominent visual behavior is object fixation [16]. To study fixation behavior, we performed closed-loop experiments in which the fly's intended turn—measured as the difference in wing beat amplitude between the right and left wing (ΔWBA)—was fed back to control yaw angular velocity, ω, of visual objects via a coupling coefficient specifying the feedback gain, g, according to the equation $\omega = -g \cdot \Delta WBA$ (Figure S1B). We refer to a black stripe (on a white background) as "stripe" and to a random-pixel figure (on a random-pixel background) as "figure," and use we "object" as the general term.

Recently, it was shown that walking flies with blocked T4 and T5 cells exhibit no optomotor response and decreased, but robust, object fixation [1]. We hypothesized, based on studies suggesting slow responses to flicker [17] at modest contrast [18], that T4-T5-independent position circuitry [1] might be unable to mediate object fixation in conditions of high feedback gain.

We used GAL4-UAS to express tetanus toxin light chain (TNT) [19] in T4-T5 cells to block chemical synaptic transmission ("T4-T5-blocked flies") and tested fixation quality during closed-loop tethered flight at a contrast of 0.32. Control flies expressed an inactive form of TNT. The behavioral data are summarized in probability distributions of object position (horizontal histogram) and object velocity (vertical histogram) together with the phase-space trajectories (i.e., object velocity as a function of object position) underlying these distributions (e.g., Figure 1A, top).

At low feedback gain ($g = 5\ s^{-1}$; Figure 1A), similar to results found in walking flies [1], fixation of a black stripe in T4-T5-blocked flies is significantly reduced, but not abolished. This is evidenced by flatter distributions of stripe position and velocity (Figure 1A, middle) as compared to control flies (Figure 1A, top). Control flies hold the stripe significantly longer in the frontal half of the visual field than do T4-T5-blocked flies (Figure 1A, bottom). In a separate set of control experiments in open loop (Figure S1C), we confirmed that T4-T5-blocked flies indeed exhibit a significant response to the position of the stripe, as expected [1].

When we tested flies in a high-gain regime ($g = 25\ s^{-1}$; Figure 1B), stripe fixation in T4-T5-blocked flies was further reduced as illustrated by an even flatter distribution of stripe position and velocity, while fixation was excellent in control flies (Figure 1B, middle versus top). Again, the stripe is kept less in the frontal half of the visual field than by control flies but longer than could be expected by chance (Figure 1B, bottom). The degraded stripe fixation shows that intact T4-T5 cells are important under these high-gain conditions.

In a further set of experiments (Figure 2), we quantified fixation of a random checkerboard figure against a random checkerboard background, i.e., figure-ground discrimination—an experiment in which luminance cues for detecting the figure are reduced. Indeed, in T4-T5-blocked flies, we found no evidence of fixation at high gain ($g = 25\ s^{-1}$; Figure 2B, blue); blocked flies did not keep the figure significantly longer in the frontal half of the visual field than expected by chance (Figure 2B, bottom, blue). Nevertheless, control flies reliably fixated, showing the necessity of intact T4-T5 cells for fixation under these conditions (Figure 2B, top versus middle, blue). Interestingly, T4-T5-blocked flies also showed no evidence of fixation at low gain (Figure 2A, blue). Again, T4-T5-blocked flies did not keep the figure significantly longer in front than expected by chance, and the robust figure-ground discrimination of control flies was significantly different from that of

[2]Co-first author
*Correspondence: andrew.straw@imp.ac.at

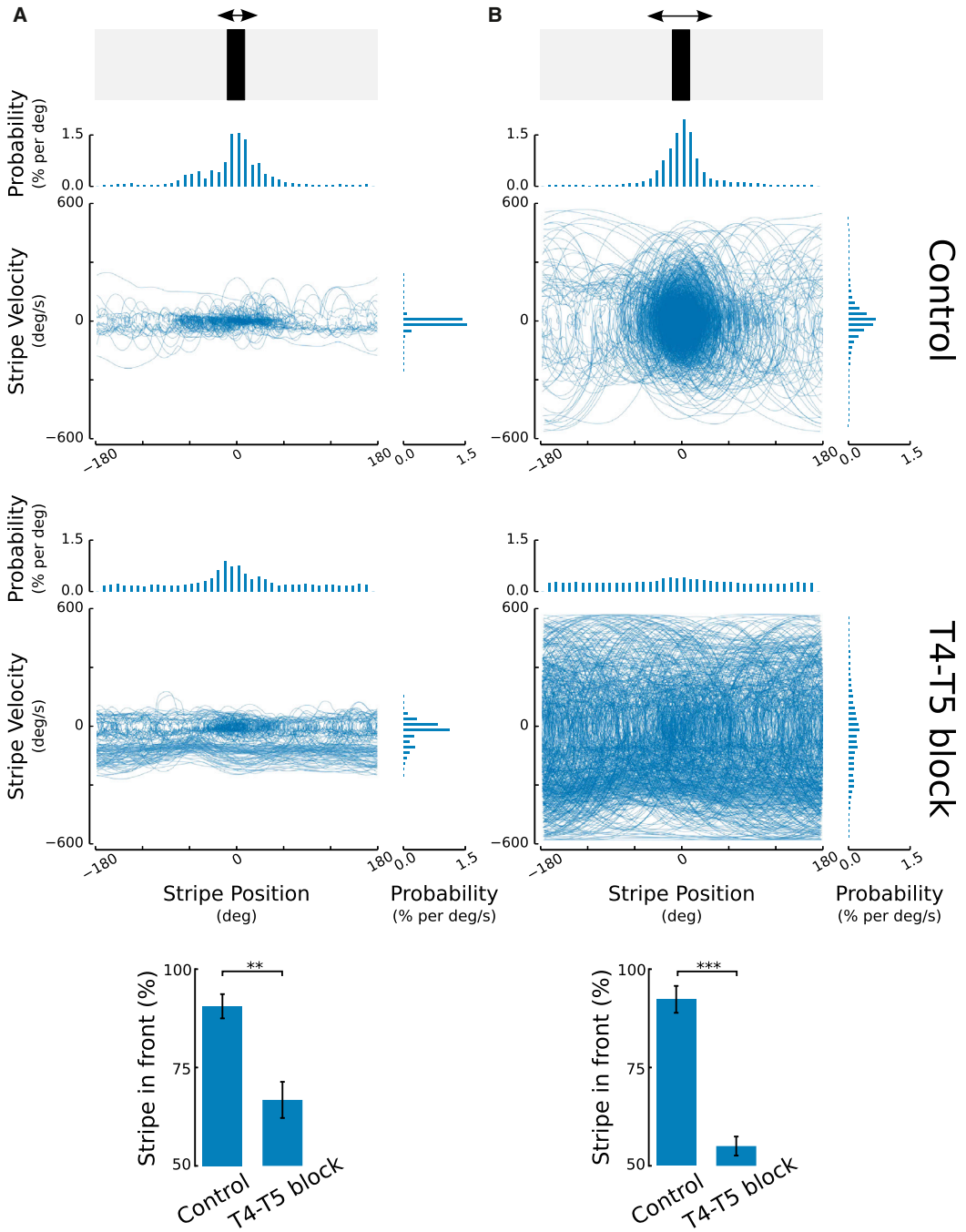

Figure 1. At High Feedback Gain, Intact T4-T5 Cells Are Necessary for Robust Stripe Fixation

Fixation behavior measured during closed-loop flight for a black stripe (width = 22.5°) on a white background. The pictograms show the stimulus; black arrows indicate gain settings. From time-series data of stripe position and velocity, phase-space trajectories are plotted in which stripe velocity is plotted against stripe position. Histograms show the probability in a given range of values. Bar charts show the average percentage of time the stripe is in the frontal field of view (error bars indicate the SEM).

(A) Behavioral results for control flies (top) and T4-T5-blocked flies (middle) for low gain, $g = 5\ s^{-1}$. Control flies keep the stripe significantly longer in the frontal half of the visual field than do T4-T5-blocked flies (p = 0.002, Mann-Whitney U test, two tailed, N = 10; bottom). Both genotypes differ significantly from chance (control flies, p = 0.001; T4-T5-blocked flies, p = 0.01; binomial test, one tailed, N = 10).

(B) As in (A), but for high gain, $g = 25\ s^{-1}$. Stripe fixation in T4-T5-blocked flies is further decreased but is still significantly different from chance (p = 0.03, binomial test, one tailed, N = 11; bottom). Again, control flies keep the stripe significantly longer in the frontal half of the visual field than do T4-T5-blocked flies ($p = 10^{-4}$, Mann-Whitney U test, two tailed, N = 11).

See also Figure S1 for a diagram of the apparatus and an example trajectory.

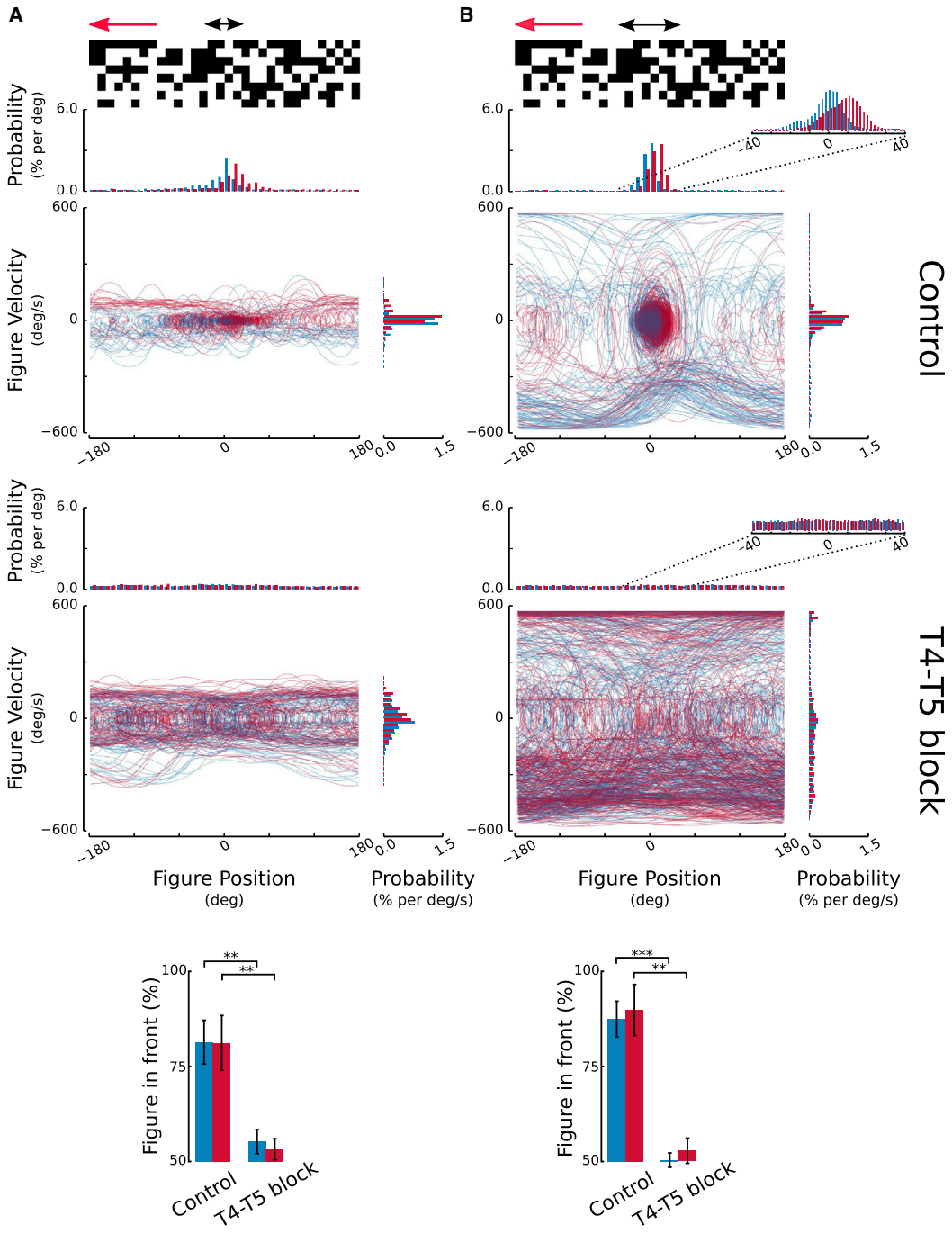

Figure 2. Blocking T4-T5 Cells Abolishes Fixation in Figure-Ground Discrimination Task

Fixation behavior measured during closed-loop flight in a figure-ground discrimination task (figure width = 22.5°) for a stationary background (blue) and a background moving at a velocity of $-2^{\circ}\ s^{-1}$ (red). The pictograms show the stimulus; black arrows indicate gain settings, and red arrows indicate background movement. Bar charts show the average percentage of time the figure is in the frontal field of view (error bars indicate the SEM).

(A) Behavioral results for control flies (top) and T4-T5-blocked flies (middle) for low gain, $g = 5\ s^{-1}$. Control flies show robust fixation behavior for both the stationary and the moving background. The position of figure fixation is shifted as a result of background movement. Both in the presence and absence of background movement, the performance of control flies was significantly better than for T4-T5-blocked flies ($p < 0.002$ for a stationary and $p < 0.004$ for a moving background, Mann-Whitney U test, two tailed, N = 11; bottom) that showed no evidence of fixation and did not keep the figure significantly longer in the frontal field of view than expected by chance ($p = 0.1$ for both stationary and moving backgrounds, binomial test, one tailed, N = 11).

(B) Behavioral results for control flies (top) and T4-T5-blocked flies (middle) for high gain, $g = 25\ s^{-1}$. T4-T5-blocked flies again showed significantly less fixation than control flies ($p < 0.0002$ for a stationary and $p < 0.003$ for a moving background, Mann-Whitney U test, two tailed, N = 10; bottom), and their responses were not significantly different from chance ($p = 0.2$ for a stationary and $p = 0.4$ for a moving background, binomial test, one tailed, N = 10).

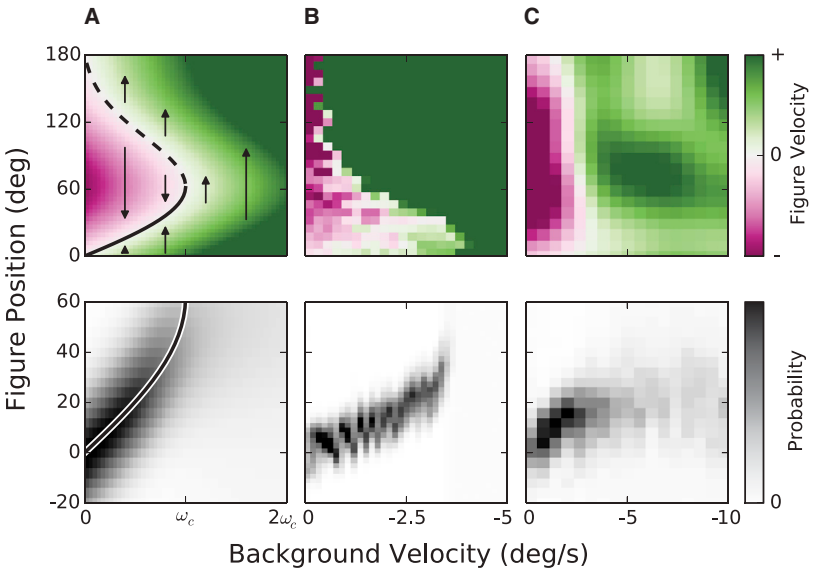

Figure 3. Models Based on Asymmetric Wide-Field Motion Processing Predict Fixation Behavior in Front of a Moving Background

Top: color-coded dynamics of figure fixation dependent on background velocity (regions with negative figure velocity are colored in purple, and regions of positive velocities are shown in green). Bottom: magnified view of probability of figure position as a function of background velocity.

(A) Fixation behavior predicted by the analytical model for *Drosophila*, showing model responses to the closed-loop coupled figure (black arrows indicate dynamics). Positions at which responses are zero (fixed points) are indicated by a line, with the solid line denoting stable equilibrium—predicting figure fixation—and the dashed line denoting an unstable equilibrium (top). The probability of figure position as a function of background velocity together with the black line indicating stable equilibrium is shown (bottom). Velocity is given relative to critical velocity, ω_c. See also Figure S2 and Code S1 (also available at http://strawlab.org/asymmetric-motion/).

(B) Fixation behavior predicted by the physiologically inspired model for *Calliphora*. Turning responses were calculated by computation of mean closed-loop figure velocity in the first 2 s after onset of background movement (top). The probability of figure position as a function of background velocity is shown (bottom). Due to different spatiotemporal properties of the *Calliphora* model, we would not expect the prediction to quantitatively match models or measurements of *Drosophila* behavior. See also Figure S3 and Code S1.

(C) Experimental measurement of fixation behavior showing smoothed figure dynamics at different positions as a function of background velocities (top). The probability of figure position as a function of background velocity is shown (bottom). Mean responses from a 600 s experiment of N = 16 flies (control genotype).

T4-T5-blocked flies (Figure 2A, bottom, blue). We also rotated the background slowly in open loop and found, similar to [1], that control flies still fixate a figure with open-loop background motion, albeit at a location offset from directly ahead, shifted opposite to the direction of background motion (Figures 2A and 2B, red). T4-T5-blocked flies were not able to fixate the figure with a moving background at high- or low-gain settings (Figures 2A and 2B, middle, red), just as they failed to fixate a figure with a stationary background.

Our behavioral experiments thus show that at high gain, object fixation in T4-T5-blocked flies is severely decreased, indicating that intact T4-T5 cells are required for robust fixation under these conditions. In addition, we found a requirement of the T4-T5 cells for fixation in our figure-ground discrimination paradigm, an effect that was true at high and low gains.

Object Responses by Asymmetric Motion Processing

Given the requirement of intact T4-T5 cells under the above conditions, we wondered whether neurons downstream of T4-T5 might mediate object fixation in the absence of parallel pathways. A critical insight came from the discovery that the T4-T5-dependent component of turning responses is asymmetric with respect to object velocity—front-to-back motion elicits stronger responses than back-to-front motion [1]. Based on this recent finding and a similar asymmetry observed in horizontal system (HS) cells [3, 4], we hypothesized that wide-field motion-integrating neurons, such as HS cells, may be able to mediate object responses without a separate position circuit. Although HS cells show residual responses in T4-T5-blocked flies [5], electrophysiological and behavioral measurements suggest that HS cells are not part of a T4-T5-independent position circuit [1]. From a theoretical perspective, it is known that asymmetric torque responses to motion are sufficient to mediate turns toward objects independent of a system that explicitly encodes position [2, 20].

An intuitive explanation for how asymmetric motion responses can give rise to object fixation is as follows. If an object on the right is moving rightward (front to back), a strong rightward turn is elicited. If this object moves leftward (back to front), the motion response will cause a leftward turn, but, due to asymmetry, this is smaller in magnitude than the rightward turn. Thus, over time, alternating movement (e.g., arising from noise) leads to net turning toward the object. If a mirror-symmetric system exists on the other side, as expected from bilateral symmetry, an equilibrium object position emerges at the midline.

The theoretical question that we addressed is whether asymmetric motion responses, observed in most lobula plate tangential cell recordings [3, 21–23], would be predicted to cause object responses similar to those measured behaviorally. To minimize the number of free parameters, we based our models as closely as possible on the response properties of the extensively investigated HS cells [3, 4], long thought to be involved in the generation of yaw torque in response to wide-field motion [6–12]. The other basic assumptions in our models are that torque produced by the fly is proportional to the difference between the output of left and right HS cells with an additional noise source.

The first model is based on a phenomenological description of basic response properties of *Drosophila* HS cells [4] that allows closed-form analysis. The second model is derived very closely from a more physiologically realistic model of *Calliphora* HS cells that predicts membrane potential for arbitrary visual inputs [24]. As partly anticipated for a stationary background [17, 25–27], both our models predict object fixation with only a wide-field motion-integrating channel and no separate small-field or position channel (Figures 3A and 3B).

In the simplified analytical model, we describe the response of each HS cell, $W(f)$, by the spatial integral over the product of

its receptive field, $R(\varphi)$, defining the local motion sensitivity, and its motion response, $M(f)$, as

$$W(f) = \int_{-\pi}^{\pi} R(\varphi) M(f) \mathrm{d}(\varphi),$$

where φ is the angular position and f is the temporal frequency of the stimulus. The particular equation describing the receptive field was chosen to have a simple form, and the motion response was based on the steady-state amplitude of the Hassenstein-Reichardt correlator [28, 29]. Parameters were adjusted to fit electrophysiological data from equatorial HS cells in *Drosophila* [4]. The most important requirement is that the motion response is asymmetric, i.e., the hyperpolarization in response to back-to-front motion is smaller in amplitude than the depolarization in response to front-to-back motion. A comprehensive description of the model is provided in the Supplemental Experimental Procedures together with Figure S2 and Code S1.

We discovered that our model predicts object fixation, and, furthermore, when we predicted fixation in front of a moving background, fixation position was shifted from zero opposite to background motion (Figure 3A). This phenomenon was also observed in behavioral experiments (Figures 2 and 3C and [1]) but was previously explained based on a summation of the outputs of the T4-T5-dependent motion circuit and a T4-T5-independent position circuit [1]. In our model, however, there is only a pair of HS cells that were reasoned unlikely to be part of the T4-T5-independent position circuit [1].

In the face of background motion, it might seem counterintuitive that two wide-field motion-integrating neurons can yield object fixation behavior. But our model predicts that the response to simultaneous closed-loop figure and open-loop background motion has two torque terms that remain in equilibrium and thus that fixation is maintained until the background exceeds a critical velocity. More formally, for a stationary background, our model predicts two fixed points at which responses vanish, a stable one in front and an unstable one behind the fly. Thus, perturbations from a position directly in front of the fly would shrink, whereas perturbations in back would grow. With increasing background velocity, these fixed points approach each other. The stable and unstable branch (Figure 3A, top, solid and dashed line) describe the dependency of the fixed points on the background velocity. The system dynamics are color coded and depicted by arrows to indicate that a figure would move toward the stable and away from the unstable branch. At a critical background velocity, ω_c, the fixed points meet and vanish (Figure 3A, top). Thus, the dynamical system shows a classical saddle-node bifurcation. At higher background velocities, the total torque is dominated by the response component due to the open-loop background, much like an optomotor response (green in Figure 3). For a more intuitive comparison with behavioral data, we computed the probability distribution of the figure position as a function of background velocity. As background velocity increases, the position of its mode follows the stable branch of the bifurcation while the distribution gets broader (Figure 3A, bottom).

Because this analytical model is based explicitly on a pair of visual neurons, it can predict responses to arbitrary piecewise-defined visual stimuli under both open- and closed-loop conditions. We found that for a particular configuration, closed-loop object fixation without input from a visual background, it is formally equivalent to the classical model proposed by Poggio and Reichardt based on torque measurements (e.g., [2, 30]; see the Supplemental Experimental Procedures). As in this classical framework, the torque acting on an object in closed-loop can be mathematically decomposed into a restoring term that drives the object to a stable position and a dampening term that opposes object motion.

We wondered if the simplifications that allowed us to perform a stability analysis were consistent with known physiology and therefore tested whether more realistic HS cell responses would lead to qualitatively similar predictions. We therefore implemented a model for *Calliphora* HS cell responses [24] and again computed torque as the scaled difference between two mirror-symmetric units. For a complete description of this model, refer to the Supplemental Experimental Procedures together with Figure S3 and Code S1.

The physiological model indeed predicts fixation in front of stationary and moving backgrounds (Figure 3B), which is qualitatively similar to the basic analytical model (Figure 3A). We calculated the initial velocity of a figure as a function of azimuthal position and background velocity (Figure 3B, top) together with the probability histograms of figure position (Figure 3B, bottom) to visualize the system dynamics and the shift of the fixation position. Although differences between *Calliphora* and *Drosophila* prevent a detailed quantitative comparison, both the dynamics and fixation position are in qualitative agreement with the analytical model.

To test the predictions of our models, we measured turning responses in flies to which we presented a closed-loop figure moving in front of an open-loop background. The overall pattern of behavioral turning responses to such stimuli measured experimentally (Figure 3C, top) is similar to the model predictions (Figures 3A and 3B, top). In particular, the fixation position shifts from directly in front of the fly into the direction opposite to background motion, and the probability distribution of figure position gets broader as the background velocity is increased (compare Figure 3C, bottom, to Figures 3A and 3B, bottom). Overall, the measured dynamics are consistent with the saddle-node bifurcation predicted by the analytical model. The main difference is that the analytical model predicts fixation at angular positions at which flies ceased to fixate the figure and exhibited optomotor-like turning. This would follow directly from a decrease in asymmetry at more lateral positions. Such decreased lateral asymmetry has been shown for the torque response [1], but electrophysiological measurements addressing this question are, to our knowledge, not published.

Discussion

Our behavioral data obtained for tethered flight show that there are conditions in which a T4-T5-independent circuit allows for object fixation, consistent with a study on walking flies [1]. We discovered that intact T4-T5 cells are required for fixation under the high feedback gain or figure-ground conditions tested. Moreover, we showed that models based on a bilateral pair of neurons with asymmetric motion responses, such as the HS cells downstream of T4-T5, predict object fixation in the absence of parallel pathways. This potential ability of HS-like cells to support object fixation was partly anticipated [17, 25–27]. Here we provide, for the first time, a complete implementation of models based on asymmetric motion-processing to predict behavioral responses to arbitrary visual stimuli. We show that both neuronal models predict object fixation, including fixation on a moving background, a behavior previously suggested to require a separate position circuit [1].

Despite their predictive power, our models do not rule out the involvement of other neurons in object responses. Indeed, previous work [1] and our behavioral results for T4-T5-blocked flies support the existence of at least one additional system. We suggest that our models, whose implementation we include in full (Supplemental Experimental Procedures and http://strawlab.org/asymmetric-motion/), may serve as a starting point and null hypothesis for studies on the role of cells potentially contributing to object responses.

Removing HS cells decreases behavioral response to wide-field motion but has a smaller effect on object fixation [31, 32]. Residual object-orienting behavior might result from a T4-T5-independent circuit alone or with contributions from non-HS neurons downstream of T4-T5. The asymmetric motion response of the modeled HS cells is the key component that allows fixation and many other neurons may exhibit similar asymmetric response properties. Any bilateral pair of such neurons would be predicted to enable figure-ground discrimination and object fixation.

The T4-T5-independent position circuit depends on local luminance changes [1] reminiscent of flicker responses described in house flies [33, 34]. We suggest that the T4-T5-independent circuit is too slow to mediate stripe fixation at high gain, perhaps due to slow responses to luminance changes at moderate contrast. Indeed, the latency of *Drosophila* wing responses to flickering stimuli exceeds one second at a contrast of 0.44 [18]. Behavioral experiments in *Calliphora* led to the conclusion that flicker-mediated responses worked on time scales much larger than the ones found in the fast turning responses of tracking and landing [17]. It is unclear why T4-T5-blocked flies failed at the figure-ground discrimination task even at low gain with a stationary background. One possible explanation is that spatial and temporal low-pass filtering in the remaining circuits responsible for fixation in T4-T5-blocked flies would lead to decreased sensitivity for this specific kind of stimulus. For example, flicker-sensitive neurons in *Eristalis* showed minimal responses to moving patterns at spatial frequencies that elicit robust responses in HS cells [35, 36], suggesting potential differences in the spatial or temporal sampling of the different circuits involved. Thus, a logical next step is to investigate specific dynamics, neuronal sampling, and contrast and luminance sensitivity of the T4-T5-dependent and T4-T5-independent object responses.

Drosophila shows, in contrast to the aerial chasing behavior of house flies and blow flies, a repulsive reaction to small objects [37], a behavior not predicted by the present models. Indeed, small-field-selective neurons [38–40] might play a role in such behaviors. In light of our models, the question arises whether sensitivity to non-Fourier figure motion, as measured in wide-field motion integrators [41], would predict a single HS-like neuronal substrate as being sufficient to mediate what was previously suggested to be information carried in two parallel streams [42, 43].

Behaviors analogous to object fixation and optomotor response in flies are present in a wide range of animals, including humans. Vertebrates minimize retinal optic flow by the optokinetic reflex similar to the flies' optomotor response. Vertebrate eyes perform saccades toward stationary objects and smooth-pursuit movements to keep objects on the fovea—reminiscent of flies fixating objects in their frontal field of view. Classically, it was assumed that a position pathway underlies saccades independently of a motion pathway serving smooth pursuit, but this juxtaposition of the position and motion pathway has been questioned because of increasing evidence for mutual interactions and synergies (reviewed in [44]). The present models illustrate how a circuit based on two neurons could account for fundamental visual behaviors. Imagine, in a thought experiment, a vertebrate eye whose two eye muscles guiding horizontal movements are coupled to HS-like neurons on either side of the fovea. The resulting hypothetical eye would show optokinetic reflexes, would fixate stationary objects at its midline, and would stabilize moving objects. How asymmetric motion detection interacts with the position pathway in mammals is currently unclear as different studies either supported a bias for motion from the periphery toward (e.g., [45]) or away from (e.g., [46]) the fovea. Our results indicate that an apparently sophisticated repertoire of visuomotor behaviors can, in principle, arise from a neural circuit with just two bilateral asymmetric wide-field motion integrators, and we speculate that the use of asymmetric motion processing might be a common principle of visuomotor systems across phyla.

Supplemental Information

Supplemental Information includes Supplemental Experimental Procedures, three figures, and code and can be found with this article online at http://dx.doi.org/10.1016/j.cub.2014.10.042.

Author Contributions

L.M.F., A.P., and A.D.S. conceived the experiments and performed the modeling. L.M.F. performed the experiments. L.M.F., A.P., and A.D.S. analyzed the experimental data. L.M.F., A.P., and A.D.S. wrote the manuscript.

Acknowledgments

We thank G. Rubin and A. Nern for the T4-T5 driver line R42F06-Gal4, B. Dickson for the UAS-TNT and UAS-TNTin flies, J. Stowers for the drawing of the tethered flight apparatus, K. Panser and S. Villalba for technical advice, and T. Poggio, C. Wehrhahn, G. Maimon, and anonymous reviewers for comments on the manuscript. This work was funded by ERC Starting Grant 281884 and IMP core funding.

Received: May 29, 2014
Revised: September 19, 2014
Accepted: October 14, 2014
Published: November 13, 2014

References

1. Bahl, A., Ammer, G., Schilling, T., and Borst, A. (2013). Object tracking in motion-blind flies. Nat. Neurosci. *16*, 730–738.
2. Poggio, T., and Reichardt, W. (1973). A theory of the pattern induced flight orientation of the fly Musca domestica. Kybernetik *12*, 185–203.
3. Hausen, K. (1982). Motion sensitive interneurons in the optomotor system of the fly. II. The horizontal cells: receptive field organization and response characteristics. Biol. Cybern. *46*, 67–79.
4. Schnell, B., Joesch, M., Forstner, F., Raghu, S.V., Otsuna, H., Ito, K., Borst, A., and Reiff, D.F. (2010). Processing of horizontal optic flow in three visual interneurons of the Drosophila brain. J. Neurophysiol. *103*, 1646–1657.
5. Schnell, B., Raghu, S.V., Nern, A., and Borst, A. (2012). Columnar cells necessary for motion responses of wide-field visual interneurons in Drosophila. J. Comp. Physiol. A Neuroethol. Sens. Neural Behav. Physiol. *198*, 389–395.
6. Hausen, K. (1982). Motion sensitive interneurons in the optomotor system of the fly. I. The horizontal cells: structure and signals. Biol. Cybern. *45*, 143–156.
7. Hausen, K., and Wehrhahn, C. (1983). Microsurgical lesion of horizontal cells changes optomotor yaw responses in the blowfly Calliphora erythrocephala. Proc. R. Soc. Lond. B *219*, 211–216.
8. Egelhaaf, M., Hausen, K., Reichardt, W., and Wehrhahn, C. (1988). Visual course control in flies relies on neuronal computation of object and background motion. Trends Neurosci. *11*, 351–358.

9. Hausen, K., and Wehrhahn, C. (1989). Neural circuits mediating visual flight control in flies. I. Quantitative comparison of neural and behavioral response characteristics. J. Neurosci. *9*, 3828–3836.
10. Hausen, K., and Wehrhahn, C. (1990). Neural circuits mediating visual flight control in flies. II. Separation of two control systems by microsurgical brain lesions. J. Neurosci. *10*, 351–360.
11. Haikala, V., Joesch, M., Borst, A., and Mauss, A.S. (2013). Optogenetic control of fly optomotor responses. J. Neurosci. *33*, 13927–13934.
12. Schnell, B., Weir, P.T., Roth, E., Fairhall, A.L., and Dickinson, M.H. (2014). Cellular mechanisms for integral feedback in visually guided behavior. Proc. Natl. Acad. Sci. USA *111*, 5700–5705.
13. Maimon, G., Straw, A.D., and Dickinson, M.H. (2010). Active flight increases the gain of visual motion processing in Drosophila. Nat. Neurosci. *13*, 393–399.
14. Stowers, J.R., Fuhrmann, A., Hofbauer, M., Streinzer, M., Schmid, A., Dickinson, M.H., and Straw, A.D. (2014). Reverse engineering animal vision with virtual reality and genetics. Computer *47*, 38–45.
15. Götz, K.G. (1964). Optomotorische Untersuchung des visuellen Systems einiger Augenmutanten der Fruchtfliege Drosophila. Biol. Cybern. *2*, 77–92.
16. Kennedy, J.S. (1940). The visual responses of flying mosquitoes. Proc. Zool. Soc. Lond. *109*, 221–242.
17. Wehrhahn, C., and Hausen, K. (1980). How is tracking and fixation accomplished in the nervous system of the fly? A behavioural analysis based on short time stimulation. Biol. Cybern. *38*, 179–186.
18. Duistermars, B.J., Care, R.A., and Frye, M.A. (2012). Binocular interactions underlying the classic optomotor responses of flying flies. Front. Behav. Neurosci. *6*, 6.
19. Sweeney, S.T., Broadie, K., Keane, J., Niemann, H., and O'Kane, C.J. (1995). Targeted expression of tetanus toxin light chain in Drosophila specifically eliminates synaptic transmission and causes behavioral defects. Neuron *14*, 341–351.
20. Poggio, T., and Reichardt, W. (1981). Visual fixation and tracking by flies: Mathematical properties of simple control systems. Biol. Cybern. *40*, 101–112.
21. Hausen, K. (1976). Functional characterization and anatomical identification of motion sensitive neurons in the lobula plate of the blowfly Calliphora erythrocephala. Z. Naturforsch. *31 c*, 628–633.
22. Egelhaaf, M., Borst, A., Warzecha, A.K., Flecks, S., and Wildemann, A. (1993). Neural circuit tuning fly visual neurons to motion of small objects. II. Input organization of inhibitory circuit elements revealed by electrophysiological and optical recording techniques. J. Neurophysiol. *69*, 340–351.
23. Eckert, H. (1980). Functional properties of the H1-neurone in the third optic ganglion of the blowfly. Phaenicia. J. Comp. Physiol. *135*, 29–39.
24. Lindemann, J.P., Kern, R., van Hateren, J.H., Ritter, H., and Egelhaaf, M. (2005). On the computations analyzing natural optic flow: quantitative model analysis of the blowfly motion vision pathway. J. Neurosci. *25*, 6435–6448.
25. Wehrhahn, C. (1981). Fast and slow flight torque responses in flies and their possible role in visual orientation behaviour. Biol. Cybern. *40*, 213–221.
26. Reichardt, W., Poggio, T., and Hausen, K. (1983). Figure-ground discrimination by relative movement in the visual system of the fly. Biol. Cybern. *46*, 1–30.
27. Wehrhahn, C. (1980). Visual fixation and tracking in flies. In Mathematical Models in Molecular and Cell Biology, L.A. Segel, ed. (Cambridge: Cambridge University Press), pp. 568–605.
28. Reichardt, W., and Varju, D. (1959). Übertragungseigenschaften im Auswertesystem für das Bewegungssehen. Z. Naturforsch. *14 b*, 674–689.
29. Borst, A., and Bahde, S. (1986). What kind of movement detector is triggering the landing response of the housefly? Biol. Cybern. *55*, 59–69.
30. Reichardt, W., and Poggio, T. (1975). A theory of the pattern induced flight orientation of the fly Musca domestica II. Biol. Cybern. *18*, 69–80.
31. Geiger, G., and Naessel, D. (1982). Visual processing of moving single objects and wide-field patterns in flies: behavioural analysis after laser-surgical removal of interneurons. Biol. Cybern. *149*, 141–149.
32. Bausenwein, B., Wolf, R., and Heisenberg, M. (1986). Genetic dissection of optomotor behavior in Drosophila melanogaster. Studies on wild-type and the mutant optomotor-blind^{H31}. J. Neurogenet. *3*, 87–109.
33. Pick, B. (1974). Visual flicker induces orientation behaviour in the fly Musca. Z. Naturforsch. *29 c*, 310–312.
34. Pick, B. (1976). Visual pattern discrimination as an element of the fly's orientation behaviour. Biol. Cybern. *23*, 171–180.
35. de Haan, R., Lee, Y.-J., and Nordström, K. (2013). Novel flicker-sensitive visual circuit neurons inhibited by stationary patterns. J. Neurosci. *33*, 8980–8989.
36. Straw, A.D., Warrant, E.J., and O'Carroll, D.C. (2006). A "bright zone" in male hoverfly (Eristalis tenax) eyes and associated faster motion detection and increased contrast sensitivity. J. Exp. Biol. *209*, 4339–4354.
37. Maimon, G., Straw, A.D., and Dickinson, M.H. (2008). A simple vision-based algorithm for decision making in flying Drosophila. Curr. Biol. *18*, 464–470.
38. Egelhaaf, M. (1985). On the neuronal basis of figure-ground discrimination by relative motion in the visual system of the fly. II. Figure-dectection cells, a new class of visual interneurones. Biol. Cybern. *52*, 195–209.
39. Reichardt, W., Egelhaaf, M., and Guo, A. (1989). Processing of figure and background motion in the visual system of the fly. Biol. Cybern. *61*, 327–345.
40. Seelig, J.D., and Jayaraman, V. (2013). Feature detection and orientation tuning in the Drosophila central complex. Nature *503*, 262–266.
41. Lee, Y.-J., and Nordström, K. (2012). Higher-order motion sensitivity in fly visual circuits. Proc. Natl. Acad. Sci. USA *109*, 8758–8763.
42. Aptekar, J.W., Shoemaker, P.A., and Frye, M.A. (2012). Figure tracking by flies is supported by parallel visual streams. Curr. Biol. *22*, 482–487.
43. Theobald, J.C., Shoemaker, P.A., Ringach, D.L., and Frye, M.A. (2010). Theta motion processing in fruit flies. Front. Behav. Neurosci. *4*, 35.
44. Orban de Xivry, J.-J., and Lefèvre, P. (2007). Saccades and pursuit: two outcomes of a single sensorimotor process. J. Physiol. *584*, 11–23.
45. Raymond, J.E. (1994). Directional anisotropy of motion sensitivity across the visual field. Vision Res. *34*, 1029–1037.
46. Georgeson, M.A., and Harris, M.G. (1978). Apparent foveofugal drift of counterphase gratings. Perception *7*, 527–536.

Current Biology, Volume *24*

Supplemental Information

Asymmetric Processing of Visual Motion for Simultaneous Object and Background Responses

Lisa M. Fenk, Andreas Poehlmann, and Andrew D. Straw

Figure S1

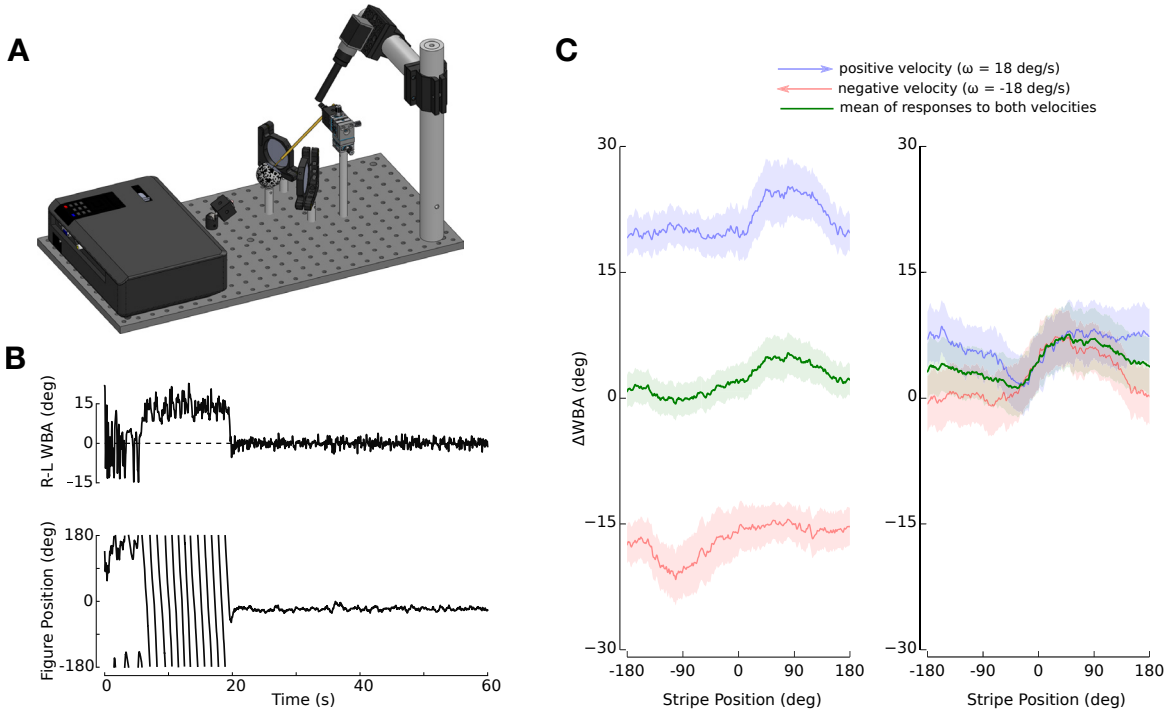

Figure S1, related to Figure 1. Behavioral setup and closed-loop and open-loop behavior

A Tethered flight apparatus. Rigidly tethered flies are placed in a virtual environment. Simultaneous tracking of the wing beat amplitude allows closing the visuo-motor feedback loop with artificial coupling using a gain parameter. **B** Example of a data trace recorded in a closed-loop fixation experiment. The upper trace gives the right minus left wing-beat amplitude (R-L WBA) as a function of time. The figure angular velocity, ω, is coupled to the difference in wing-beat amplitude, $\triangle$WBA, via the closed-loop gain, g ($\omega = -g \cdot \triangle$WBA, here: $g = 25\ s^{-1}$). The lower trace gives the figure position as a function of time showing that the fly keeps the figure in its frontal field of view after an initial spinning period. **C** Turning response of flies (smoothed mean $\triangle$WBA $\pm$ SEM) to a black stripe (22.5 deg width) in open-loop on a white background moving at a positive angular velocity (blue) and a negative angular velocity (red), together with the arithmetic mean of the responses to the two motion directions (green). The stripe started at an initial position behind the fly ($\pm$ 180 deg) with a positive velocity and after 20 cycles, the velocity was switched to the negative value. In both control (left panel) and T4-T5-blocked (right panel) flies, a clear position response was observed. Additionally, as expected, control flies showed a large syndirectional turning response (left panel). The overall mean $\triangle$WBA (averaged across all positions) in response to positive stripe velocity differs significantly from the response to negative stripe velocity ($p = 0.0002$, $N = 18$, two tailed Wilcoxon signed rank test) with a median difference of 37 deg. This syndirectional turning is, as expected, substantially reduced in T4-T5-blocked flies (right panel); the overall mean $\triangle$WBA responses to positive and negative background motion were not significantly different in blocked flies ($p = 0.09$, $N = 15$, Wilcoxon signed-rank test, two tailed) with a median difference of 2 deg. Note that at stripe positions in the rear, there appears to be a directional response. Indeed, due to the open-loop protocol, one would expect a continued turning response after the stripe has moved out of the fly's field of view to result in a small directional component. Position response was evaluated statistically as follows. The mean $\triangle$WBA from the range of negative stripe positions differs significantly from the mean across positive stripe positions for both control flies as well as T4-T5-blocked flies ($p = 0.01$, $N = 18$ and $p = 0.003$, $N = 15$, respectively, Wilcoxon signed-rank test, two tailed) with a median difference of 3.4 deg for control flies and 3.6 deg for T4-T5-blocked flies. Because of motor saturation in control flies due to the strong syndirectional turning, it is difficult to compare the absolute magnitude of the position response between the two genotypes.

Figure S2

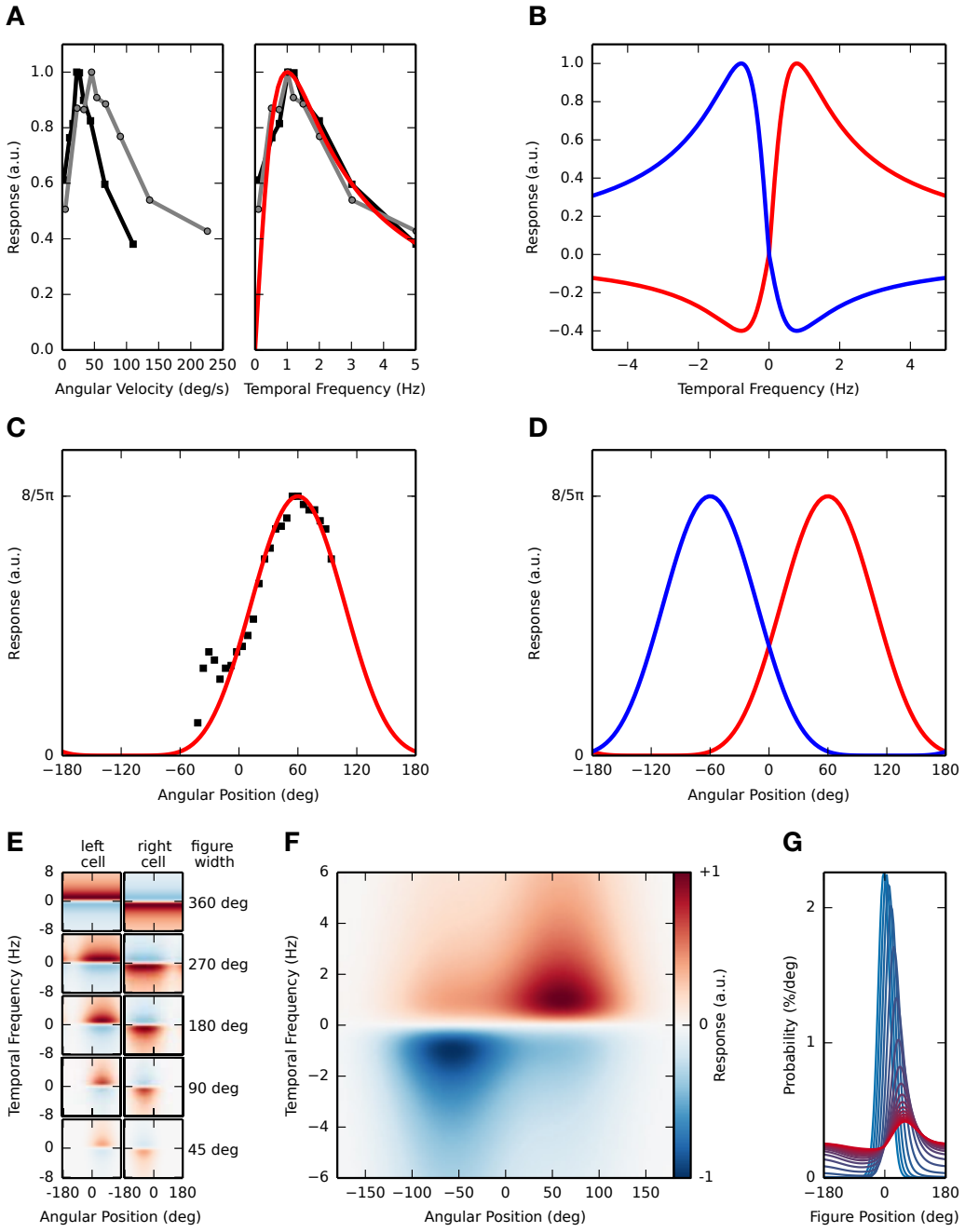

Figure S2, related to Figure 3. Phenomenological model of asymmetric motion processing for figure-ground discrimination

A Experimentally measured motion response of HS-cells to preferred direction motion from Schnell *et al.* [S9] for angular velocity (left) and temporal frequency (right). Model motion response (red line) was manually fit to the temporal frequency data. **B** Motion response in preferred and null direction for left (red) and right (blue) model cells. **C** Model receptive field was manually fit (red line) to experimental data (black points) from Schnell *et al.* [S9]. **D** Receptive fields for left (red) and right (blue) model cells. **E** Responses of left and right cells (left and right panels, respectively) to small-field stimuli of varying width, β. **F** Torque resulting from the model in response to a (22.5 deg width and wavelength) figure. **G** Probability of figure position under open-loop background conditions. Colors correspond to open-loop background velocity ranging from 0 (blue) to twice the critical background velocity (red).

Figure S3

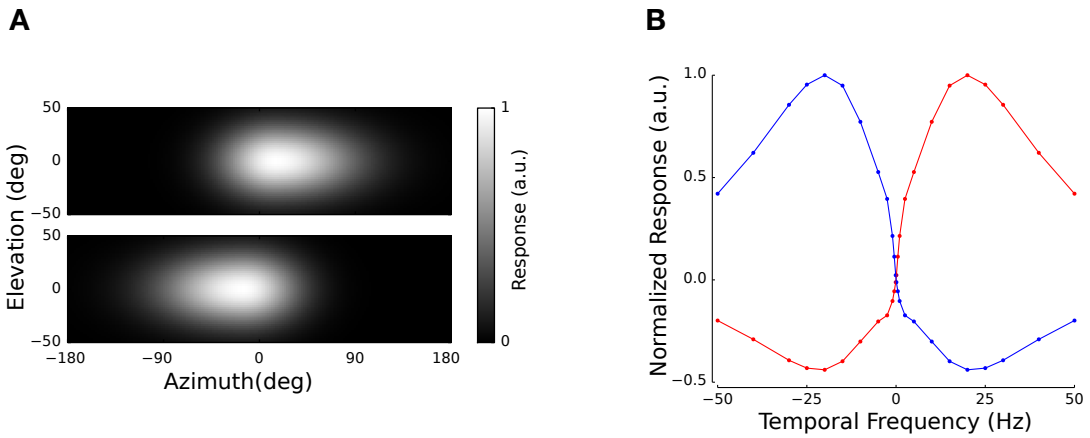

Figure S3, related to Figure 3. Physiologically inspired model of asymmetric motion processing for figure-ground discrimination

A Receptive field of the left (upper panel) and right (lower panel) model wide-field motion detecting neuron after Lindemann *et al.* [S4]. **B** Motion response in each a left model neuron (red) and a right model neuron (blue) computed for a sinusoidally modulated grating (10 deg wavelength).

Supplemental Experimental Procedures

1 Flies

We used 4-day-old female flies that were raised on standard food at 25 °C on a 12-h light, 12-h dark cycle. Flies were anesthetized by cooling to 3.2 °C on a custom-built thermo-electric cold plate (IMP Mechanical Workshop, Vienna) and fixed to a tungsten tether rod with a small drop of blue-light solidifying glue (Bondic). The glue droplet was applied such that the head was fixed to the body without occluding ocelli. Flies were allowed at least 20 minutes recovery time before the experiments. We used T4-T5 blocked flies by expressing tetanus toxin light chain (w^+/w^- ; UAS-TNTe/+ ; R42F06-GAL4/+) and T4-T5 control flies where we expressed an inactive form of the toxin (w^+/w^- ; UAS-TNTin/+ ; R42F06-GAL4/+). All experiments were conducted at room temperature (22-25 °C).

2 Virtual reality apparatus for tethered flight

The experiments were conducted in a custom built virtual reality arena. Rigidly tethered flies are placed in the center of a ping-pong ball used as a spherical projection screen for visual stimuli. We filmed the flies from above using a camera (Basler ac640m, lens: InfiniStix 94mm 1x) equipped with an infrared filter (Lee filters, transmission above 730nm) at 100 fps and illuminate the arena from below with a infrared diode (Osram Golden Dragon 1 Ampere, 850 nm) to track the flies' wing movements. The infrared illumination allows the separation of the visual stimulation and the tracking. Custom software within the Motmot framework [S1] was used to track the leading edge of the wing-stroke envelope in real time. The delay of the tracking is less than 20 ms [S2]. As the flies' wing-beat frequency is approximately 200 Hz, an exposure time of 9.9 ms ensures that each frame contains roughly two wing stroke cycles and that the leading edge reversal is not subject to temporal aliasing in a condition in which the stroke reversal was not imaged [S2]. Estimation of right and left wing beat amplitudes happened at 100 Hz. We used the difference between the right and the left wing beat amplitudes ($\triangle$WBA) to close the loop in our experiments (see below). We excluded data when flies stopped flying for plotting, but not for visual feedback, and position was low-pass filtered only for plotting. Including visual stimulus latency (see below), the total latency of this system is less than 50 ms.

3 Visual stimuli and data analysis

Visual stimuli were generated with FlyVR (http://flyvr.org) [S3] driving a video card (based on the NVIDIA GeForce GTX 650 chipset) and projected on the ball with a projector (ViewSonic PJD6381) at 120 Hz refresh rate. Total latency from software command to luminance changes on the screen was measured at 22 ms. The contrast of the visual stimuli inside the spherical display was 0.32 (Michelson units) and the mean luminance was 130 cd/m^2. Three images are projected on the spherical display – one directly onto the ball, and two indirectly using two mirrors – to cover the whole 360 deg visual parameter. Object angular velocity, ω, is given as $\omega = -g \cdot \triangle$WBA, where g is the gain. We clipped object velocity to $\pm$ 573 deg/s (4.8 degrees per frame with our 120 Hz projector) at both gain settings to ensure a smooth apparent motion stimulus. In the first set of closed-loop experiments, (Figure 1AB) we tested a black stripe on a white background for 120 s. This same stimulus was used in open-loop for the data shown in Figure S1C. In a second assay (Figure 2AB, Figure S1B) we presented a random pixel figure (angular width: 22.5 deg) in front of a random pixel background (angular size of a pattern pixel: 11.25 deg) that was stationary for 60 s and then moved at constant speed (-2 deg/s) for another 60 s. For comparison of the predicted bifurcation to the flies' behavior we presented again a random pixel figure in front of a random pixel background and linearly increased the speed of the background over ten minutes to a final value of -10 deg/s. To plot the measured dynamics of fixation behavior (Figure 3C, top), we considered periods in which absolute figure velocity was less than 250 deg/s, to eliminate periods in which flies did not exhibit figure responses and these data are presented as a smoothed 2D histogram. Plots of figure position probability (Figure 3C, bottom) is a 2D histogram of all data.

4 Physiologically realistic model

We implemented the *Calliphora* HS-cell model from Lindemann *et al.* ('variant 7') [S4]. Briefly summarizing, the visual stimulus is sampled by a two-dimensional photoreceptor array modeled by Gaussian spatial

low-pass filters, after which the signal is passed to the first temporal filtering stage to simulate lamina large monopolar cells. The resulting signal is then fed into elementary motion detectors (EMDs). In their most basic form, they multiply the temporally unfiltered with a temporally low-pass filtered signal. In an elaborated version, Lindemann *et al.* added a temporal high-pass-filter to the classically unfiltered signal, previously shown to improve simulations [S5]. The output of the EMDs are weighted according to the spatial sensitivity of HS-cells [S6], and finally, the output of two mirror-symmetrical EMD units are treated as the conductances of excitatory and inhibitory synapses of the integrating cell [S4] as suggested by [S7]. To implement a strong asymmetry in response to preferred and null direction motion, we deviated from the published model by changing the ratio of inhibitory to excitatory reversal potentials from -0.95 to -0.5, consistent with electrophysiological measurements of HS-cells in response to rotating stimuli [S8, S9]. The complete software is included (Code S1, also available at http://strawlab.org/asymmetric-motion/) and the basic properties of the modeled cells are shown in Figure S3. The data shown in Figure 3B were computed using Euler-Maruyama integration (time step 1 ms) with Gaussian white noise (σ = 0.001 rad/s^2) on the angular acceleration. The angular acceleration was coupled to the difference between the left and right HS-cell via a proportionality constant of -3000 (a.u.). The visual stimuli consisted of a checkerboard figure (width: 20 deg) in front of a checkerboard background (both 20 deg wavelength).

5 The phenomenological model

Here we describe a phenomenological model of fly visual behaviors based on a few well-known properties of wide-field motion integrators such as the lobula plate tangential cells (LPTCs) of flies. A primary goal was to formulate a very simple model to facilitate rigorous mathematical analysis. It predicts turning responses of the fly to piecewise-defined open- and closed-loop stimuli. The model abstracts fly behavior to a one degree of freedom system (azimuth) and reduces stimuli to horizontal piecewise-defined patterns at zero elevation. We provide a theoretical framework to analytically predict turning responses here, as well as a software implementation in Supplemental Code S1 (also available at http://strawlab.org/asymmetric-motion/). All retinal positions are specified as azimuthal angle from the visual midline (right handed coordinate system).

The internal parameters of the model are, with a single exception, based exclusively on measurements from electrophysiological experiments of well investigated LPTCs, *Drosophila* Horizontal System (HS) cells [S9]. The remaining free parameter, C_T, is used to account for experimental coupling conditions and predict behavioral responses under a variety of those conditions. The parameter is a constant specifying the cell output to torque coupling, and we discuss it below.

5.1 The motion response

A fundamental property of an HS-cell is its change in membrane potential when a wide-field stimulus, such as horizontal sinusoidal grating covering the whole visual field, is rotated azimuthally around the fly. We call the function that describes the dependence of membrane potential responses to movement of the visual stimulus the motion response. Its dependent variable is the temporal frequency, f_t, which is described by $f_\mathrm{t} = \omega/\lambda_\mathrm{p}$ given a stimulus with a pattern wavelength, λ_p, and an angular velocity, ω. We use the measured relative motion response from Figure 2B of [S9], to fit the parameters of our function. The mathematical form of our function is given by the Reichardt correlator ([S10] after [S11]). Like most LPTCs, HS-cells respond with depolarizing and hyperpolarizing responses in the so-called preferred and null directions, respectively. The relative motion response to preferred direction stimuli with constant pattern wavelength is:

$$M_\mathrm{PD}(f_\mathrm{t}) = \frac{\tau_\mathrm{opt} f_\mathrm{t}}{1 + (\tau_\mathrm{opt} f_\mathrm{t})^2} \tag{1}$$

Adjusting the parameter, $f_\mathrm{opt} = \tau_\mathrm{opt}^{-1}$, to 1 Hz, approximates the data reasonably well (Figure S2A).

A critical feature of our model is the asymmetry of the response to the direction of motion of the stimulus. In particular, the motion response to null direction stimuli is not only inverted in sign but also reduced in amplitude. Basing our estimate on the values published in Figure 1D of [S9], we account for this by a factor C_ND = 0.4. The relative motion response for stimuli moving in both directions can be written as:

$$M(f_\mathrm{t}) = \begin{cases} M_\mathrm{PD}(f_\mathrm{t}) & \text{if } f_\mathrm{t} \geq 0 \\ -C_\mathrm{ND} M_\mathrm{PD}(-f_\mathrm{t}) & \text{otherwise} \end{cases}$$

The normalized response to a moving sinusoidal pattern in both the null (amplitude is *negative*) and the preferred (amplitude is *positive*) direction in temporal frequency space, $f_t = \omega/\lambda_p$, for a pair of neurons with opposite direction selectivities (e.g. contralateral cells) is shown in Figure S2B.

5.2 The receptive field

For a small stimulus, the response of an LPTC is also dependent on retinal position. We use the local motion sensitivity measured at zero degrees elevation from Figure 3C of [S9] to define the spatial receptive field for our model. Because we simulated visual stimuli along the unit circle, the receptive field is required to be 2π periodic, and we therefore choose a trigonometric function. However, its exact nature is not important and was chosen for convenience. Our model receptive field (see Figure S2C) is given as:

$$R(\varphi) = \frac{8}{5\pi} \cos\left(\frac{1}{2}(\varphi \pm \varphi_{max})\right)^6 \tag{2}$$

In this model, φ_{max} is the azimuthal angle at which the model cell responds most strongly to a small field stimulus and the factor $\frac{8}{5\pi}$ normalizes the area under the curve to 1.

The receptive fields of the left (red) and right (blue) model cells are symmetric around zero, as shown in Figure S2D.

5.3 The cell's response

We model the cell's complete output as the integral over all angular positions weighted with the receptive field:

$$W(f_t) = \int_{-\pi}^{\pi} R(\varphi) M(f_t)\, d\varphi \tag{3}$$

For clarity, we expand this to explicitly show all parameters (enclosed in square brackets):

$$W(f_t, [\varphi_{max}, f_{opt}, C_{ND}]) = \int_{-\pi}^{\pi} R(\varphi, [\varphi_{max}]) M(f_t, [f_{opt}, C_{ND}])\, d\varphi$$

As described above, each of these three parameters, φ_{max}, f_{opt}, C_{ND}, was adjusted by eye to the experimental data of [S9]. This model describes the noise-free normalized graded potential of a wide-field motion integrator cell. We do not adjust these parameters for any predictions that we make later.

5.4 Introducing the figure-ground stimulus

So far, the model did not consider responses to spatially complex stimuli. The motion response (equation 1) was defined for a panoramic sinusoidal grating, which for a certain angular velocity, ω, and pattern wavelength, λ_p, generates a temporal frequency, $f_t = \omega/\lambda_p$. The receptive field (equation 2) was defined for a small stimulus. We now introduce a figure-ground stimulus, where the background pattern is occluded by the figure, with the following parameters:

- figure width β
- figure position φ_F
- figure pattern wavelength λ_F
- figure velocity ω_F
- ground pattern wavelength λ_G
- ground velocity ω_G

All the parameters above are inherent to the stimulus, not to the model. This is important because the responses to the figure or to the background — which we derive below — evolve from these parameters, and are not properties of the model cell. Please note that in this text, we use the word "figure" to describe a small-field visual object, even when there is no background contrast.

To use these stimulus parameters in the model, we define ω_{FG} and λ_{FG} dependent on the angular position, φ, the figure position, φ_F, and width, β, for the figure-ground stimulus.

$$\lambda_{FG}(\varphi, [\varphi_F, \beta]) = \begin{cases} \lambda_F & \text{if } \varphi_F - \frac{\beta}{2} \leq \varphi \leq \varphi_F + \frac{\beta}{2} \\ \lambda_G & \text{otherwise} \end{cases}$$

$$\omega_{FG}(\varphi, [\varphi_F, \beta]) = \begin{cases} \omega_F & \text{if } \varphi_F - \frac{\beta}{2} \leq \varphi \leq \varphi_F + \frac{\beta}{2} \\ \omega_G & \text{otherwise} \end{cases}$$

With this we can rewrite the cell response as:

$$\begin{aligned} W(f_t) = W(\omega_{FG}/\lambda_{FG}) &= \int_{-\pi}^{\pi} R(\varphi) M(\omega_{FG}/\lambda_{FG})\, \mathrm{d}\varphi \\ &= \int_{-\frac{1}{2}\beta}^{+\frac{1}{2}\beta} R(\varphi_F + \varphi) M(\omega_F/\lambda_F)\, \mathrm{d}\varphi + \int_{+\frac{1}{2}\beta}^{2\pi-\frac{1}{2}\beta} R(\varphi_F + \varphi) M(\omega_G/\lambda_G)\, \mathrm{d}\varphi \end{aligned}$$

We can interpret these two summands as a response to the figure, and a response to the background. But, again, they originate from the properties of the stimulus, not from the properties of the wide-field motion integrator. We define the figure and ground responses as:

$$W_F(\varphi_F, \omega_F, [\lambda_F, \beta]) = \int_{-\frac{1}{2}\beta}^{+\frac{1}{2}\beta} R(\varphi_F + \varphi) M(\omega_F/\lambda_F)\, \mathrm{d}\varphi$$

$$W_G(\varphi_F, \omega_G, [\lambda_G, \beta]) = \int_{+\frac{1}{2}\beta}^{2\pi-\frac{1}{2}\beta} R(\varphi_F + \varphi) M(\omega_G/\lambda_G)\, \mathrm{d}\varphi$$

Since the basic property of our figure-ground stimulus is that the figure occludes the background, the background response, W_G, is of course dependent on the figure position, φ_F, as a variable and the figure width, β, as a parameter.

If we use a figure of width, β, and pattern wavelength, λ_F, in front of a contrast-free background ($\lambda_G = \infty$), we can plot the response of the cell in phase space (see Figure S2F).

5.5 From cell output to torque

We model the torque output of the fly to be proportional to the difference of the left and the right model cell responses. We introduce a factor, C_T, which scales the normalized output to torque. This is the only free parameter of our model.

$$T(f_t) = C_T \left[W^{(\text{left})}(f_t) - W^{(\text{right})}(f_t) \right]$$

To simulate a noisy cell response, we add noise to the torque response of our system at this point to get:

$$T^*(f_t, t) = T(f_t) + N(t) = C_T \left[W^{(\text{left})}(f_t) - W^{(\text{right})}(f_t) \right] + N(t)$$

We rewrite this torque response for a figure-ground stimulus, using the following abbreviations:

$$R_{\mathsf{F}}^{(\text{left/right})}(\varphi_{\mathsf{F}}) = \int_{-\frac{1}{2}\beta}^{+\frac{1}{2}\beta} R^{(\text{left/right})}(\varphi_{\mathsf{F}} + \varphi)\,\mathrm{d}\varphi$$

$$R_{\mathsf{G}}^{(\text{left/right})}(\varphi_{\mathsf{F}}) = \int_{+\frac{1}{2}\beta}^{2\pi-\frac{1}{2}\beta} R^{(\text{left/right})}(\varphi_{\mathsf{F}} + \varphi)\,\mathrm{d}\varphi$$

$$X^{(-)} = X^{(\text{left})} - X^{(\text{right})}$$

$$X^{(+)} = X^{(\text{left})} + X^{(\text{right})}$$

Putting this and the figure-ground stimulus parameters into $T(f_t)$ gives:

$$\begin{aligned} T(f_t) &= T(\varphi_{\mathsf{F}}, \omega_{\mathsf{F}}, \omega_{\mathsf{G}}, [\lambda_{\mathsf{F}}, \lambda_{\mathsf{G}}, \beta]) = C_{\mathsf{T}} W^{(-)}(\varphi_{\mathsf{F}}, \omega_{\mathsf{F}}, \omega_{\mathsf{G}}, [\lambda_{\mathsf{F}}, \lambda_{\mathsf{G}}, \beta]) \\ &= C_{\mathsf{T}}\left(W_{\mathsf{F}}^{(-)}(\varphi_{\mathsf{F}}, \omega_{\mathsf{F}}, [\lambda_{\mathsf{F}}, \beta]) + W_{\mathsf{G}}^{(-)}(\varphi_{\mathsf{F}}, \omega_{\mathsf{G}}, [\lambda_{\mathsf{G}}, \beta])\right) \end{aligned}$$

For the sake of simplicity, we set the background contrast to zero for now ($\lambda_{\mathsf{G}} = \infty \rightarrow W_{\mathsf{G}}^{(-)} = 0$).

$$T(\varphi_{\mathsf{F}}, \omega_{\mathsf{F}}) = \frac{C_{\mathsf{T}}}{2}\left[R_{\mathsf{F}}^{(-)}(\varphi_{\mathsf{F}}) M^{(+)}(\omega_{\mathsf{F}}/\lambda_{\mathsf{F}}) + R_{\mathsf{F}}^{(+)}(\varphi_{\mathsf{F}}) M^{(-)}(\omega_{\mathsf{F}}/\lambda_{\mathsf{F}})\right]$$

This gives the response properties of a figure in front of a homogeneous background. For different figure widths, the phase space representation of this output is shown in Figure S2E. The receptive fields of both model cells make the initially homogeneous and optomotor like torque response (360 °) more and more position specific with decreasing figure width.

Note: The mathematical conversion on the figure terms can be applied to the ground terms in the same manner. For the figure-ground stimulus with $\lambda_{\mathsf{G}} < \infty$ we would get:

$$\begin{aligned} T(\varphi_{\mathsf{F}}, \omega_{\mathsf{F}}, \omega_{\mathsf{G}}) = &\frac{C_{\mathsf{T}}}{2}\left[R_{\mathsf{F}}^{(-)}(\varphi_{\mathsf{F}}) M^{(+)}(\omega_{\mathsf{F}}/\lambda_{\mathsf{F}}) + R_{\mathsf{F}}^{(+)}(\varphi_{\mathsf{F}}) M^{(-)}(\omega_{\mathsf{F}}/\lambda_{\mathsf{F}})\right] \\ &+ \frac{C_{\mathsf{T}}}{2}\left[R_{\mathsf{G}}^{(-)}(\varphi_{\mathsf{F}}) M^{(+)}(\omega_{\mathsf{G}}/\lambda_{\mathsf{G}}) + R_{\mathsf{G}}^{(+)}(\varphi_{\mathsf{F}}) M^{(-)}(\omega_{\mathsf{G}}/\lambda_{\mathsf{G}})\right] \end{aligned}$$

5.6 The dynamic equation

Above we derived an analytical model for the torque output of a fly based on the fundamental properties of motion integrator cells. In the following sections, we use this model to predict fly behavior during different figure-ground discrimination tasks, where two coupling conditions will be important. These are closed-loop and open-loop. For an open-loop stimulus, the torque produced does not influence the stimulus. The stimulus moves along a predefined trajectory in space time, and we measure torque output over time. In a closed-loop scenario, we apply the torque produced by the model on the part of the stimulus in closed-loop. For example, for a closed-loop figure (position: φ_{F}, velocity: $\dot{\varphi}_{\mathsf{F}}$) with no or stationary background, we obtain a Langevin type dynamic equation of the form:

$$\begin{aligned} \Theta\ddot{\varphi}_{\mathsf{F}} &= T^*(\varphi_{\mathsf{F}}, \dot{\varphi}_{\mathsf{F}}) \\ &= \frac{C_{\mathsf{T}}}{2}\left[R_{\mathsf{F}}^{(-)}(\varphi_{\mathsf{F}}) M^{(+)}(\dot{\varphi}_{\mathsf{F}}/\lambda_{\mathsf{F}}) + R_{\mathsf{F}}^{(+)}(\varphi_{\mathsf{F}}) M^{(-)}(\dot{\varphi}_{\mathsf{F}}/\lambda_{\mathsf{F}})\right] + N(t) \end{aligned}$$

Here we introduced an additional constant, Θ, which describes the effective moment of inertia in the model. In our tethered flight experiments, this corresponds to the inverse of the coupling gain, g, described in the manuscript. As can be seen easily Θ and C_{T} are not linearly independent, so for this case only the sign of Θ will be important. The case where Θ is set to a negative value corresponds to the natural condition in which the generated torque moves the figure in the opposing direction, referred to as *normal gain*.

5.7 Equivalence with Poggio and Reichardt 1973 model for specific conditions

As mentioned in the main text, because this analytical model is based explicitly on a pair of visual neurons, it can predict responses to arbitrary visual stimuli in both open- and closed-loop. We found that for a particular stimulus configuration (closed-loop figure fixation without input from a visual background), it is formally equivalent to the classical model proposed by Poggio and Reichardt based on torque measurements [S12, S13] (Eq. 2). For the specific notation refer to [S13]. One can identify

$$R_F^{(-)}(\varphi_F)M^{(+)}(\dot{\varphi}_F/\lambda_F) \mathrel{\widehat{=}} D^{\dagger}(\varphi(t), \dot{\varphi}(t))$$
$$R_F^{(+)}(\varphi_F)M^{(-)}(\dot{\varphi}_F/\lambda_F) \mathrel{\widehat{=}} \rho(\varphi(t), \dot{\varphi}(t))$$

as the even ($f(x) = f(-x)$) and odd ($f(x) = -f(-x)$) symmetric parts of the torque response in $\dot{\varphi}$.

We now linearize the Langevin equation around $\dot{\varphi}_F = 0$. Since our system is described by stochastic processes we use [S14] to justify the linearization. This assumes that the temporal average of the squared velocity does not vanish $\langle\dot{\varphi}^2\rangle > 0$ and the figure is almost stationary $\dot{\varphi} \approx 0$, which is a valid assumption since we are only interested in the quasi stationary behavior of the system.

For the even term, the linearization around $\dot{\varphi} \approx 0$ returns a constant and terms of the order of 2 or higher.

$$\langle M^{(+)}(\dot{\varphi})\rangle = M_0^{(+)} + O(\dot{\varphi}^2)$$

which depends on the initial slope of the motion response and on the asymmetry, C_{ND}, of the motion responses. For a symmetric motion response, this constant would be equal to zero. The asymmetry is therefore required for the system to have a restoring force, which is essential for figure fixation. Additionally, it is important to understand that $M_0^{(+)} = 0$ if $\langle\dot{\varphi}^2\rangle = 0$, i.e. in the absence of noise. It is a common misunderstanding that the linearization would throw away the asymmetric response to a moving figure.

After linearizing the even term, we can write:

$$\frac{C_T}{2} R_F^{(-)}(\varphi_F) M_0^{(+)} = \frac{\partial}{\partial\varphi} U(\varphi)$$

Which describes the restoring force of the system. Since we assume the potential energy of the dynamic system to be path independent, we can define a scalar potential, $U(\varphi)$, as written above. Due to our circular boundary conditions, $U(\varphi) = U(\varphi + n2\pi)$ is the periodic potential in which the figure is moving. Please note that this potential depends on the shape of the receptive field and, more importantly, on the properties of the presented stimulus. It results from the stimulus properties and a spatially integrating (wide-field) motion responsive cell having an anisotropic receptive field and an asymmetric motion response.

For the odd term, the linearization around $\dot{\varphi} \approx 0$ returns only a linear term (see [S14]) and terms of the order of 3 or higher.

$$\langle M^{(-)}(\dot{\varphi})\rangle = M_0^{(-)}\dot{\varphi} + O(\dot{\varphi}^3)$$

The odd function $M^{(-)}(\dot{\varphi})$ is by definition already point symmetric and shows no asymmetry. For small velocities this linearization is valid.

After linearizing the odd term, we get:

$$\frac{C_T}{2} R_F^{(+)}(\varphi_F) M_0^{(-)}\dot{\varphi} \approx r\dot{\varphi}$$

in [S13], they assume $R^{(+)}(\varphi) = r$ to be constant. Since the odd term describes the dampening force of the system for quasi stationary processes, this assumption is completely reasonable from a modelling perspective (note that $R_F^{(+)}(\varphi) > 0$ is true for all φ).

With all this, we can write down the linearized torque response to a figure as the Langevin equation:

$$\begin{aligned}\Theta\ddot{\varphi}_F &= T^*(\varphi_F, \dot{\varphi}_F)\\ &= \frac{C_T}{2}\left[R_F^{(-)}(\varphi_F)M^{(+)}(\dot{\varphi}_F/\lambda_F) + R_F^{(+)}(\varphi_F)M^{(-)}(\dot{\varphi}_F/\lambda_F)\right] + N(t)\\ &\approx \frac{\partial}{\partial\varphi_F} U(\varphi_F) + r\dot{\varphi}_F + N(t)\end{aligned}$$

using standard techniques, this Langevin equation can be transformed into a Fokker-Planck type equation, which describes the distribution arising from the time evolution of this stochastic differential equation. This representation allowed us to calculate probability distributions for the figure fixation process.

$$\frac{\partial}{\partial t}P = -\omega\frac{\partial}{\partial\varphi}P - \frac{\partial}{\partial\omega}\Big(\frac{\partial}{\partial\varphi}U + r\omega\Big)P + \zeta\frac{\partial^2}{\partial\omega^2}P$$

For this case, closed-loop figure fixation, this equation is equivalent to the theoretical framework presented in [S12, S13]. Again, note that we did not derive this equation from observed torque responses of tethered flies, but from the measured response properties of the wide-field motion integrator cells — the HS-cells — in *Drosophila*. Furthermore, our spatially explicit representation of visual stimuli and our explicit treatment of open- or closed-loop dynamics allow use of our framework in other scenarios, as performed below.

To summarize the above, the subtracted output of two opposing *HS-like* model cells predicts figure fixation in *Drosophila*.

5.8 Theoretical predictions

In the following experiments, the fly is in closed-loop control of a figure displayed in front of a moving background. It was previously shown that flies fixate a figure in front of a moving background at a position shifted from zero in the direction opposite to the background movement direction, and it was suggested that this results from a summation of a motion independent response and a motion response [S15].

However, we now show that our model, with only a single pathway, also predicts figure displacement. The quasistationary dynamic equation for our system looks like:

$$\begin{aligned}\Theta\ddot{\varphi}_\mathsf{F} &= T(\varphi_\mathsf{F}, \dot{\varphi}_\mathsf{F}, \omega_\mathsf{G}) \\ &= \frac{C_\mathsf{T}}{2}\Big[R^{(-)}_\mathsf{F}(\varphi_\mathsf{F})M^{(+)}(\dot{\varphi}_\mathsf{F}/\lambda_\mathsf{F}) + R^{(+)}_\mathsf{F}(\varphi_\mathsf{F})M^{(-)}(\dot{\varphi}_\mathsf{F}/\lambda_\mathsf{F})\Big] \\ &+ \frac{C_\mathsf{T}}{2}\Big[R^{(-)}_\mathsf{G}(\varphi_\mathsf{F})M^{(+)}(\omega_\mathsf{G}/\lambda_\mathsf{G}) + R^{(+)}_\mathsf{G}(\varphi_\mathsf{F})M^{(-)}(\omega_\mathsf{G}/\lambda_\mathsf{G})\Big]\end{aligned}$$

We would now like to perform a stability analysis of figure fixation. For this, we calculate the points in space for which the torque response vanishes and then check each of these fixed points to determine if it is a stable or an unstable equilibrium.

Since we are only interested in the fixed points of the system, the forces in this equation should vanish, and we can again linearize around a stable figure position and rewrite the dynamic equation to:

$$\Theta\ddot{\varphi}_\mathsf{F} = \frac{C_\mathsf{T}}{2}\Big[\frac{\partial}{\partial\varphi_\mathsf{F}}V(\varphi_\mathsf{F}, \omega_\mathsf{G}) + r\dot{\varphi}_\mathsf{F}\Big]$$

with

$$\frac{\partial}{\partial\varphi_\mathsf{F}}V(\varphi_\mathsf{F}, \omega_\mathsf{G}) = \frac{\partial}{\partial\varphi_\mathsf{F}}U(\varphi_\mathsf{F}) + R^{(-)}_\mathsf{G}(\varphi_\mathsf{F})M^{(+)}(\omega_\mathsf{G}/\lambda_\mathsf{G}) + R^{(+)}_\mathsf{G}(\varphi_\mathsf{F})M^{(-)}(\omega_\mathsf{G}/\lambda_\mathsf{G})$$

At the fixed points of the system, the force, $\frac{\partial}{\partial\varphi_\mathsf{F}}V(\varphi_\mathsf{F}, \omega_\mathsf{G})$, vanishes. By solving for the positions where torque was zero, we calculated the fixed points as we altered background velocity, with the results shown in Figure 3A (top) of the main text.

We furthermore evaluated whether these were stable or unstable. In Figure 3A (top), the solid black line is the stable position of a quasistationary figure dependent on the background velocity. At this stable point, the restoring force in the system pushes the figure back to the stable branch (indicated by the color coding). The dashed black line is the unstable position of the figure and perturbation from this equilibrium would grow and push the figure away.

With increasing background velocity, the stable and unstable points approach each other. At a critical background velocity, ω_c, the fixed points meet and vanish (Figure 3A, top) and therefore the figure can no longer be fixated. This is a classical saddle-node bifurcation. At higher background velocities, the total torque is dominated by the response component due to the open-loop background, much like an optomotor response, and exceeds the fraction generated by the response to the figure.

To calculate the probability distribution, $P(\varphi)$, of figure positions dependent on background velocity, we solve the Fokker-Planck equation derived above, but for the potential, $V(\varphi_F, \omega_G)$. The analytical solution for this type of Fokker-Planck equation for arbitrary potentials can be found in [S13]. With this, we can calculate the probability distribution for the figure in closed-loop, and compare it to the stationary solution of the bifurcation (see Figure S2G and Figure 3A bottom). Note how the mode of the distribution shifts in position and how the distribution becomes flatter when getting closer to the critical velocity.

5.9 Summarizing the phenomenological model

We derived an analytical model for an asymmetric motion detection pathway from fundamental response properties of HS-cells. We showed that this model is capable of performing figure fixation in a manner equivalent to a classical model [S12, S13]. Furthermore, utilizing a novel aspect of our model, its explicit dependence on arbitrary visual input, we also showed that it predicts the displacement of the fixation point as a function of background motion. This behavior was previously argued to result from a motion independent position pathway [S15]. Thus, from a theoretical perspective, a motion pathway alone leads to responses that have been argued to require a position pathway.

Supplemental References

S1. Straw, A. D., and Dickinson, M. H. (2009). Motmot, an open-source toolkit for realtime video acquisition and analysis. Source Code Biol. Med. 4, 5.

S2. Maimon, G., Straw, A. D., and Dickinson, M. H. (2010). Active flight increases the gain of visual motion processing in Drosophila. Nat. Neurosci. *13*, 393–399.

S3. Stowers, J. R., Fuhrmann, A., Hofbauer, M., Streinzer, M., Schmid, A., Dickinson, M. H., and Straw, A. D. (2014). Reverse engineering animal vision with virtual reality and genetics. Computer *47*, 38–45.

S4. Lindemann, J. P., Kern, R., van Hateren, J. H., Ritter, H., and Egelhaaf, M. (2005). On the computations analyzing natural optic flow: quantitative model analysis of the blowfly motion vision pathway. J. Neurosci. *25*, 6435–6448.

S5. Borst, A., Reisenman, C., and Haag, J. (2003). Adaptation of response transients in fly motion vision. II: Model studies. Vision Res. *43*, 1309–1322.

S6. Krapp, H. G., Hengstenberg, R., and Egelhaaf, M. (2001). Binocular contributions to optic flow processing in the fly visual system. J Neurophysiol *85*, 724–734.

S7. Borst, A., Egelhaaf, M., and Haag, J. (1995). Mechanisms of dendritic integration underlying gain control in fly motion-sensitive interneurons. J. Comput. Neurosci. *2*, 5–18.

S8. Hausen, K. (1982). Motion sensitive interneurons in the optomotor system of the fly. II. The horizontal cells: receptive field organization and response characteristics. Biol. Cybern. *46*, 67–79.

S9. Schnell, B., Joesch, M., Forstner, F., Raghu, S. V, Otsuna, H., Ito, K., Borst, A., and Reiff, D. F. (2010). Processing of horizontal optic flow in three visual interneurons of the Drosophila brain. J. Neurophysiol. *103*, 1646–1657.

S10. Borst, A., and Bahde, S. (1986). What kind of movement detector is triggering the landing response of the housefly? Biol. Cybern. *55*, 59–69.

S11. Reichardt, W., and Varju, D. (1959). Übertragungseigenschaften im Auswertesystem für das Bewegungssehen [(Conclusions from experiments on the beetle Chlorophanus viridis)]. Zeitschrift für Naturforsch. B *14*, 674–689.

S12. Poggio, T., and Reichardt, W. (1973). A theory of the pattern induced flight orientation of the fly Musca domestica. Kybernetik *12*, 185–203.

S13. Reichardt, W., and Poggio, T. (1975). A theory of the pattern induced flight orientation of the fly Musca domestica II. Biol. Cybern. *18*, 69–80.

S14. Kazakov, I. Y. (1961). Problems of the theory of statistical linearization and its applications. In Automatic and remote control. Proc. I. Int. Congr. IFAC, Moscow 1960, J. Coales, ed. (London: Butterworth).

S15. Bahl, A., Ammer, G., Schilling, T., and Borst, A. (2013). Object tracking in motion-blind flies. Nat. Neurosci. *16*, 730–738.

6 Quantifying T4/T5 motion-vision dependent object tracking in *Drosophila* tethered flight

photo by Sayan Soselisa

type	*unpublished manuscript*
authors	Andreas Poehlmann (AP), Sayan J. Soselisa (SJS), Lisa M. Fenk (LMF), Andrew D. Straw (ADS)
contributions	AP, SJS, LMF and ADS conceived the experiments and simulations. AP and SJS performed the experiments. AP analyzed the experimental data. AP performed the modeling and simulations. AP, SJS, LMF and ADS wrote the manuscript.

Quantifying T4/T5 motion-vision dependent object tracking in *Drosophila* tethered flight

Andreas Poehlmann[1,3], **Sayan J. Soselisa**[1,3], **Lisa M. Fenk**[2,3], **Andrew D. Straw**[1,3]

[1]Institute of Biology I and Bernstein Center Freiburg, Hauptstr. 1, 79104 Freiburg, Germany
[2]Laboratory of Integrative Brain Function, The Rockefeller University, New York, NY 10065, USA
[3]Research Institute of Molecular Pathology, Vienna Biocenter, Dr. Bohr-Gasse 7, 1030 Vienna, Austria

Abstract How neural circuits govern behavior is a key question in neuroscience. Circuits that process visual information to control *Drosophila* locomotion have been studied in detail, but contributions of various pathways to flight control remain unclear. Here, we measure the system dynamics of vertical black bar tracking in tethered flight for flies with intact and synaptically silenced T4 and T5 motion processing neurons, allowing us to investigate motion-vision dependent object responses. We find the estimated T4/T5 dependent contribution to be well approximated by an existing visual system model based on asymmetric elementary motion detectors. Furthermore, the model predicts many different tracking behaviors, including some previously argued to require motion-vision independent circuitry. Together, experiment and theory suggest that T4/T5 dependent circuits mediate, in addition to wide-field optomotor responses, short time scale object tracking behavior. This uniquely shows how one individual neuronal pathway can contribute to distinctly different behaviors.

Introduction

Vision is a key element in the survival and behavior of many animals. Especially while flying, many species have to rely predominantly on visual input. The fast dynamics during flight require visually-guided flight behavior like chasing, tracking, and avoidance behaviors to operate on very short timescales. How these fast object behaviors are implemented on an algorithmic and neuronal level is yet to be fully understood. With its comparatively small brain consisting of only about 100.000 neurons and low resolution compound eyes, *Drosophila melanogaster* is a well suited model system for these studies.

Two important visual behaviors in *Drosophila* are the optomotor response to panoramic motion, and small field object tracking. The optomotor response is a behavior which serves to minimize visual motion with compensatory movements (***Hassenstein and Reichardt, 1956***) and is used for orientation stabilization. The neuronal substrate responsible for mediating the optomotor response has been well characterized. Optomotor responses in walking flies are strongly impaired when T4 and T5 neurons (local motion detectors) are genetically silenced (***Bahl et al., 2013***). These cells provide main visual input to horizontal system (HS) cells (***Schnell et al., 2012***), wide-field motion sensitive neurons that were long thought to be involved in optomotor responses. Indeed, activation of HS cells leads to turns of the head and wings (***Haikala et al., 2013***), whereas inactivation of HS cells was shown to reduce optomotor responses of the head (***Kim et al., 2017***). When presented with visual motion stimuli, behavioral output (***Goetz, 1964***), neuronal responses of T4 and T5 (***Silies et al., 2014***) and responses of downstream HS cells (***Schnell et al., 2010***) are consistent with mathematical descriptions of variants of the Hassenstein-Reichardt elementary motion detector (EMD) (***Hassenstein and Reichardt, 1956***; ***Reichardt, 1987***). The field of insect vision research is currently narrowing down the exact neuronal implementation of these EMDs which mediate motion responses and optomotor behavior (***Borst et al., 2010***; ***Silies et al., 2014***).

Object tracking behavior, on the other hand, describes the active reorientation of the fly to keep small

field objects at the visual midline. The neuronal substrate responsible for mediating object tracking is yet to be fully discovered. It has been shown, that object fixation behavior towards vertical bars in walking flies is independent of the output of T4 and T5 neurons (***Bahl et al., 2013***). Albeit, it has also been shown that tethered flight object tracking in a figure ground discrimination task depends on intact T4/T5 neurons (***Fenk et al., 2014***). Since optomotor behavior relies on visual motion information, and object tracking behavior requires positional information in the visual stimulus per definition, it may be interesting to consider if the neuronal circuits mediating either behavior are separate. The fact that the linearized mathematical description of single degree of freedom tracking behavior dynamics separates into one purely position-dependent and one motion-dependent term (***Poggio and Reichardt, 1973***; ***Reichardt and Poggio, 1975***) can be seen as further evidence supporting separate circuitry. It is often argued, that motion-dependent systems cannot be responsible for object tracking because they are susceptible to low-frequency drift away from the tracked object (***Fox et al., 2013***). This interpretation is problematic, since it has been shown that neuronal system models based on properties of a single type of visual neurons are able to mediate the responses associated to the position-dependent term as well as the responses associated to the motion-dependent term (***Poggio and Reichardt, 1973***, ***1981***; ***Fenk et al., 2014***).

As mentioned, it has been shown that object tracking can be mediated by T4/T5 independent and T4/T5 dependent circuits (***Bahl et al., 2013***; ***Fenk et al., 2014***). In tethered flight, T4/T5 independent object tracking was much more pronounced under artificially weak closed loop coupling conditions, which led us to hypothesize that T4/T5 independent object tracking operates on longer timescales compared to T4/T5 mediated object tracking (***Fenk et al., 2014***). Because of the unclear overlap of object responses mediated by T4/T5 dependent and T4/T5 independent circuits, we try to separate the two systems on a temporal level by exploring object tracking behavior under external perturbation. Here we show that a T4/T5 independent object tracking system is sufficient to explain fly behavior in closed loop tethered flight under slow speed perturbations, whereas at faster speeds, intact T4/T5 cells are required for tracking. We measure the transfer function for black bar tracking with intact flies and motion-blind flies in which the T4 and T5 neurons have been synaptically silenced. Under the assumption that the fly's visual tracking behavior can be well approximated by a linear time-invariant system (as tested by ***Roth et al. 2012***), the transfer function is a full description of the input-output relations. We further show that an estimated object tracking transfer function exclusively based on T4/T5 output can be well approximated using a simulated transfer function of a Hassenstein-Reichardt correlator model with an asymmetric motion response. Additionally, we simulate many object behaviors, including some which have been previously used to argue for additional object tracking circuitry independent of the neuronal circuit responsible for motion responses.

Results

Perturbed object tracking of flies with intact and with blocked T4/T5 cells

We wanted to investigate if the two neuronal circuits underlying object tracking behavior operate on different timescales. Assuming one of these circuits mediates tracking behavior on short timescales, we expect that genetically blocking its input neurons will impair the fly's ability to compensate fast perturbations in the angular position as well as the angular velocity domain.

We ran tethered closed loop object tracking experiments on flies in which synaptic transmission was blocked in T4 and T5 neurons by expressing tetanus toxin ("T4/T5 block flies", *;UAS-TNTe,tsh-GAL80;GMRSS00324-splitGAL4;*), and on flies that express an inactive variant of the toxin in the same neurons ("T4/T5 control flies", *;UAS-TNTin,tsh-GAL80;GMRSS00324-splitGAL4;*). Using the cell-specific split GAL4 driver line (***Schilling and Borst, 2015***) minimizes the possibility of inducing motor defects. We used a tethered flight setup as depicted in ***Figure 1—figure supplement 1A*** to show a visual stimulus that consisted of a 20 deg wide black bar moving on a white background. The fly's wing movement was analyzed using a video camera and realtime image processing software running at 120 Hz. The difference in leading wingstroke angles (delta wing beat amplitude Δ_{WBA}) which is approximately proportional to yaw torque was measured in realtime and coupled back to give the fly control over its simulated orientation towards the bar (***Figure 1—figure supplement 1B***). Experiments consisted of closed loop fixation interrupted by 10 s long trials during which a constant angular torque bias was added to the tethered flight

dynamics. Torques were randomly selected from a predefined set. To make comparison between perturbation torque and measured Δ_{WBA} easier, torque is converted to its equivalent Δ_{WBA} perturbation offset throughout the following section.

Figure 1A shows averaged Δ_{WBA} for three trials with equidistantly spaced, increasing absolute perturbation torque values. To still be able to fixate the bar, flies need to compensate the added perturbation by adjusting their Δ_{WBA} to the given trial condition. Control flies were able to compensate the perturbation almost completely up to bias amplitudes slightly above 15 deg, and start to show decreased performance for higher amplitude trials. T4/T5 blocked flies on the other hand, show decreased performance already below 15 deg perturbations. Furthermore, they take several seconds to reach an average Δ_{WBA} plateau that is far below the required amplitude to compensate the perturbation and therefore fail to keep the stripe stationary. Investigating the plateau Δ_{WBA} reached by flies across varying perturbation offsets (***Figure 1B***) reveals that for very small offsets both blocked and control flies are able to adjust to the trial conditions (plateau amplitude on diagonal), but for absolute offsets larger than about 15 deg, blocked flies fail to adjust. The plateau Δ_{WBA} returns to almost zero for higher perturbation amplitudes. Δ_{WBA} distributions during non-perturbed bar tracking show that the maximum observed Δ_{WBA} range in T4/T5 blocked flies is larger compared to control flies (***Figure 1—figure supplement 1C***), confirming that failure to compensate the perturbation is not due to a genetically introduced motor defect limiting maximum wing movement, but due to a reduced visual response to the bar.

Figure 1C shows distributions of angular position during the last 5 s of the trial duration, at which point transient changes in the position distribution are negligible. While the width and mode of the distributions are very similar between control and blocked flies during low amplitude trials, the distributions for blocked flies become relatively uniform for perturbation offsets larger than 11.5 deg. The fact that the mode of the angular position distribution is similarly shifted during small torque offset trials for both genotypes suggests that the fixation behavior is not fundamentally different from the fixation behavior that only control flies are capable of at higher offsets. As a distribution-independent measure of fixation quality, we plot the full width at half maximum (FWHM) of angular position distributions during the last 5 s of the trial in ***Figure 1D***. While blocked flies are able to keep the stripe comparably stationary at low perturbation amplitudes, they rapidly fail to do so with increasing perturbation amplitude. Interpreting these results using theoretical work from ***Reichardt and Poggio*** (***1976***) indicates, that while the positional term describing tracking responses in the underlying dynamic equations for these perturbed object tracking trials is similarly shaped for blocked and control flies, it has to have a smaller maximum amplitude for blocked flies. This would then explain why tracking responses in blocked flies are completely disrupted at lower perturbation offsets compared to control flies, and why measurements of positional responses comparing blocked and control flies without external perturbation should not differ in shape, but in amplitude (as seen in ***Bahl et al. 2013***).

Object tracking dynamics of flies with intact and with blocked T4/T5 cells

Since this hypothesized reduced amplitude of the positional term does not necessarily mean that the tracking performance differs between block and control flies or that the time scale on which object responses operate are different, we wanted to investigate the dynamics of object tracking under time varying perturbation conditions. We used a similar method to the one previously described in ***Roth et al.*** (***2012***) to measure the open-loop system dynamics of object tracking under perturbed closed-loop conditions. It directly measures the transfer function describing the fly's ability to track moving black vertical bars. The frequency dependence of the transfer function's gain (absolute amplitude) and phase give direct and intuitive insight into how well a fly is able to follow the trajectory of a moving bar and how much it lags behind the bar's movement. During the experiment, the fly's Δ_{WBA} is close-loop coupled to the stimulus, so that the fly is in control over its orientation in the world coordinate system (see ***Figure 2—figure supplement 1A***). A black vertical bar of width 15 deg is centered at angular position 0 deg in world coordinates, and its position is perturbed during the experiment. The perturbation is defined by a logarithmic chirp of increasing frequency and decreasing amplitude (see Materials and Methods). This limits the maximum apparent angular velocity during the stimulus presentation, and still covers a wide range of perturbation frequencies, which allows us to recover the empirical transfer function under the assumption of linearity (shown to be valid within margins of error by ***Roth et al. 2012***).

Figure 2A shows the averaged fly orientation in the world coordinate system as well as the Δ_{WBA} for control

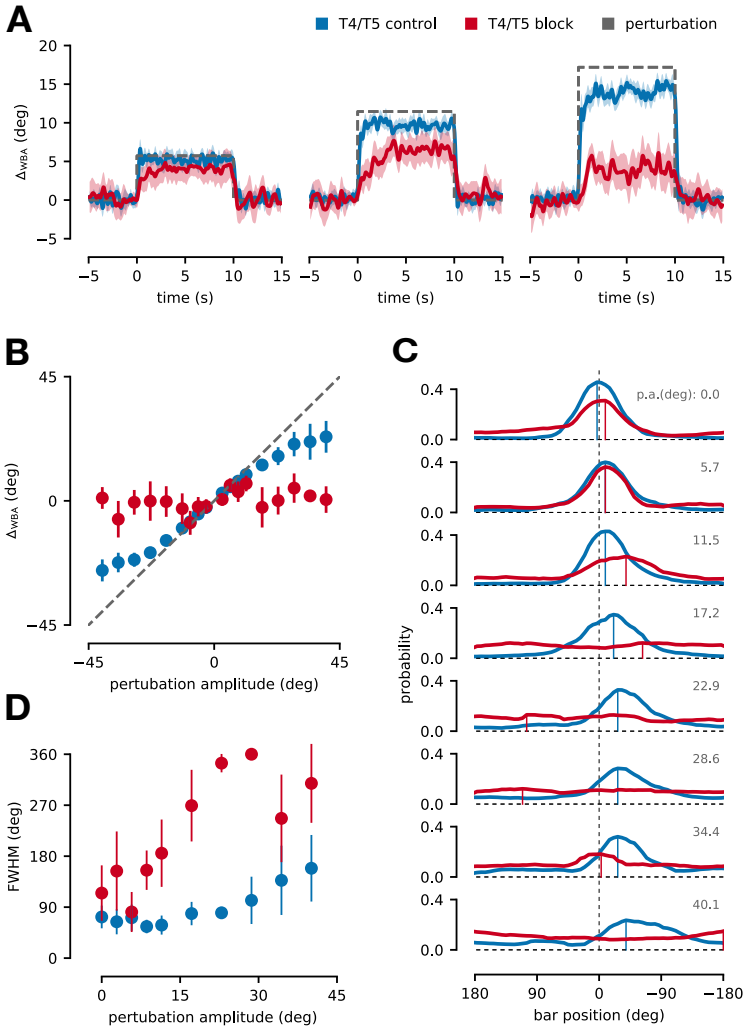

Figure 1. Delta wing beat amplitude offset experiment. Control flies blue, N=11, total number of trials m=55. Blocked flies red, N=9, m=45, **(A)** Averaged delta wing beat amplitude traces over time for equidistantly spaced, increasing perturbation torque values. Shaded area indicates standard error of mean across flies. The dashed black line shows the Δ_{WBA} equivalent of perturbation torque over time for each trail. Control flies manage to almost fully compensate perturbation offsets up to roughly 15 deg but show decreasing ability to do so at higher perturbations. Blocked flies already start to fail at perturbations offsets of about 10 deg and take longer to plateau at a lower value. For increasing perturbation offsets blocked flies responses tend towards zero again. **(B)** Average plateau delta wing beat amplitude during last 5 s of perturbation. Dashed line indicates perturbation offset. Errorbars show standard deviation across individual flies. Control flies can compensate up to higher perturbation offsets. Blocked flies' plateau amplitudes tend towards zero for higher offsets. **(C)** Histograms of bar position for different perturbation offsets during last 5 s of trial. Negative offset amplitude trials have been mirrored and grouped together with positive amplitude trials. Top to bottom shows increasing perturbation amplitude offsets. Mode of distribution is marked with vertical line. At small offsets, distribution modes are shifted in same directions for control and blocked flies. **(D)** FWHM of bar position distributions during offset perturbation. Dataset mirrored and combined like in (C). Errorbars indicate standard deviation across flies. The FWHM increases dramatically for blocked flies with increasing perturbation amplitude beyond 15 deg.

Figure 1–Figure supplement 1. **(A)** Tethered flight setup schematic. **(B)** Δ_{WBA} tracker visualization. **(C)** Δ_{WBA} distributions during closed loop.

and blocked flies during the chirp stimulus. Initially, flies of both genotypes are are able to change their orientations to follow the perturbation, and require only small modulation in Δ_{WBA} since the bar is moving comparatively slowly. Control flies keep the bar at the visual midline over the whole time course of the trial. Their orientation follows the trajectory defined by the logarithmic chirp and the Δ_{WBA} is most strongly modulated at around 60 s. At roughly 80 s the fly does not completely follow every oscillation of the bar anymore, but still keeps it perfectly in front. Blocked flies, on the other hand, lose the ability to reliably track the bar at around 40 s, as indicated by the FWHM of the bar position distribution reaching 360 deg (see ***Figure 2—figure supplement 1B***). Additionally the stimulus progression had to be reset more often compared to control flies (refer to Materials and Methods and ***Figure 2—figure supplement 1C***). In the Δ_{WBA} time series the blocked flies show an almost random response, fluctuating around zero, with large error. This could indicate that they can't visually detect the bar anymore at these perturbation frequencies.

Interpreting the chirp perturbation as the input to a linear system and the temporally integrated Δ_{WBA} as its output (using the closed-loop dynamic equation), we can calculate the empirical transfer function for both genotypes (see Materials and Methods). ***Figure 2B*** shows the recovered transfer functions for control and blocked flies, plotting both gain and phase. A gain of 1 indicates a perfect match to the input offset position amplitude and a phase of 0 indicates zero lag following of the bar. Control flies are able to follow the perturbations in the position domain up to frequencies of about 2 Hz, after which the gain drops dramatically. The flies are still fixating the bar even at higher frequency (average bar position is at the visual midline, see ***Figure 2—figure supplement 1B***), but do not follow the oscillations anymore. The measured empirical transfer function is in slight discrepancy with ***Roth et al. (2012)*** which measured a dip in object tracking performance at around 1 Hz. It is possible that this measured dip is an artefact of the shadow based Δ_{WBA} tracking method. When observing the flies at perturbation frequencies of around 1 Hz we measure an almost threefold increase in leg extensions (***Figure 2—figure supplement 1D***), consistent with T4/T5 mediated landing responses (***Schilling and Borst, 2015***). This leg extension behavior could interfere with shadow based measuring techniques, but can be dealt with in image based measuring techniques, like the one used here (see Materials and Methods and ***Figure 1—figure supplement 1B***). T4/T5 block flies are able to follow perturbations at low frequencies, but show a continuous drop in tracking performance starting at 0.6 Hz. The almost linear drop in phase starting at 0.2 Hz indicates a slow response time for the T4/T5 blocked tracking response, in line with the bad tracking performance at higher frequencies. At perturbation frequencies of 1 Hz, the blocked flies' performance is almost an order of magnitude worse than in control flies. The higher the perturbation frequency, the less the blocked flies are able to keep the bar stationary. This strongly suggests that while T4/T5 independent object tracking is sufficient for very slow moving objects, faster moving object tracking requires intact T4/T5 neurons, which further supports our previous observation. In other words, the T4/T5 independent object tracking system is only able to mediate black bar tracking up to perturbation frequencies of $\approx$ 0.6 Hz, at which the T4/T5 dependent object tracking system is mainly responsible for tracking behavior as measured directly by the transfer functions presented here. During flight maneuvering we expect that only motion-vision based object responses operate fast enough to reliably facilitate object tracking.

Simulation of pure motion-vision based object tracking dynamics

In previous work we showed that simple models based on asymmetric motion responses are able to mediate object fixation (***Fenk et al., 2014***). We tested our numerical model adapted to *Drosophila* (see Materials and Methods) under the same logarithmic chirp perturbed closed-loop object tracking conditions as our real fly experiments. Ideally, we would want to compare the results of the simulations to responses of flies in which every visual response not mediated by T4/T5 is genetically blocked. Since the neuronal substrate for these object responses is currently unknown, this is not yet possible. The best possible approximation can be obtained by assuming that object tracking behavior across flies can be described as the linear sum of the T4/T5 independent and T4/T5 dependent system. Using this approach, we recover an estimation of the pure T4/T5 response as the difference of the averaged control and block fly responses. ***Figure 2C*** shows fly orientation and Δ_{WBA} for the estimated pure T4/T5 system (orange) as well as the simulated asymmetric motion model (green). While it is very hard to make any meaningful comparison in the position domain, the Δ_{WBA} results are in good agreement for higher perturbation frequencies. The empirical pure T4/T5 object tracking transfer function, as well as the

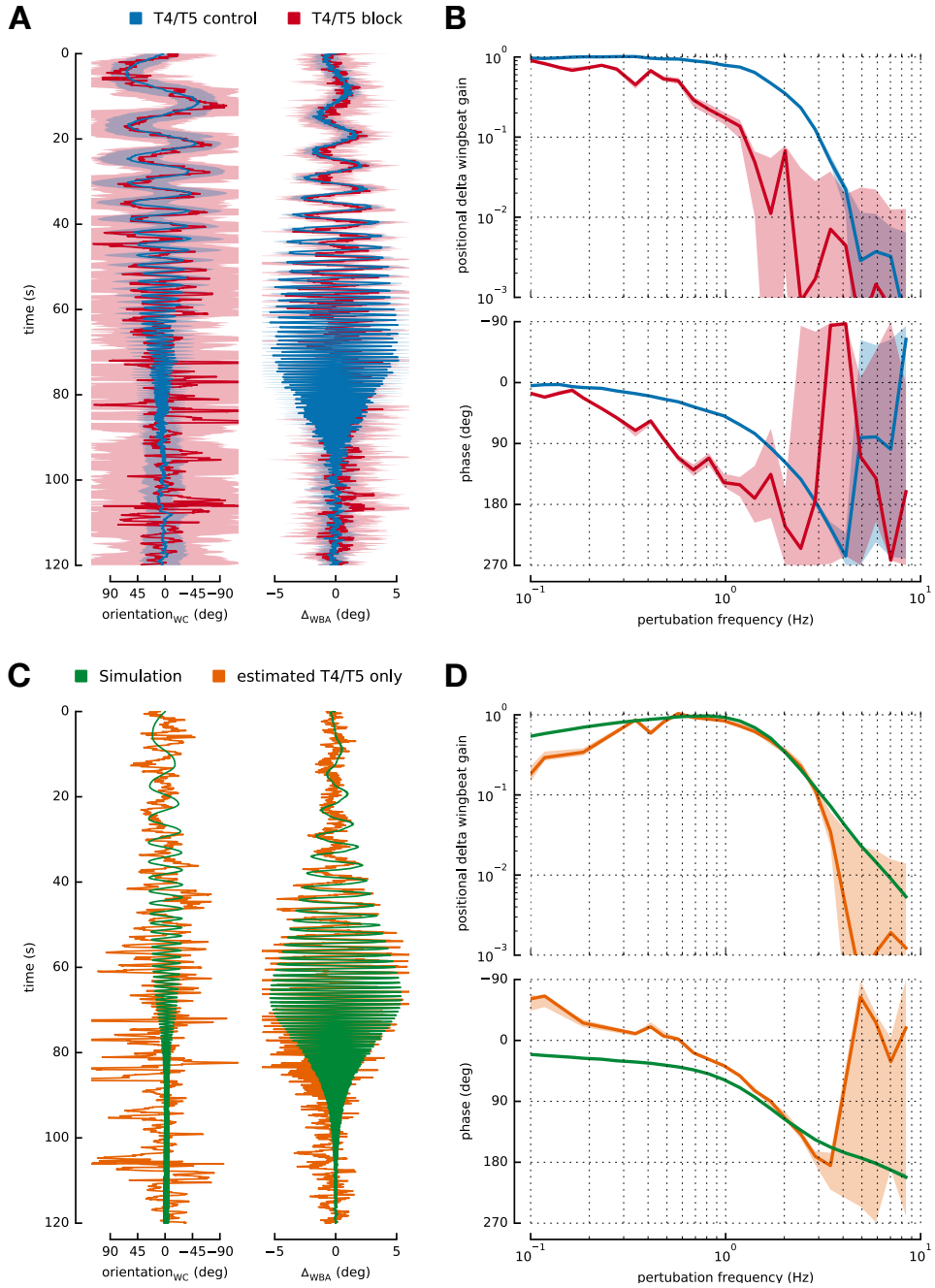

Figure 2. Logarithmic chirp experiment. Control flies blue, N=14, total number of trials m=66. Blocked flies red, N=14, m=64, **(A)** Averaged fly orientation in world coordinate system and median Δ_{WBA} over time. Shaded area shows FWHM for position plot and median absolute deviation for Δ_{WBA} plot. Position: Control flies follow the object position perturbation almost perfectly. Blocked flies do so for low perturbation frequencies but fail to orient correctly at higher frequencies. Δ_{WBA}: While almost identical in performance at low perturbation frequencies, blocked flies fail to keep up with control flies starting at $\approx 60\,s$. **(B)** Bode plot of empirical transfer functions recovered from closed loop chirp experiments. Blocked flies tracking performance drops at lower frequencies compared to control flies. At 1 Hz blocked tracking performance is almost an order of magnitude worse than control performance. **(C)** Identical to (A), showing estimated T4/T5 only responses and numerical simulation results of an asymmetric motion system. Error estimates have been omitted for both. **(D)** Identical to (B). Approximated pure T4/T5 motion system responses should be interpreted as lower boundary on real transfer function. Above 0.6 Hz the approximated and numerical transfer functions are in remarkable agreement.

Figure 2–Figure supplement 1. **(A)** Coordinate systems. **(B)** Bar LC positions. **(C)** Reset event probability. **(D)** Leg extension probability.

simulated asymmetric motion model transfer function, are shown in ***Figure 2D***. Considering the crude way of approximating the pure T4/T5 system response, the experimental and simulation data are in remarkable agreement at frequencies above 0.6 Hz. The discrepancy at lower frequencies can be easily explained by the fact that at these frequencies the T4/T5 independent system is already sufficient to compensate the perturbations. If the two object tracking systems mediate redundant object responses at low frequencies, it directly follows that estimates of the pure T4/T5 motion response (under the assumption of linearity) will always underestimate the real contribution of the T4/T5 motion system. Our approximation should be interpreted as the lower boundary of object tracking responses of a pure T4/T5 motion system. A similar argument can be made for the phase, where the observed nonsensical phase lead of the estimated pure T4/T5 motion system should be seen as the lower bound.

Overall the experimentally approximated and numerically simulated pure motion system transfer functions agree at frequencies above 0.6 Hz, at which the influence of a T4/T5 independent system should be negligible. Interestingly, the simulated asymmetric motion system predicts very robust fixation at high frequency perturbations, which the blocked flies completely fail at, but control flies excel at. It should be noted, that since our numerical model is a pure motion vision Hassenstein-Reichardt correlator based model, it shows no response in the limit of zero velocity. The measured transfer functions for blocked flies and control flies together with the simulated asymmetric motion system transfer functions suggest, that black bar tracking responses are redundantly mediated by a T4/T5 independent and T4/T5 dependent system up to frequencies of about 0.6 Hz. For higher perturbation frequencies the object tracking behavior seems to be mainly mediated by the T4/T5 dependent motion-vision system.

Prediction of closed loop object tracking tasks using motion-vision only

The high frequency component of the empirical transfer function for perturbed closed loop bar tracking is well explained by our pure motion response based model. We therefore decided to simulate already published object tracking experiments under various closed loop tethered flight conditions. All following experiments were originally done on flies with intact T4/T5 neurons, and some were used to justify or hypothesize the need for additional non-motion based object response circuitry in the fly visual system based on the observed behavior. To be able to intuitively understand the results shown in this section it is best to think about these experiments in terms of the analytical description formulated in ***Fenk et al.*** (***2014***). Briefly summarizing, given a small field object stimulus, a motion-vision based visual system model with asymmetric response amplitudes towards progressive and regressive motion can be mathematically described by a linearized differential equation, which separates into a position dependent term and a motion dependent term. The position dependent term is mainly defined by the difference in receptive fields of the inputs to the elementary motion detectors. The motion response is mainly defined by the delay time constants used in the correlator model. For a small field bar stimulus on a structured background, the linearized second order differential equation can basically be expressed as:

$$\ddot{\varphi} + r\dot{\varphi} = -g_{\mathrm{FG}} D_{\mathrm{FG}}(\varphi) - g_{\mathrm{FG}} M_{\mathrm{FG}}(\dot{\varphi}) - g_{\mathrm{BG}} M_{\mathrm{BG}}(\omega_{\mathrm{BG}})$$

where φ describes the bar position relative towards the visual midline, r emulates the aerodynamic dampening, g_{FG} and g_{BG} are the close loop figure and background gain, D_{FG} and M_{FG} are the position and motion response terms originating from the small field stimulus and the asymmetric motion response, M_{BG} is the motion response term for the background, and ω_{BG} is the angular velocity of the background. Under normal gain coupling conditions D_{FG} yields a stable fixpoint at the visual midline. M_{FG} and M_{BG} (if moving together with the bar) render velocity $0\,\mathrm{deg\,s^{-1}}$ a stable condition.

We encourage the reader to directly compare our simulation results with the published work. Care has been taken to stylistically reproduce the published experimental figures using our model simulation results, to facilitate direct comparison.

Monocular object tracking behavior has been previously measured in *Drosophila* to investigate the influence of the binocular overlap region on the angular position dependence of object responses (***Geiger et al., 1981***). ***Figure 3A*** shows simulation results for black bar position histograms for flies under normal coupling and various eye occlusion conditions. From top to bottom, these conditions are no occlusion, left eye covered with screen,

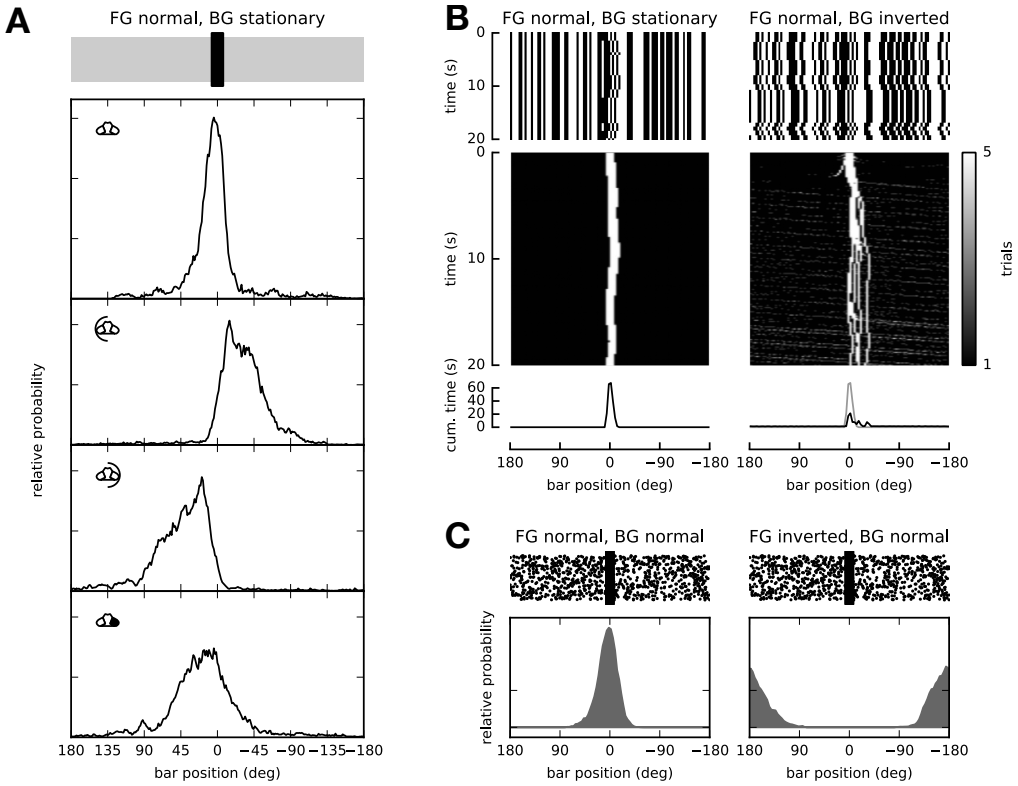

Figure 3. Closed loop simulation results. **(A)** Comparison of tracking behavior of flies under normal conditions (top), with a screen placed in front of the left eye (2nd from top), with a screen placed in front of the right eye (2nd from bottom) and the right eye covered with paint (bottom). One eyed fixation distributions roughly double in width compared to normal fixation. Most likely fixation positions are shifted away from the occluded eye. See ***Geiger et al.*** (***1981***) Figure 6. **(B)** Inverted background gain simulation. Top row: space-time plots of stimuli. Middle row: space-time plot of tracking positions. Bottom row: histogram of cumulative time of bar at angular position. Left column: Bar coupled normally, background stationary. The bar is fixated in front of the fly across several trials, as can be seen by maximum of histogram. Right column: Bar coupled normally, background coupled inversely. While the stationary bar position at the visual midline is inherently unstable, it can stay there for some amount of time. The histogram shows a smaller but positionally consistent mode. See ***Fox et al.*** (***2013***) Figure 2. **(C)** Closed loop tracking of inversely coupled bar. Left: Background and bar are coupled normally and therefore move together. The bar is fixated at the visual midline. Right: Background coupled normally, bar coupled inversely. The stationary bar is still a stable condition but the stable position is now at the back of the fly. See ***Heisenberg and Wolf*** (***1984***) Figure 105.

Figure 3–Figure supplement 1. Simulated torque responses towards a moving black bar.

right eye covered with screen and right eye covered with paint. Since the background is unstructured, the only relevant term for tracking is the position dependent term $D_{\mathrm{FG}}(\varphi)$. When no eye is occluded the bar is fixated at the visual midline, where D_{FG} has its zero crossing. When the screen was placed on one side, fixation was only possible when an additional torque offset was added to the torque produced by the simulated fly, and half of this offset torque was used to produce the covered eye results (identical to ***Geiger et al. 1981***). This is intuitively easy to understand when considering that the occlusion of one eye will basically set D_{FG} to zero on one half of the visual field, effectively removing its zero-crossing required for fixation. Adding a constant torque offset to the bar, shifts the position response vertically, creating a new zero-crossing along the edge of D_{FG}, which, depending on its slope, is shifted away from the visual midline (see ***Fenk et al. 2014*** for reference; in agreement with ***Virsik and Reichardt 1976***). That covering an eye with paint creates a less steep slope of the fixation histogram is easily explained by the decreased slope at the visual midline of D_{FG} when only one receptive field is considered. Together with a shift of the onset of the position response during open loop rotation experiments (see ***Figure 3—figure supplement 1***), our model reproduces the tracking experiments from ***Geiger et al.*** (***1981***) using an asymmetric motion vision based model, with no additional non-motion based position system.

Inverted background gain coupling experiments have been previously used to hypothesize the active suppression of responses to moving wide field stimuli in the presence of a small field object (***Fox et al., 2013***). ***Figure 3B*** shows the result of an inverted background gain coupling simulation. The left column shows the simulation results for a stationary background. Across several trials, the bar is fixated at the visual midline. The right column then shows a rather artificial experimental scenario in which the torque generated by the fly is normally coupled to a small figure initially in front of the fly, but also inversely coupled to the background pattern. This means that movement of the bar produces opposite movement of the background pattern. It is argued that the reduced but non zero tracking behavior, as evident by the maximum of the bar position histograms, is proof that there must be wide field ground systems and figure systems operating in parallel. Since g_{FG} is positive, the position in front and angular velocity zero would be a stable fixpoint. But the inverted background coupling together with the strong motion response towards the background renders the stationary bar inherently unstable. For very small deviations from the unstable position in front of the fly the bar can stay roughly at the visual midline for a reasonable amount of time. If it deviates too much, the system locks into another stable behavioral mode, which is determined by the maximum torque produced by a spinning wide field pattern, and manifests as constant spinning of the background and the bar. To extend the time a bar can stay at the unstable point at the visual midline, we can reduce the closed loop gain to a weak coupling condition. Our simulation results reproduce this experiment with only a single pure wide field asymmetric motion system, however only under the condition of weak closed loop coupling compared to previous experiments (like in ***Figure 3A***). But examination of maximum bar velocities (slopes of bar position traces) in ***Fox et al.*** (***2013***) suggest that these experiments were indeed run under weak coupling conditions (as indicated by the maximum observed slope of roughly $120\,\mathrm{deg\,s^{-1}}$). Running these experiments with initial bar positions at the side would immediately reveal that the position at the visual midline is unstable.

Another artificial scenario which was used in learning experiments is inverted figure coupling with normally coupled background (***Heisenberg and Wolf, 1984***). ***Figure 3C*** shows tracking behavior under these conditions. Again thinking about this in terms of the analytical model, this time the correctly coupled large background motion response, which outweighs the inversely coupled bar motion response, renders the zero velocity state stable. The inverted gain on the bar forces the positional term of the bar response to be unstable at the visual midline but now stable at the back of the fly. Our asymmetric motion model correctly predicts the initially measured anti-fixation behavior, but can of course not predict the learning behavior as shown in ***Heisenberg and Wolf*** (***1984***).

In summary, our asymmetric motion based visual system model correctly predicts closed loop tracking behaviors with eye occlusion, under normal and inverted figure coupling as well as normal and inverted background coupling.

Prediction of open loop object tracking tasks using motion-vision only

To further demonstrate the predictive power of our asymmetric motion model, we wanted to investigate different types of open loop behaviors that have been previously published.

Oscillating bar stimuli have been used to measure positional object responses because they reliably elicit visual tracking behavior (***Maimon et al., 2008***). ***Figure 4A*** shows the simulation of a fly responding to an open loop oscillating bar. The space-time plot (left) shows the time representation of the stimulus. A black bar of width 15 deg is oscillating at one of 5 different locations indicated by the black ticks on top. The Δ_{WBA} output of the simulated fly follows the oscillation of the bar. If the average position of the bar is to one side, the asymmetry in the motion response output leads to a shift of the average Δ_{WBA} to the same side. This is the most intuitive way to understand why asymmetric motion vision based systems lead to position system like responses. The right subplot shows the average Δ_{WBA} dependent on the average bar position. As it can be seen, this is in perfect agreement to predictions of the analytical model presented previously in ***Fenk et al.*** (***2014***) and basically shows the difference of the left and right receptive field of our visual model. The aversion behavior shown in ***Maimon et al.*** (***2008***) for black bars with smaller vertical extent can not be predicted by this one dimensional model.

Other more complex behaviors include responses to theta motion stimuli, which consist of moving objects which are themselves only defined by their internal pattern motion. ***Figure 4B*** shows simulation results of theta motion experiments like in ***Theobald*** (***2010***). The top row leaves the bar position amplitude fixed, while varying the bar/pattern amplitude ratio from −1 to 1. The bottom row leaves the pattern position amplitude fixed, while varying the pattern/bar amplitude ratio from −1 to 0 (refer to ***Theobald*** (***2010***) Figure 5/6 for space-time representations of each stimulus). It has been argued that the decrease in delay time across varying pattern/bar displacements from roughly 500 ms down to sub 100 ms, as well as the decrease in phase from roughly 120 deg down to sub 20 deg for varying bar/pattern displacement is a direct manifestation of the superposition of the outputs of separate subsystems with different dynamical properties. These subsystems would separately encode the 1st order motion of the object itself and the pattern motion inside the object. One of these systems would have short latency response and the other one a long latency response. It is hard to justify this argument when our asymmetric motion vision based model is able to reproduce this change in delay and phase without implementing multiple subsystems.

Finally, we wanted to investigate tracking behavior under a figure-ground discrimination experimental paradigm. ***Figure 4C*** shows results from spatio temporal action field (STAF) simulations as presented in ***Fox et al.*** (***2013***). STAF experiments simultaneously measure the impulse response towards two separate stepwise-moving patterns. One small-field figure pattern occludes the other wide-field background pattern. Impulse responses are then measured dependent on the position of the figure pattern during the measurement. The figure STAFs represent responses towards the figure pattern. Ground STAFs represent responses towards the background pattern. The figure and ground STAFs for increasing figure width show that starting at around 60 deg figure width we see a decrease in the amplitude of the ground STAF for positions in front of the fly. This becomes most evident when increasing the figure width even further. It has been argued that an active suppression of the ground response is responsible for the observed decrease in the ground STAF. This hinges on an observation that, when replacing the active figure with a gray pattern of the same width moving together with the background pattern, the suppression in the ground STAF does not happen. Our asymmetric motion based visual system model reproduces the same active ground suppression STAFs for figures of widths above 90 deg (***Figure 4C***) and displays the lack of ground suppression for the gray occlusion experiments (***Figure 4C—figure supplement 1***). The fact that the model does not reproduce the STAFs for very small figure widths is likely due to the wide receptive field width used in the model. But we want to emphasize that a Hassenstein-Reichardt correlator based model with an asymmetric motion response shows figure responses in STAF experiments and active background suppression, without having any of these properties implemented. Not all properties of the figure and ground STAFs can be recovered by simulating the experiments with these pure motion system models, but our simulation clearly illustrates how complex inputs to a very simple system can generate very complex outputs, without the need of active suppression mechanisms or parallel visual streams.

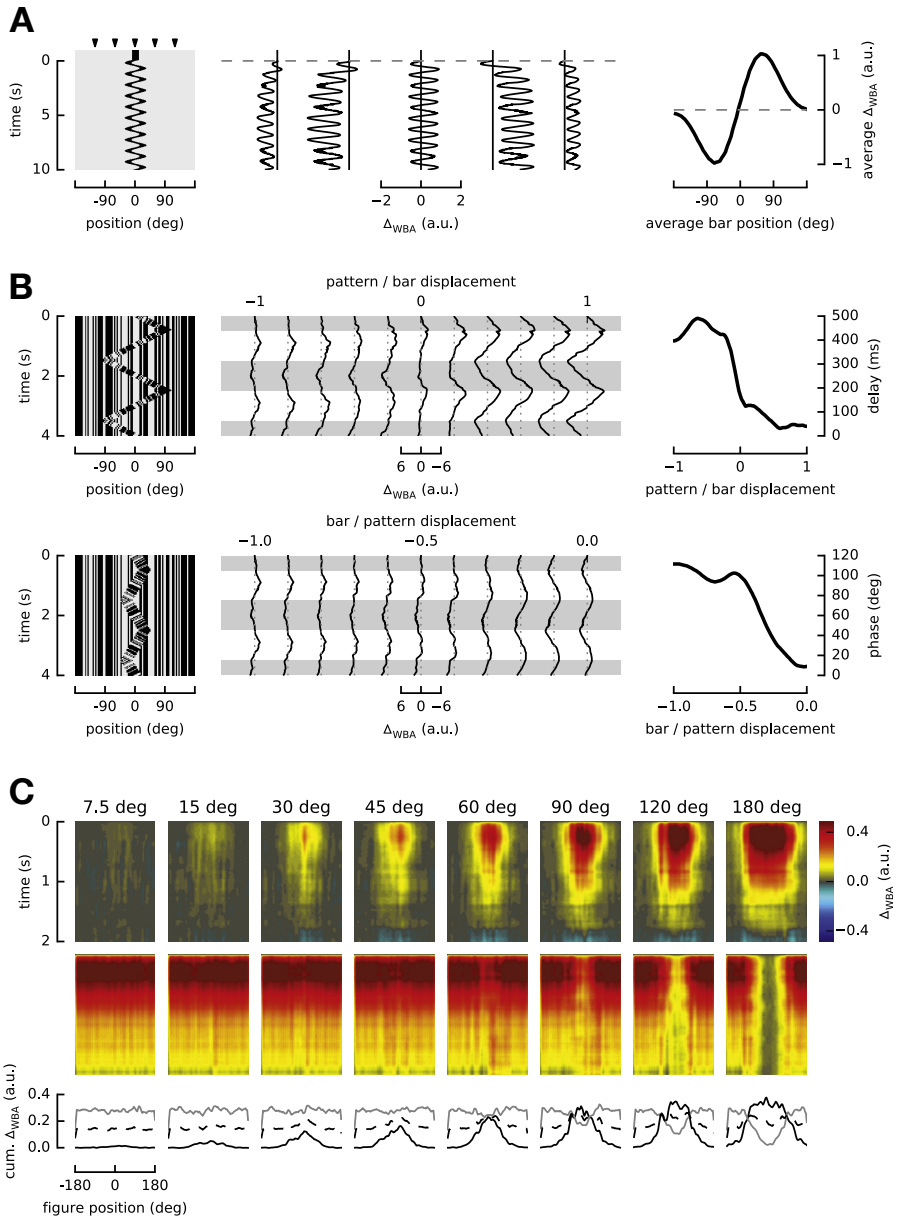

Figure 4. Open loop simulation results. **(A)** Δ_{WBA} responses to oscillating black bar of 15 deg width at different positions. Left: space-time representation of oscillating bar stimulus. Black ticks on top indicate the 5 different test conditions, at −120 deg, −60 deg, 0 deg, 60 deg and 120 deg. Center: Δ_{WBA} traces for the 5 tested stimuli. Δ_{WBA} shows position response like offset towards objects at either side. Right: Average Δ_{WBA} amplitude during trial for varying average bar positions. The resulting shape nice recovers the difference in receptive fields of the motion vision system. See ***Maimon et al.*** (***2008***) Figure 4. **(B)** Δ_{WBA} responses to theta motion stimuli. Left column: space-time representation of stimuli. Small bar is moving in a triangle wave pattern with periodicity of 2 s. Inner bar pattern is moving with same triangle wave function but 180 deg phase shifted. Middle column: Δ_{WBA} traces for respective stimuli. Right column: delay and phase dependency on amplitude ratios between bar and pattern amplitudes. Top row: pattern/bar amplitude varying between −1 and 1. The delay in Δ_{WBA} responses ranges from roughly 500 ms down to sub 100 ms when varying the ratio. Bottom row: bar/pattern amplitude varying between −1 and 0. The phase shifts from ≈ 120 deg down to sub 20 deg when varying the ratio. See ***Theobald*** (***2010***) Figure 5/6. **(C)** Figure-Ground STAFs for varying figure widths. Top to bottom: Figure STAFs, Ground STAFs and averaged response of the first 100 ms of the STAFs. Left to right: Increasing figure width. The Figure STAF response becomes prominent enough at roughly 60 deg to start to show a reduction in amplitude in the ground STAF. See ***Fox et al.*** (***2013***) Figure 6.

Figure 4–Figure supplement 1. Ground suppression control.

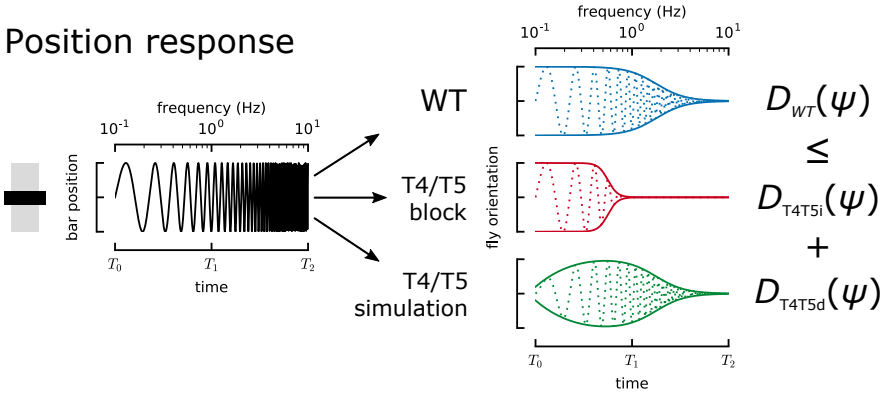

Figure 5. Summary: object tracking responses of a black vertical bar are mediated by T4/T5 independent (T4T5i) and T4/T5 dependent (T4T5d) circuits. Position responses are redundantly mediated by both systems at low perturbation frequencies. During short time scale perturbation, important during flight, only motion-computation based (T4/T5 dependent) systems are able to mediate object tracking.

Discussion

With our behavioral experiments, we were able to measure the empirical transfer functions for object tracking behavior in tethered flight for control flies, as well as for flies in which we blocked synaptic transmission in T4 and T5 cells. The transfer functions clearly show that motion-blind T4/T5-block flies are able to fixate an object that is perturbed at frequencies below 0.6 Hz, but fail to do so at higher perturbation frequencies. Additionally, we show that the difference in object tracking capability between control and blocked flies is well approximated using a simple Hassenstein-Reichardt-type elementary motion detector model with asymmetric motion response. This suggests that while object tracking can be mediated by a T4/T5 independent system for slow moving objects, it requires T4/T5 input if the object moves faster. We hypothesize that during free flight, where response times are critical, tracking behavior is predominantly mediated by a T4/T5 dependent motion-vision based circuitry (see ***Figure 5***).

Additionally, we used the asymmetric motion visual system model to predict multiple different types of closed loop and open loop fly behavior, ranging from simple tracking behavior, across more complex anti-fixation behavior to theta motion responses and figure-ground discrimination. That the model is able to predict this variety of experimental results without requiring adjustment of its internal parameters for each specific stimulus condition shows that motion-vision based object responses are robust enough to withstand the rigors of dynamic applications of biological systems. The argument that pure visual motion based systems are ill-suited for object tracking, because they fail to compensate low-frequency drift (***Fox et al., 2013***), can not be accepted, especially when many of the stimuli presented to measure position responses contain motion-information at temporal frequencies above 0.6 Hz. When attributing complex object behavior to yet to be found new visual circuitry, we suggest to use our more parsimonious model, to see if these responses can already be explained by an asymmetric motion system. Very complex position responses can be mediated by motion vision based models, as long as they show a difference in response amplitudes for progressive and regressive motion.

Materials and Methods

Flies

We used flies raised on yeast food at 25 °C. Female flies 4 days past eclosion were used for experiments. All experimental flies were the heterozygous F1 offspring of *GMRSS00324-splitGAL4* males *(w−;R59E08-AD;R42F06-DBD;)* (***Schilling and Borst, 2015***) and females carrying *UAS-TNTe* (active) or *UAS-TNTin* (inactive) and *teeshirt-GAL80* to block *GAL4* expression in the ventral nerve cord and peripheral neurons *(w−;UAS-TNTe,tsh-GAL80;+;)* or *(w−;UAS-TNTin,tsh-GAL80;+;)*. Each fly was cold anesthetized for tethering and given a 30 min recovery period before being exposed to visual stimuli.

Tethered flight setup

Experiments where done in a custom built tethered flight rig similar to the one used in ***Fenk et al.*** (***2014***) but with a cylindrical screen with 10 cm diameter and 12 cm height. The closed loop latency of the system from delta wing beat amplitude change to photon was measured as 28 ms. The wing beat tracker runs at 120 Hz and is robust against partial occlusion due to leg extensions even if they are intersecting with the leading wing edge on the tracking image (***Figure 1—figure supplement 1B***). As measured in ***Hesselberg and Lehmann*** (***2007***), the fly is given closed-loop control over its orientation φ via:

$$I\ddot{\varphi}(t) = -C\dot{\varphi}(t) + \tau(t)$$

Here, the rotational inertia I is defined to be 0.52×10^{-12} N m s^2. Aerodynamic rotational dampening C is set to 54×10^{-12} N m s. The estimated torque τ generated by the fly is calculated from delta wing beat amplitude Δ_{WBA} via:

$$\tau(t) = k\Delta_{WBA}(t)$$

with $k = 2.9 \times 10^{-10}$ N m deg^{-1}.

Torque bias stimulus

The torque bias stimulus consisted of unbiased and biased closed loop object tracking trials, in which a 20 deg wide black bar could be tracked by the fly. The feedback loop was modulated during 10 s perturbation trials in which a constant angular torque offset was added, which is equivalent to adding a constant Δ_{WBA} offset to the measured Δ_{WBA}. Since the feedback dynamics are dominated by aerodynamic dampening, the constant torque offset effectively manifests as an angular velocity bias on the bar. Each trial was triggered after the fly fixated the bar for at least 2 s. The minimum waiting time between two trials was 10 s. Torque ranges were initially determined so that we could observe T4/T5 blocked flies failing to track the bar. During experimental trials, preselected torques were randomized and tested in both directions.

Chirp stimulus

The chirp stimulus consisted of a 15 deg wide black bar moving at a predefined trajectory in world coordinates, identical to ***Roth et al.*** (***2012***). The trajectory was given by a logarithmic chirp ranging from 0.05 Hz to 12.5 Hz over the time period of 120 s. The chirp amplitude A was modulated by $A(\omega) = A_0\ (0.918 + 0.264\ \text{s} \cdot \omega)^{-1}$, dependent on the angular frequency ω and the initial amplitude $A_0 = 60$ deg. The fly was in active control over its orientation in the world coordinate system, so that it could track the bar. To get reliable data for T4/T5 blocked flies, we had to interrupt the stimulus if flies were locked in a behavior that would spin the bar around. If the fly lost track of the object (indicated by the bar spinning around the fly more than 5 times per 5 s) we stopped the closed loop stimulus, reset the bar position to the visual midline of the fly for 5 s and returned closed loop control to the fly at the time when the first spin occurred. While this was rarely necessary for the control flies, it was required to get reliable data for the blocked flies (see ***Figure 2—figure supplement 1C***).

Transfer function extraction

To recover the transfer functions from closed loop trials, we treat the tethered flight setup and the fly as a input-output system, where the perturbation signal over time is the input and the temporally integrated Δ_{WBA} is the output of the system. This includes the dynamics of the setup in the transfer function, but helps to improve the accuracy of the method for blocked flies, which fail to reliably track the bar across most of the trial. Since the setup dynamics only show low pass filter characteristics, and are dominated by the processing and display delay of 28 ms corresponding to $\approx$ 35 Hz they can be ignored for the 12.5 Hz limited responses measured here. Δ_{WBA} is integrated via the closed-loop coupling dynamic equations described in the setup section. To recover gain and phase of the transfer function, the integrated output signal is divided into overlapping intervals in the time domain which are equidistantly spaced in the frequency domain. Each interval is then used to estimate amplitude and phase of the logarithmic chirp input signal using the output signal data. To estimate amplitude and phase we use a Bayesian estimation routine based on a Markov-Chain-Monte-Carlo method. Priors are chosen to be completely uninformative. Sampling is done until posteriors are reasonably well converged. Best

estimates of actual gain and phase are chosen as the maximum likelihood values from resulting posterior distributions. Error estimates are 90 % confidence interval ranges calculated from posterior distributions.

Numerical modelling

Numerical simulations use a Hassenstein-Reichardt-type elementary motion detector based visual system model, previously described in ***Lindemann* (*2005*)** with an asymmetric motion response (***Fenk et al., 2014***). The model was reduced to one dimension with inter-ommatidial angles of 5 deg and receptive fields matching horizontal system cell responses at 0 deg elevation from ***Schnell et al.* (*2010*)**. The *Calliphora* adequate LMC input filters were replaced with plain first order high-pass filters with a characteristic time of 80 ms. Time constants in first order low and high pass filters in both arms of the correlators were set to 140 ms to comply with results from *Drosophila* behavioral experiments (***Leonhardt et al., 2016***). Scaled model output is interpreted as Δ_{WBA} and limited via a first order low pass filter to a maximum change rate of 60 deg /s to emulate maximum observed change rate of Δ_{WBA} in control flies. Closed-loop simulations emulate the 28 ms tethered rig setup delay. Simulated experiments try to emulate high resolutions screens or LED cylinders dependent on experiment. Internal model parameters are identical across all simulations if not explicitly mentioned otherwise.

References

Bahl A, Ammer G, Schilling T, Borst A. Object tracking in motion-blind flies. Nature Neuroscience. 2013 apr; 16(6):730–738. https://doi.org/10.1038%2Fnn.3386, doi: 10.1038/nn.3386.

Borst A, Haag J, Reiff DF. Fly Motion Vision. Annual Review of Neuroscience. 2010 jun; 33(1):49–70. https://doi.org/10.1146%2Fannurev-neuro-060909-153155, doi: 10.1146/annurev-neuro-060909-153155.

Fenk LM, Poehlmann A, Straw AD. Asymmetric Processing of Visual Motion for Simultaneous Object and Background Responses. Current Biology. 2014 dec; 24(24):2913–2919. https://doi.org/10.1016%2Fj.cub.2014.10.042, doi: 10.1016/j.cub.2014.10.042.

Fox JL, Aptekar JW, Zolotova NM, Shoemaker PA, Frye MA. Figure-ground discrimination behavior in Drosophila. I. Spatial organization of wing-steering responses. Journal of Experimental Biology. 2013 nov; 217(4):558–569. https://doi.org/10.1242%2Fjeb.097220, doi: 10.1242/jeb.097220.

Geiger G, Boulin C, Bücher R. How the two eyes add together: monocular properties of the visually guided orientation behaviour of flies. Biological Cybernetics. 1981 jun; 41(1):71–78. https://doi.org/10.1007%2Fbf01836128, doi: 10.1007/bf01836128.

Goetz KG. Optomotorische Untersuchung des visuellen systems einiger Augenmutanten der Fruchtfliege Drosophila. Kybernetik. 1964 jun; 2(2):77–92. https://doi.org/10.1007%2Fbf00288561, doi: 10.1007/bf00288561.

Haikala V, Joesch M, Borst A, Mauss AS. Optogenetic Control of Fly Optomotor Responses. Journal of Neuroscience. 2013 aug; 33(34):13927–13934. https://doi.org/10.1523%2Fjneurosci.0340-13.2013, doi: 10.1523/jneurosci.0340-13.2013.

Hassenstein B, Reichardt W. Systemtheoretische Analyse der Zeit-, Reihenfolgen- und Vorzeichenauswertung bei der Bewegungsperzeption des Rüsselkäfers Chlorophanus. Zeitschrift für Naturforschung B. 1956; 11(9-10):513–524.

Heisenberg M, Wolf R. Vision in Drosophila. Springer Berlin Heidelberg; 1984. https://doi.org/10.1007%2F978-3-642-69936-8, doi: 10.1007/978-3-642-69936-8.

Hesselberg T, Lehmann FO. Turning behaviour depends on frictional damping in the fruit fly Drosophila. Journal of Experimental Biology. 2007 dec; 210(24):4319–4334. https://doi.org/10.1242%2Fjeb.010389, doi: 10.1242/jeb.010389.

Kim AJ, Fenk LM, Lyu C, Maimon G. Quantitative Predictions Orchestrate Visual Signaling in Drosophila. Cell. 2017 jan; 168(1-2):280–294.e12. https://doi.org/10.1016%2Fj.cell.2016.12.005, doi: 10.1016/j.cell.2016.12.005.

Leonhardt A, Ammer G, Meier M, Serbe E, Bahl A, Borst A. Asymmetry of Drosophila ON and OFF motion detectors enhances real-world velocity estimation. Nature Neuroscience. 2016 feb; 19(5):706–715. https://doi.org/10.1038%2Fnn.4262, doi: 10.1038/nn.4262.

Lindemann JP. On the Computations Analyzing Natural Optic Flow: Quantitative Model Analysis of the Blowfly Motion Vision Pathway. Journal of Neuroscience. 2005 jul; 25(27):6435–6448. https://doi.org/10.1523%2Fjneurosci.1132-05.2005, doi: 10.1523/jneurosci.1132-05.2005.

Maimon G, Straw AD, Dickinson MH. A Simple Vision-Based Algorithm for Decision Making in Flying Drosophila. Current Biology. 2008 mar; 18(6):464–470. https://doi.org/10.1016%2Fj.cub.2008.02.054, doi: 10.1016/j.cub.2008.02.054.

Poggio T, Reichardt W. A theory of the pattern induced flight orientation of the fly Musca domestica. Kybernetik. 1973 may; 12(4):185–203. https://doi.org/10.1007%2Fbf00270572, doi: 10.1007/bf00270572.

Poggio T, Reichardt W. Visual fixation and tracking by flies: Mathematical properties of simple control systems. Biological Cybernetics. 1981 mar; 40(2):101–112. https://doi.org/10.1007%2Fbf00344289, doi: 10.1007/bf00344289.

Reichardt W. Evaluation of optical motion information by movement detectors. Journal of Comparative Physiology A. 1987; 161(4):533–547. https://doi.org/10.1007%2Fbf00603660, doi: 10.1007/bf00603660.

Reichardt W, Poggio T. A theory of the pattern induced flight orientation of the fly Musca domestica II. Biological cybernetics. 1975 jan; 18(2):69–80. http://www.ncbi.nlm.nih.gov/pubmed/4718020.

Reichardt W, Poggio T. Visual control of orientation behaviour in the fly: Part I. A quantitative analysis. Quarterly Reviews of Biophysics. 1976 aug; 9(03):311. https://doi.org/10.1017%2Fs0033583500002523, doi: 10.1017/s0033583500002523.

Roth E, Reiser MB, Dickinson MH, Cowan NJ. A task-level model for optomotor yaw regulation in drosophila melanogaster: A frequency-domain system identification approach. In: *2012 IEEE 51st IEEE Conference on Decision and Control (CDC)* Institute of Electrical and Electronics Engineers (IEEE); 2012. https://doi.org/10.1109%2Fcdc.2012.6426231, doi: 10.1109/cdc.2012.6426231.

Schilling T, Borst A. Local motion detectors are required for the computation of expansion flow-fields. Biology Open. 2015 jul; 4(9):1105–1108. https://doi.org/10.1242%2Fbio.012690, doi: 10.1242/bio.012690.

Schnell B, Joesch M, Forstner F, Raghu SV, Otsuna H, Ito K, Borst A, Reiff DF. Processing of Horizontal Optic Flow in Three Visual Interneurons of the Drosophila Brain. Journal of Neurophysiology. 2010 jan; 103(3):1646–1657. https://doi.org/10.1152%2Fjn.00950.2009, doi: 10.1152/jn.00950.2009.

Schnell B, Raghu SV, Nern A, Borst A. Columnar cells necessary for motion responses of wide-field visual interneurons in Drosophila. Journal of Comparative Physiology A. 2012 mar; 198(5):389–395. https://doi.org/10.1007%2Fs00359-012-0716-3, doi: 10.1007/s00359-012-0716-3.

Silies M, Gohl DM, Clandinin TR. Motion-Detecting Circuits in Flies: Coming into View. Annual Review of Neuroscience. 2014 jul; 37(1):307–327. https://doi.org/10.1146%2Fannurev-neuro-071013-013931, doi: 10.1146/annurev-neuro-071013-013931.

Theobald. Theta motion processing in fruit flies. Frontiers in Behavioral Neuroscience. 2010; https://doi.org/10.3389%2Ffnbeh.2010.00035, doi: 10.3389/fnbeh.2010.00035.

Virsik RP, Reichardt W. Detection and tracking of moving objects by the fly Musca domestica. Biological Cybernetics. 1976; 23(2):83–98. https://doi.org/10.1007%2Fbf00336012, doi: 10.1007/bf00336012.

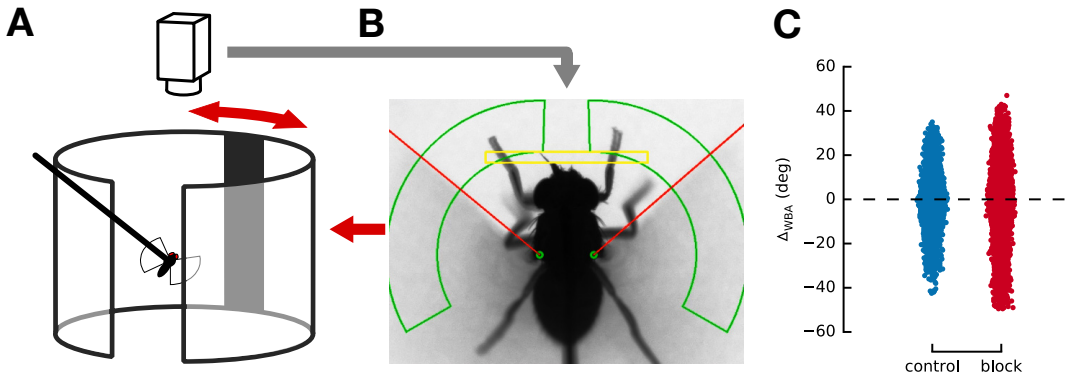

Figure 1–Figure supplement 1. (A) Closed loop tethered flight setup. The fly is mounted on a thin tungsten tether in the center of a cylindrical projection screen. The visual stimulus is projected onto the screen with a lcd projector. A camera mounted above the fly is tracking the wing movement of the fly. Realtime analysis of delta wing beat amplitude allows for closed loop coupling with stimulus. **(B)** View of camera image used for realtime tracking of Δ_{WBA}. Green framed areas indicate image portion in which the leading wing edge is tracked (detected edge marked by red line). Yellow framed area indicates image portion used to determine if the fly extends it's legs. Leg extensions do not interfere with leading edge tracking of wing stroke in this image based method, but could interfere in shadow based methods. **(C)** Scatter plot of observed delta wing beat amplitudes during object fixation. The blocked flies show a broader distribution compared to the control flies.

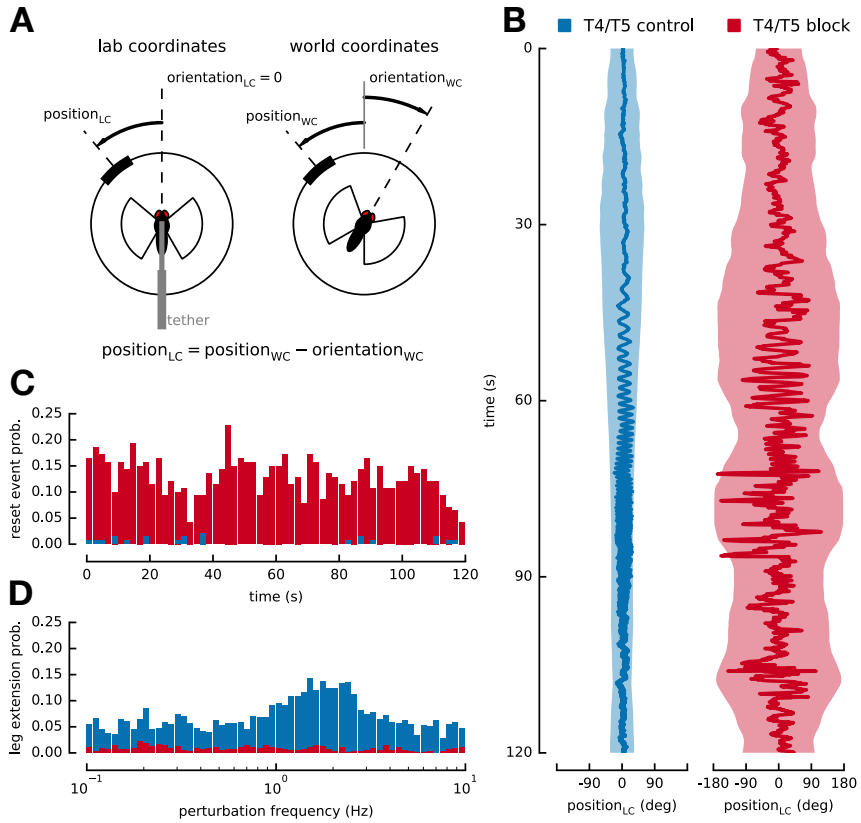

Figure 2–Figure supplement 1. **(A)** Lab and world coordinates during chirp stimulus explained. **(B)** Filtered average bar position in lab coordinate system over time. Shaded area marks FWHM of tracking distribution. Control flies fixate the bar almost perfectly. Blocked flies lose their ability to track reliably at around 45 s, indicated by a FWHM of almost 360 deg. **(C)** Reset event probability over time during chirp event. When the bar spins more that 3 times in 5 s, the stimulus is reset, to a stationary bar in front of the fly for 5 s, after which the stimulus resumes at a time prior to 'time of first spin' minus 5 s (see Materials and Methods). Stimulus interruptions are almost absent in control flies. Blocked flies average at a probability of about 10 %. **(D)** Leg extension event probability over time during chirp experiment. Blocked flies show almost no leg extension behavior. Control flies show an increased amount of leg extension between perturbation frequencies of 1 Hz and 3 Hz, which could explain the difference in empirical transfer functions.

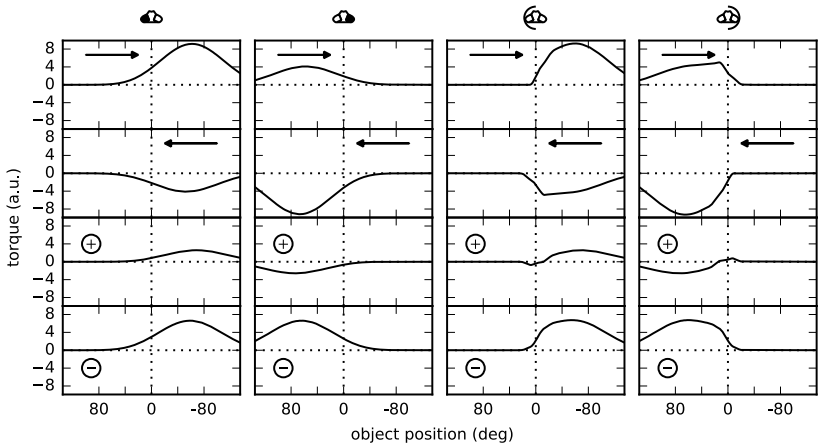

Figure 3–Figure supplement 1. Simulated torque responses toward a moving black bar for flies where half of the visual field was occluded by a screen and for flies where one eye was covered with paint. Top two rows show the response to a bar moving from left to right and right to left respectively. Bottom rows show sum (position response) and difference (motion response) of the two top rows. Since this is a motion-vision only based model, progressive and regressive responses differ in comparison to experiments, but position responses and motion responses created by summation and subtraction qualitatively agree with experimental results. See ***Geiger et al.*** (***1981***) Figure 5.

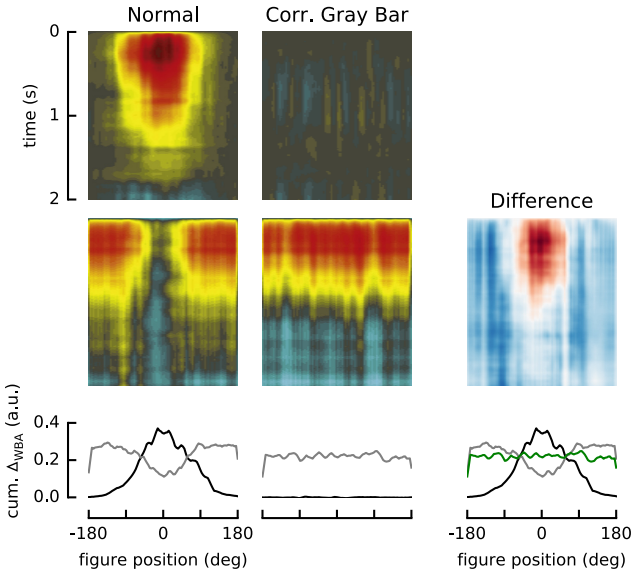

Figure 4–Figure supplement 1. Control simulation for background suppression argument. Top to bottom: Figure STAFs, Ground STAFs and averaged response of the first 100 ms of the STAFs. The left column shows a normal experiment that shows background suppression with background pattern and uncorrelated figure. The center column shows an experiment, where the figure was replaced with a gray bar of identical width, which moves correlated together with the background. The suppression in the ground STAF response vanishes vanishes when using a correlated gray bar as figure. The right column is plotted to facilitate easy comparison. See ***Fox et al.*** (***2013***) Figure 5.